

UNCLASSIFIED

AD NUMBER
AD881981
NEW LIMITATION CHANGE
TO Approved for public release, distribution unlimited
FROM Distribution: Further dissemination only as directed by Eustis Directorate, U.S. Army Air Mobility R & D Laboratory, Fort Eustis, Virginia 23604; Dec 1970 or higher DoD authority.
AUTHORITY
USAAMRDL ltr, 11 Jun 1971

THIS PAGE IS UNCLASSIFIED

AD 881981

CB (20)

AD

USAAVLABS TECHNICAL REPORT 69-66

AN ACTUATOR-DISC ANALYSIS OF HELICOPTER WAKE GEOMETRY AND THE CORRESPONDING BLADE RESPONSE

By  
M. Joglekar  
R. Loewy

December 1970

AD No. \_\_\_\_\_  
EEO FILE 0000

EUSTIS DIRECTORATE  
U. S. ARMY AIR MOBILITY RESEARCH AND DEVELOPMENT LABORATORY  
FORT EUSTIS, VIRGINIA

CONTRACT DAAJ02-68-C-0047 NEW  
UNIVERSITY OF ROCHESTER  
ROCHESTER, NEW YORK

This document is subject to special export controls, and each transmittal to foreign governments or foreign nationals may be made only with prior approval of Eustis Directorate, U. S. Army Air Mobility Research and Development Laboratory, Fort Eustis, Virginia 23004.



BDC  
RECEIVED  
APR 2 1971  
C

214



DEPARTMENT OF THE ARMY  
EUSTIS DIRECTORATE  
U.S. ARMY AIR MOBILITY RESEARCH AND DEVELOPMENT LABORATORY  
FORT EUSTIS, VIRGINIA 23604

This report has been reviewed by the Eustis Directorate,  
U. S. Army Air Mobility Research and Development  
Laboratory, and is considered to be technically sound.  
The report is published for the dissemination of in-  
formation and the stimulation of thought.

## ABSTRACT

Assuming that a helicopter rotor in forward flight can be represented by a flat circular disc with an appropriate steady pressure discontinuity across it, expressions were developed for relating the pressure field (1) to the total aerodynamic thrust and the total steady pitching and rolling moments experienced by the rotor or (2) to the time-dependent aerodynamic flapping moments at the roots of the blades as they rotate. The selected pressure field (1) satisfies the requirement of a loss of lift at the center and periphery of the disc, (2) accounts for first and second azimuthal harmonic variations in the lift density, and (3) satisfies Laplace's equation, which is the governing equation for the linearized steady flow of an incompressible fluid.

A digital computing program was written for calculating the velocity field from the selected pressure field and for calculating the positions of streamlines emanating from points above the disc. Two sample cases were chosen, corresponding to the UH-1 rotor at advance ratios,  $\mu$ , of 0.26 and 0.08 respectively. The computed streamlines for both cases show the tip-vortex phenomenon, indicating Prandtl-Lanchester trailing vortices emanating from the tip areas of the circular wing.

The geometry of the vortex wake that is shed and trailed from the blades was predicted from the above-mentioned streamline calculations. The computed deviations from a helical wake were greater for the  $\mu = 0.08$  case than for the  $\mu = 0.26$  case.

In order to examine the sensitivity of blade-load calculations to wake geometry, an existing computer program for calculating blade airloads was modified to accept the computed wake geometry, as contrasted to the rigid helix usually assumed. The blade-load predictions of this program using the computed wake geometry input were compared with the predictions resulting from a helical wake-geometry input and with experimentally measured airloads for the two cases mentioned above. The comparison indicates that for the UH-1 two-bladed teetering rotor system, the computed airloads are more sensitive to the wake geometry for the slower flight ( $\mu = 0.08$ ) than for the faster one ( $\mu = 0.26$ ). This weaker dependence at higher forward speeds may be due to (1) the wake being blown farther behind the rotor and/or (2) the relative predominance of cyclic pitch input, tangential velocity variation, and blade flapping motion in the total time-varying environment of the blades at a higher speed.

### FOREWORD

The subject investigation was performed under the direction of Mr. William Nettles of U. S. Army Aviation Materiel Laboratories, Fort Eustis, Virginia. The work was authorized by DA Task 1F162204A13904.

In preparing parts of the report, material was drawn freely from the work of Mr. R. A. Piziali, listed as Reference 2 in this report. The authors are grateful for the cooperation of Cornell Aeronautical Laboratory, and particularly to Mr. R. A. Piziali for making available the source decks for their blade-loads program BLP2.

TABLE OF CONTENTS

	<u>Page</u>
ABSTRACT . . . . .	iii
FOREWORD . . . . .	v
LIST OF ILLUSTRATIONS . . . . .	ix
LIST OF TABLES . . . . .	xii
LIST OF SYMBOLS . . . . .	xiii
CHAPTER 1 INTRODUCTION . . . . .	1
1.1 A First View of the Helicopter Wake-Geometry Problem . . . . .	1
1.2 Some Relevant Physical Phenomena . . . . .	5
1.21 Blade Dynamics . . . . .	5
1.22 Blade Aerodynamics . . . . .	6
1.23 Wake-Induced Velocity Relations . . . . .	11
1.24 Wake-Transport Relations . . . . .	12
1.3 Review of Various Approaches to Handling Rotary- Wing Aerodynamics . . . . .	13
1.31 Analytical . . . . .	13
1.32 Experimental . . . . .	14
1.33 Computational . . . . .	14
1.34 Some Complicating Factors Encountered in the Approaches Cited . . . . .	15
1.341 Physical Aspects . . . . .	15
1.342 Theoretical Difficulties . . . . .	15
1.343 Experimental and Computational Difficulties	16
1.4 Motivation for the Present Work . . . . .	16
CHAPTER 2 THEORETICAL MATERIAL . . . . .	19
2.1 Theoretical Background . . . . .	19
2.2 Capsule Statement of the Work Done . . . . .	19
2.3 Theoretical Scheme . . . . .	23
2.31 Equations of Fluid Motion . . . . .	23
2.32 Coordinate Transformations and Solutions of Laplace's Equation . . . . .	26

	<u>Page</u>
2.33 Choice of the Pressure Field, Based on Total Thrust and Net Moments . . . . .	30
2.34 Choice of the Pressure Field, Based on Blade Flapping Moments . . . . .	36
2.35 Induced Velocity Field . . . . .	44
CHAPTER 3 THE COMPUTER PROGRAM . . . . .	48
3.1 General Description . . . . .	48
3.2 Representation of Various Physical Phenomena in the CAL Program . . . . .	53
3.21 Rotor Dynamics . . . . .	53
3.22 Blade Aerodynamics . . . . .	55
3.23 Wake-Induced Effects . . . . .	58
3.24 Wake Transport . . . . .	59
3.3 Algorithm for Computing the UR Wake Geometry . . . . .	60
3.31 Subroutine RWAKE . . . . .	61
3.32 Subroutine STMLN(KEND) . . . . .	64
3.33 Subroutine FRWRD . . . . .	66
3.4 Integration With the CAL Program . . . . .	66
3.5 Peripheral Program . . . . .	69
CHAPTER 4 COMPUTED RESULTS AND INTERPRETATION . . . . .	70
4.1 UH-1 at $\mu = 0.26$ . Injection on Flat Disc . . . . .	70
4.2 UH-1 at $\mu = 0.26$ . Injection at Steady Deflected Positions of Blades . . . . .	78
4.3 UH-1 at $\mu = 0.08$ . Injection at Steady Deflected Positions of Blades . . . . .	82
CHAPTER 5 CONCLUSIONS AND POSSIBILITIES FOR FURTHER WORK . . . . .	93
LITERATURE CITED . . . . .	97
APPENDIXES	
I. Associated Functions of Legendre and Some of Their Properties . . . . .	99
II. FORTRAN IV Source Listings . . . . .	106
III. Induced Velocity at Selected Positions on the Disc Due to Selected Segments of the Nearest Tip Trail . . . . .	194
DISTRIBUTION . . . . .	197

LIST OF ILLUSTRATIONS

<u>Figure</u>		<u>Page</u>
1	Schematic Representation of the Helicopter Rotor Aerodynamics Problem. . . . .	3
2	Physical and Mathematical Blade Element Characteristics . . . . .	7
3	Induced Velocity Over Disc for Azimuthally Symmetric Lift Distribution Disc Incidence = $0^\circ$ . . . . .	20
4	Induced Velocity Over Disc for Azimuthally Symmetric Lift Distribution. Disc Incidence = $15^\circ$ . . . . .	21
5	Induced Velocity Distribution According to Mangler and Squire. Disc Incidence = $15^\circ$ . . . . .	22
6	Cartesian Coordinate Systems $x, y, z$ ("Wind system") and $x', y', z'$ ("Disc system") In Dimensional Form . . . . .	24
7	Ellipsoidal Coordinate System, Viewed in the $x'z'$ Plane . . . . .	28
8	$P_n^m(\psi)$ Plotted as a Function of Radius $r$ on the Disc . . . . .	34
9	Typical Steady and First Two Harmonic Components of Experimental Blade Loads. . . . .	37
10	Time Histories of the Lift Density at a Point $(r, \psi)$ of the Disc . . . . .	40
11	Flow Diagram for Part 1 of BLP2. . . . .	49
12	Major Steps in the Iterative Procedure for Solving the Equations in Part 2 of BLP2 . . . . .	50
13	Flow Diagram for Part 2 of BLP2 . . . . .	51

<u>Figure</u>		<u>Page</u>
14	Schematic of the Modified BLP2 . . . . .	52
15	K-Subscript Notation, Wake Configuration and Wake Vortex Strengths . . . . .	56
16	Flow Diagram for Subroutine RWAKE. . . . .	62
17	Flow Diagram for Subroutine STMLN(KEND). . . . .	65
18	Flow Diagram for Subroutine FRWRD . . . . .	67
19	Flow Diagram for Subroutine SUB14 as Modified at UR . . . . .	68
20	$Z$ -Component of the Induced Velocity on a Lifting Disc, Using the UR Program. . . . .	71
21	Typical Instantaneous Geometry of Wake Trails (UH-1, $\mu = 0.26$ , $N_b = 2$ , One of the Blades at $\psi = 75^\circ$ ) . . . . .	73
22	Geometry of Streamlines in the Steady Flow Field (UH-1, $\mu = 0.26$ ). . . . .	74
23	Three Views of a Fluid Contour, Released From 90% Radius on the Disc, One Rotor Revolution After Release (UH-1, $\mu = 0.26$ ). . . . .	75
24	Three Views of a Fluid Contour, Released From 90% Radius on the Disc, Two Rotor Revolutions After Release (UH-1, $\mu = 0.26$ ). . . . .	76
25	Time Histories of the Unsteady Parts of Measured and Computed Airloads (UH-1, $\mu = 0.26$ ). . . . .	77
26	Harmonic Analyses of Measured and Computed Airloads (UH-1, $\mu = 0.26$ ). . . . .	79
27	Time Histories of the Unsteady Parts of Measured and Computed Blade-Flapwise Bending Moments (UH-1, $\mu = 0.26$ ). . . . .	80
28	Harmonic Analyses of Measured and Computed Blade-Flapwise Bending Moments (UH-1, $\mu = 0.26$ ). . . . .	81

<u>Figure</u>		<u>Page</u>
29	Typical Instantaneous Geometry of a Wake Trail (UH-1, $\mu = 0.08$ , $N_b = 1$ , Blade at $\psi = 75^\circ$ ) . . . . .	84
30	Typical Instantaneous Geometry of a Wake Trail (UH-1, $\mu = 0.08$ , $N_b = 1$ , Blade at $\psi = 255^\circ$ ) . . . . .	85
31	Geometry of Streamlines in the Steady Flow Field (UH-1, $\mu = 0.08$ ) . . . . .	86
32	Three Views of a Fluid Contour, Released From 90% Radius on the Disc, One Rotor Revolution After Release (UH-1, $\mu = 0.08$ ) . . . . .	87
33	Three Views of a Fluid Contour, Released From 90% Radius on the Disc, Two Rotor Revolutions After Release (UH-1, $\mu = 0.08$ ) . . . . .	88
34	Three Views of a Fluid Contour, Released From 90% Radius on the Disc, Three Rotor Revolutions After Release (UH-1, $\mu = 0.08$ ) . . . . .	89
35	Three Views of a Fluid Contour, Released From 90% Radius on the Disc, Four Rotor Revolutions After Release (UH-1, $\mu = 0.08$ ) . . . . .	90
36	Time Histories of the Unsteady Parts of Measured and Computed Airloads (UH-1, $\mu = 0.08$ ) . . . . .	91
37	Time Histories of the Unsteady Parts of Measured and Computed Blade-Flapwise Bending Moments (UH-1, $\mu = 0.08$ ) . . . . .	92
38	Positions of Selected Blade-Stations and Selected Wake-Trail Segments (UH-1, $\mu = 0.26$ ) . . . . .	195

LIST OF TABLES

<u>Table</u>		<u>Page</u>
I	Rotor Blade Vibration Natural Frequencies and Comparison With Rotor Speeds, for UH-1 and H-34 . . . . .	4
II	The Terms Retained in the Expression (62) for the Disturbance Pressure P . . . . .	38
III	Various Options for Choosing the Steady Pressure Field P Through the Coefficients $C_n^m$ and $D_n^m$ . . . . .	63
IV	Comparison of Contributions of the Quasi-Steady and Wake-Induced Quantities to the Bound Vorticity Strength Components at the 85% Radial Station, UH-1, $\mu = 0.26$ and $\mu = 0.08$ . . . . .	94
V	Induced Velocity at Selected Blade-Stations due to Selected Tip-Trail Segments (UH-1, $\mu = 0.26$ ). See Figure 38. . . . .	196

LIST OF SYMBOLS

$\bar{A}_{0k}, \bar{A}_{nk}$	cosine coefficients of Fourier expansion of $G_k$
$a_{0k}, a_{nk}$	cosine coefficients of Fourier expansion of $q_k$
$A_{0k}, A_{nk}$	coefficients in trigonometric expansion for $\gamma_k$
$b$	blade semi-chord
$\vec{B}$	vector magnetic induction field
BLP2	blade airload digital computer program described in Reference 2
$\bar{B}_{nk}$	sine coefficients of nth harmonic in Fourier Expansion of $G_k$
$b_{nk}$	sine coefficients of nth harmonic in Fourier Expansion of $q_k$
$C_n^m$	"arbitrary" constant in the solution of Legendre's equation, multiplying the cosine term
$C_T$	thrust coefficient = $\frac{T}{\pi \rho R^4 \Omega^2}$
$C_{M_r}$	coefficient of rolling moment = $\frac{M_r}{T \cdot R}$
$C_{M_p}$	coefficient of pitching moment = $\frac{M_p}{T \cdot R}$
$C_t$	Mangler thrust coefficient = $\frac{T}{\pi \rho / 2 V_{\infty}^2 R^2}$

$D_n^m$	"arbitrary" constant in the solution of Legendre's equation, multiplying the sine term
$dA$	elemental area of rotor disc
$\left(\frac{\partial C_L}{\partial \alpha}\right)$	measured lift curve slope
$e_k$	$\sqrt{g_{kk}}$
$F(r,t)$	blade aerodynamic lift per unit span
$g_k$	structural damping coefficient in the $k^{\text{th}}$ natural mode
$G_k$	generalized force in the $k^{\text{th}}$ natural mode
$i$	imaginary number = $\sqrt{-1}$
$I_k$	circulation associated with the part of the bound vortex due to all parts of the airfoil angle of attack except that resulting from wake vorticity
$\vec{J}$	vector current distribution
$k_a$	azimuthal position of blade when shedding vorticity
$L$	implies the total of line filaments of vortex strength
$l$	length along vortex filament
$M_k$	generalized mass in the $k^{\text{th}}$ natural mode
$m$	"constant of separation" in solution of a partial differential equation
$M_r$	rolling moment (about the $x'$ axis)
$M_p$	pitching moment (about the $y$ axis)

$M(\psi)$	moment applied by rotor blade to shaft at angle $\psi$
$M_0, M_{c1}, M_{s1}$	harmonic components of $M(\psi)$
$N_m$	total number of normal modes chosen to represent total blade response
$N_h$	total number of harmonics retained in Fourier expansion
$\hat{n}$	unit vector, normal to a surface
$n$	"constant separation" in solution of a partial differential equation
$N_b$	total number of blades in a rotor
$N_a$	total number of azimuthal stations on rotor disc
$N_r$	total number of radial stations on rotor disc
$P(r,t)$	blade aerodynamic pitching moment per unit span
$p$	disturbance pressure
$p_0$	static pressure
$P_n^m(\nu)$	associated Legendre function of the first kind
$P$	nondimensionalized disturbance pressure $= \frac{p}{\rho V_{fs}^2}$
$Q(u,v,w)$	nondimensional induced velocity $q(u,v,w)/V_{fs}$
$Q_n^m$	associated Legendre functions of the second kind
$g_{ij}$	metric tensor

$q_k(t)$	generalized displacement (a function of time) in the $k^{\text{th}}$ normal mode
$\vec{q}$	induced velocity vector
$q_i$	component of fluid velocity in the $i$ -axis direction
$r$	radial distance from the rotor center to a point on a blade
$\vec{r}$	vector distance between source point and field point
$R$	radius of actuator disc
$R_{ijka}$	point in the three-dimensional wake model
$S_{mKj}$	induced velocity coefficients in the trip expansion for $w_{K_s}$
$t$	(independent) time coordinate (sec.)
$T$	total thrust
$T_{mKi}$	induced velocity coefficients in trig expansion for $w_{K_T}$
$u$	disturbance velocity in $x$ -direction
$U$	nondimensionalized disturbance velocity in the $x$ -direction = $\frac{u}{V_{Fe}}$
$v_k$	"impressed" normal flow due to all effects except wake vorticity
$\bar{v}_{ok}, \bar{v}_{nk}$	coefficients in trig expansion for $\bar{w}_k$
$V_1$	"tangential" relative airflow velocity component in $x$ -direction
$V_T$	total relative fluid velocity normal to the blade leading edge
$V$	volume of fluid

$V$	nondimensionalized disturbance velocity in the $y$ -direction = $\frac{V}{V_{Fs}}$
$V_i$	induced velocity
$V_{Fs}$	free-stream velocity
$v$	disturbance velocity in the $y$ -direction
$W$	nondimensionalized disturbance velocity in the $z$ -direction = $\frac{W}{V_{Fs}}$
$\overline{W}(x)$	normal relative velocity component (positive in the plus $z$ -direction)
$w$	disturbance velocity in the $z$ -direction
$w_k$	"impressed" normal flow component due to wake vorticity
$\underline{w}$	(assumed) uniform induced velocity over rotor disc
$x$	$x/R$
$x^w$	"wind coordinates"
$x_1$	blade chordwise coordinate, positive aft
$x$	Cartesian coordinate in horizontal, longitudinal direction, positive forward
$x'$	longitudinal Cartesian coordinate in plane of rotor disc, positive forward
$\hat{x}$	unit vector in direction of positive $x$ -axis
$y$	displacement of blade normal to the chord plane
$y'$	Cartesian coordinate in lateral direction, positive starboard

$\gamma_{oc}$	built-in coning angle plus steady blade bending deflection (plus, up)
$Y'$	$y'/R$
$Z, Z'$	$z/R, z'/R$
$z$	Cartesian coordinate in vertical direction, positive down
$z'$	Cartesian coordinate normal to rotor disc, positive down
$\alpha_{max}$	angle of attack corresponding to airfoil stall
$\alpha_g$	geometric angle of attack of blade (airfoil section (positive, nose up))
$\alpha$	incidence angle of rotor disc, (positive, nose down)
$\Gamma_{mk}$	maximum value of total bound, circulation, corresponding to blade stall
$\vec{\gamma}$	vector distribution of vorticity
$\Gamma$	total circulation around the blade section
$\bar{\Gamma}_i$	maximum bound vorticity on a blade at azimuth station $i$
$\gamma$	strength of vortex sheet per unit length
$\Gamma$	scalar vorticity per unit length in the wake
$\delta$	fraction of time interval which wake is advanced from blade position at which it was shed, trailed
$\Delta(\ )$	difference in ( ) between upper and lower surface, or increment in ( )
$\delta_{kj} \Gamma_j$	circulation associated with bound vorticity resulting from wake vorticity trailed and shed when blade was at azimuth $j$

$\Theta$	torsional displacement of blade
$\theta$	Glauert coordinate
$\omega_k$	$k^{\text{th}}$ natural frequency (rad/sec)
$\xi^m$	ellipsoidal coordinates
$\xi$	"dummy" variable of integration in chord or $x$ -axis direction
$\xi^m$	disc coordinates
$\phi$	velocity potential = $\Phi_1(\nu) \cdot \Phi_2(\eta) \cdot \Phi_3(\psi)$
$\pi(r, \psi)$	pressure difference at $r, \psi$ when a blade is at that point on the disc
$\rho$	air mass density
$\mu_0$	electromagnetic induction coefficient defined by $\nabla \times \vec{B} = \mu_0 \vec{J}$
$d\tau$	elemental volume
$d\Sigma$	elemental surface area (of a vortex tube)
$\nabla$	vector operator = $\frac{\partial}{\partial x} \hat{x} + \frac{\partial}{\partial y} \hat{y} + \frac{\partial}{\partial z} \hat{z}$
$\nu, \eta, \psi$	curvilinear coordinates (see Figure 7), the last corresponds to angle of azimuth on the rotor disc
$\mu$	tip speed ratio: $V_{Fs} / \Omega R$

#### Subscripts

$c$	identifies quantity evaluated around a closed contour
$k$	identifies $k^{\text{th}}$ natural mode
$m$	identifies a finite number (say of normal modes)
$i$	identifies induced

U,L	identifies upper, lower airfoil surface, respectively
T	identifies trailed vortex
BU	" bound vortex
S	" shed vortex
Q	" field point
K	" particular point on the rotor disc
,	indicates partial derivative with respect to variable(s) represented by subscript(s) which follow(s)

Superscripts

(k)	identifies $k^{\text{th}}$ natural mode
$\rightarrow$	" vector
$\sim$	" perturbation quantity
$\hat{\phantom{x}}$	" unit vector
$\bar{\phantom{x}}$	" steady component

## CHAPTER 1

### INTRODUCTION

#### 1.1 A First View of the Helicopter Wake-Geometry Problem

The desirability of an accurate determination of the wake geometry for a helicopter rotor stems primarily from the necessity of predicting the airloads experienced by the blades. These airloads, in addition to providing the lift and propulsive force, are a major source of vibratory excitation and drive the structurally important oscillatory blade bending moments. Since aerodynamic forces are determined by the flow field, the relative flow field must be known if one is to satisfactorily predict the airloads on a prescribed airfoil executing a prescribed motion.

It has been demonstrated from fixed-wing experience (see, for example, the reduced polar diagrams and reduced lift/angle of attack curves in Reference 1), that for a finite lifting body, the velocity field perturbation resulting from the distribution of the "free" vorticity in the wake must be taken into account in order to predict the aerodynamic forces (aerodynamic force is sufficiently definitive) on the body. It may be argued that this wake-induced velocity is even more important for rotary wings since (1) rotation causes the wake vorticity to remain in the vicinity of the (succeeding) blades for a much longer time and (even for the highest known advance ratios) is not blown behind the wing so quickly as with fixed-wing craft, and (2) as a result of a lower forward speed in the case of a pure helicopter, the change in angle of attack for a given downwash velocity will be larger over most of the disc than in the fixed-wing case.

In addition to the determination of the rotor airloads, the wake-induced velocity field is likely to be influential in the determination of (1) interference effects between rotors, (2) positioning and effectiveness of auxiliary surfaces, (3) interference with the fuselage and other nonlifting bodies, (4) debris entrainment, (5) projectile trajectories, etc; hence, the continuing interest in the study of helicopter wake geometry and in the resultant wake-induced velocity field.

One of the difficulties in an accurate determination of the wake-induced velocity should be immediately apparent: the interdependence of the wake geometry and the induced velocity field. The wake-

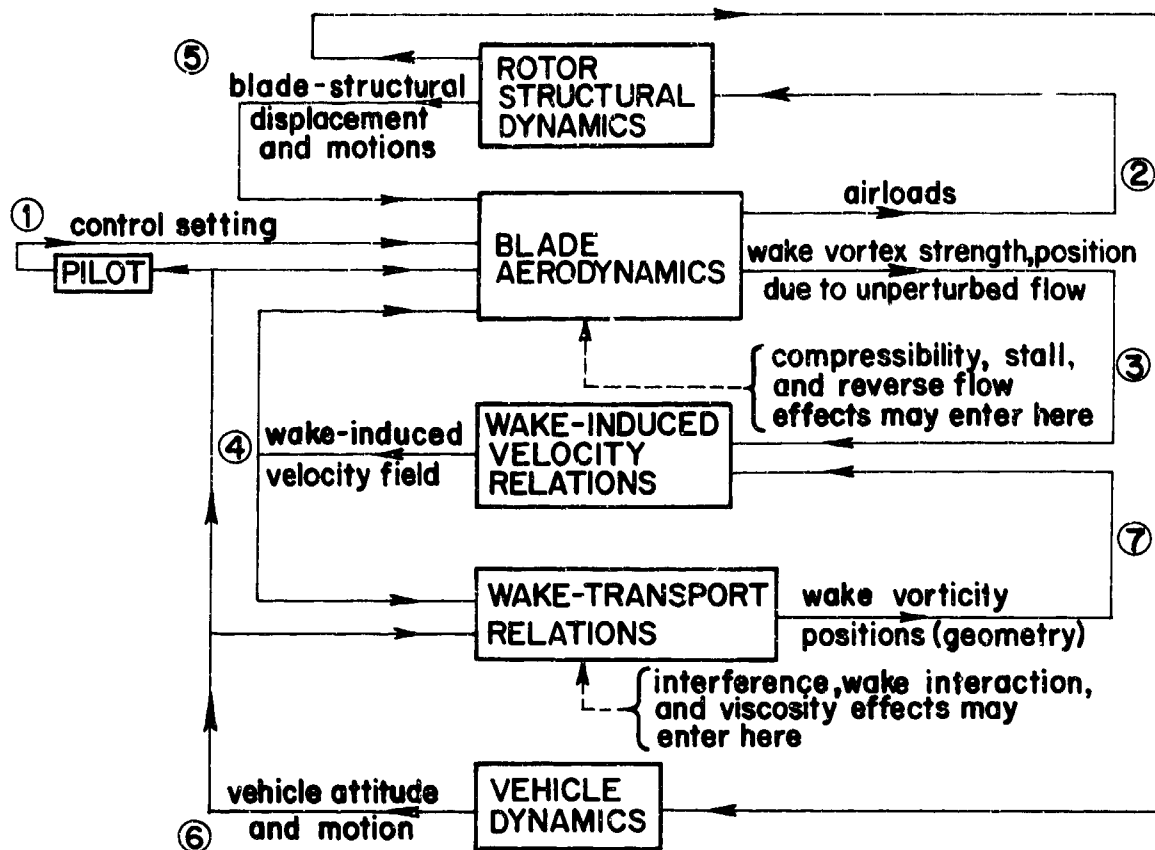
induced velocity field can be expressed only as an integral (over the wake) of a function of the wake geometry and the vorticity strengths, while the wake geometry is obtained by time integrations of the flow field along particle paths. As can be seen from subsequent sections, this one complication alone is sufficient to make the general wake-geometry determination problem difficult. This interdependence between wake geometry and induced velocity field does not arise in the customary treatment of the fixed-wing problem because one assumes there that the induced velocity is quite small as compared to the forward speed and hence the trailed vorticity is assumed to lie on a "rigid, horizontal" surface behind the wing.

Another complicating factor is the flexibility of rotor blades. Most helicopter blades currently have their first flapwise natural frequencies within a few percent of rotor speed. Table I summarizes the flapping natural frequencies for the UH-1 and H-34 rotor systems. It has been demonstrated that significant variations in downwash exist up to the 4th azimuthal harmonic. Under such circumstances, the azimuthal variations in aerodynamic loads are almost certain to excite substantial oscillatory flapping displacements as well as torsional displacements, and the resulting "plunging" velocities will affect the aerodynamic loads on the blades to the first order, while the torsional displacements (i.e., angle of attack changes due to torsion) will affect them to the zeroth order. Thus, the situation is not one of a "prescribed blade executing a prescribed motion". As a final note, it may be mentioned that the rotor control settings and attitude are themselves affected by the periodic variations in the hub loads.

Figure 1 indicates the interrelations of these various aspects of the problem. The figure can be looked upon as an information flow diagram\*, the rectangular blocks representing various phenomena as customarily treated in isolation. Thus, for example, the airloads and wake vorticity strengths resulting from the phenomenon of blade aerodynamics can be calculated if the (1) blade structural displacements and motions, (2) control settings, (3) vehicle attitude and motion, and (4) wake-induced velocity (inflow) are all known as "inputs" to the blade aerodynamic equations. These equations are, for unstalled subsonic motion, simple algebraic relations. (The assumption that makes this possible is the customary strip theory postulation that each spanwise section of the airfoil has a two-dimensional pattern of aerodynamic behavior.) We are not so fortunate in regard to some of the other phenomena; e.g., the wake-

---

\*By "information", we mean here "knowledge about the values (steady or otherwise) of specific physical quantities of interest".



Quantities of interest :

- |  |  |
|--|--|
| 1. Control settings                                  | 5. Blade displacements and motions         |
| 2. Airloads  | 6. Vehicle attitude and motion             |
| 3. Vortex strength, position due to unperturbed flow | 7. Wake vorticity position (wake geometry) |
| 4. Induced velocity field                            |  |

Figure 1. Schematic Representation of the Helicopter Rotor Aerodynamics Problem.

TABLE I. ROTOR BLADE VIBRATION NATURAL FREQUENCIES AND COMPARISON WITH ROTOR SPEEDS, FOR UH-1 AND H-34

Rotor System	Nominal Rotor Speed	Rotor Mode No.	Natural Frequency		Mode of Oscillation
			rad/sec	Rotor Speeds	
Bell UH-1 (teetering) 2 blades	315 rpm (33 rad/sec)	1	33.8	0.97	rigid flapping
		2	38.6	1.18	first symmetric flap-bending
		3	96.4	2.92	first antisymmetric flap-bending
		4	112.8	3.42	second symmetric flap-bending
		5	171.6	5.20	second antisymmetric flap-bending
Sikorsky H-34 (fully articulated) 4 blades	210 rpm (22 rad/sec)	1	23.65	1.08	rigid flapping
		2	61.45	2.79	first flap-bending
		3	111.84	5.08	second flap-bending
		4	177.19	8.05	third flap-bending
		5	297.19	13.51	fourth flap-bending

induced velocity relations (i.e., Biot-Savart law integrated over the wake) and the wake-transport relations. These are integral expressions, as mentioned above.

## 1.2 Some Relevant Physical Phenomena

Equations representing some of the phenomena shown in Figure 1 will be stated in this section. More specific description of these phenomena as represented in the computer program appears in Chapter 3.

### 1.21 Blade Dynamics

The oscillatory response of a rotor blade to variations in airloads can usually be satisfactorily represented in terms of its response in each of a judiciously chosen finite number,  $N_m$ , of its normal modes of displacement (rigid as well as elastic). If  $q_k(t)$  is the generalized displacement in the  $k^{\text{th}}$  normal mode, the flapwise and torsional displacements at a point radius  $r$  can then be written as\*

$$y(r,t) = \sum_{k=1}^{N_m} q_k(t) \cdot y^{(k)}(r) \quad (1)$$

$$\theta(r,t) = \sum_{k=1}^{N_m} q_k(t) \cdot \theta^{(k)}(r) \quad (2)$$

where  $y^{(k)}(r)$ ,  $\theta^{(k)}(r)$  is the mode shape in the  $k^{\text{th}}$  normal mode.

---

\*We are here assuming the blade to be infinitely rigid in the chordwise direction. The computations reported herein used the additional structural simplifications of Reference 2, ignoring the dependence of torsional displacements on airloads, thus assuming the torsional response of the blades to be completely known beforehand.

The differential equation for determining the generalized displacements  $q_k(t)$  is of the form

$$M_k \ddot{q}_k + i g_k M_k \omega_k^2 \dot{q}_k + M_k \omega_k^2 q_k = G_k(t) \quad (3)$$

...k=1, N<sub>m</sub>

$M_k, g_k, \omega_k$  and  $G_k$  are the generalized mass, structural damping, natural frequency, and generalized forcing function respectively in the  $k^{\text{th}}$  mode. The first three of these are dynamic "properties" of the rotating blade, as is the mode shape, and can be predetermined for each mode. The forcing function depends on the airloads experienced by the blade:

$$G_k(t) = \int_{r_1}^{r_2} [F(r,t) \cdot y^{(k)}(r) + P(r,t) \cdot \Theta^{(k)}(r)] dr \quad (4)$$

...k=1, N<sub>m</sub>

$F(r,t)$  and  $P(r,t)$  represent the time-varying aerodynamic lift and pitching moment per unit span at radius  $r$ .

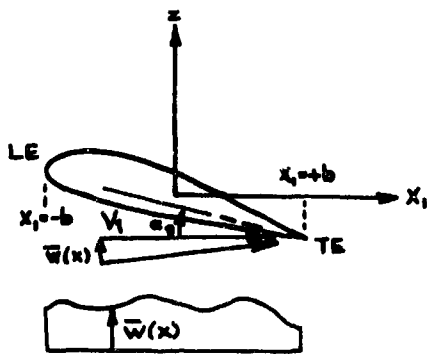
### 1.22 Blade Aerodynamics

Consider a blade segment with its leading edge at  $x = -b$  and trailing edge at  $x = +b$  in a blade-attached coordinate system; see Figure 2(a). Let the relative airflow have a "tangential" component  $V_1$  in the  $x_1$  direction and an "impressed" normal flow component  $\bar{w}(x)$  in the  $z$  direction.  $\bar{w}(x)$  is the combined effect of (1) the component of  $V_1$  normal to the blade chord as a result of the geometrical angle of attack  $\alpha_1$  and from the local camber of the airfoil section, (2) the component of the forward speed normal to the blade chord as a result of shaft tilt, spanwise blade slope, etc., (3) instantaneous flapping velocity of the blade section, (4) instantaneous torsional velocity of the blade section (due to blade flexibility as well as cyclic control inputs), and (5) induced velocity due to the wake vorticity. We wish to estimate the aerodynamic forces experienced by this blade segment.

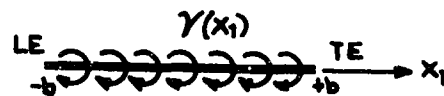
Since no through-flow can exist on the impermeable airfoil, the presence of the airfoil must give rise to such a "disturbance" that its effect will exactly cancel the "impressed" normal velocity  $\bar{w}(x_1)$  in the region  $-b \leq x_1 \leq +b$ . It can be shown (see, for example, Reference 3) that for a thin airfoil, this disturbance can be represented by a vortex sheet over the chord length, as shown in Figure 2(b). The distribution of the

strength  $\gamma(x_1)$  of this vortex sheet must be such that

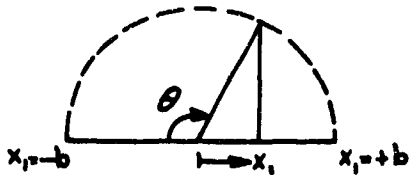
$$\bar{w}(x_1) + \frac{1}{2\pi} \int_{-b}^{+b} \frac{\gamma(\xi_1)}{\xi_1 - x_1} d\xi_1 = 0 \quad (5)$$



(a) blade element and "impressed" normal velocity distribution  $\bar{w}(x)$ .



(b) thin airfoil representation with bound vorticity distribution  $\gamma(x)$ .



(c) Glauert coordinate  $\theta$ .

$$x_1 = -b \cos \theta$$

Figure 2. Physical and Mathematical Blade Element Characteristics.

In order to uniquely specify the circulation around the airfoil section, it is customary to further require that the flow be smooth over the sharp trailing edge (Kutta hypothesis)\*. This can occur only if

$$\gamma(+b) = 0 \quad (6)$$

Subject to the condition (6), equation (5) has now to be solved. The solution, by Sohngen's formula, is

$$\gamma(x_1) = \frac{2}{\pi} \cdot \sqrt{\frac{b-x_1}{b+x_1}} \cdot \int_{-b}^{+b} \sqrt{\frac{b+\xi}{b-\xi}} \cdot \frac{\bar{w}(\xi)}{x_1-\xi} \cdot d\xi \quad (7)$$

After thus determining the bound vorticity strength  $\gamma(x_1)$  from the impressed normal velocity  $\bar{w}(x_1)$ , it now remains to deduce the pressure difference between the two faces of the airfoil. Assuming that (1) the disturbance velocities are small compared to  $V_1$ , (2) the flow is irrotational outside of the vortex sheet, and (3) the flow is incompressible, the momentum equation for unsteady flow can be reduced to

$$\frac{\partial}{\partial t} \left( -\frac{\partial \phi}{\partial x_1} \right) + V_1 \frac{\partial}{\partial x_1} \left( -\frac{\partial \phi}{\partial x_1} \right) = -\frac{1}{\rho} \cdot \frac{\partial p}{\partial x_1} \quad (8)$$

where  $p$  is the disturbance pressure and  $\phi$  is a velocity

---

\*This is tantamount to requiring a finite velocity at the trailing edge. It has been corroborated by experiment, in that the pressure distributions on the surfaces of the airfoil as predicted from such a choice of the bound vorticity distribution agree with experimental measurements (see, for example, Reference 4).

potential, such that the disturbance velocity  $u$  equals  $-\frac{\partial \phi}{\partial x_1}$ . Changing the order of differentiation in the first term and integrating from  $x_1 = -\infty$  to a point on the upper face of the vortex sheet,

$$-\frac{\partial \phi_u}{\partial t} - V_1 \frac{\partial \phi_u}{\partial x_1} + \frac{1}{\rho} p_u = f(t) \quad (9)$$

and similarly at a point on the lower face,

$$-\frac{\partial \phi_L}{\partial t} - V_1 \frac{\partial \phi_L}{\partial x_1} + \frac{1}{\rho} p_L = f(t) \quad (10)$$

But it can be shown (by considering an elemental rectangular contour around a point  $x_1$ ) that

$$\frac{\partial \phi_L}{\partial x_1} - \frac{\partial \phi_u}{\partial x_1} = u_u - u_L = \gamma(x_1, t) \quad (11)$$

and, by integrating,

$$\phi_L - \phi_u = \int_{-b}^{x_1} \gamma(\xi, t) d\xi \quad (12)$$

Using equations (9) through (12), one gets the aerodynamic pressure difference across the vortex sheet:

$$p_L(x_1) - p_u(x_1) = \Delta p(x_1) = \rho \left[ V_1 \gamma(x_1, t) + \frac{\partial}{\partial t} \int_{-b}^{x_1} \gamma(\xi, t) d\xi \right] \quad (13)$$

which is the unsteady form of Zhukovskii's theorem.

The total circulation  $\Gamma$  around the blade section, the aerodynamic lift  $F$  per unit span, and the aerodynamic pitching moment about mid-chord  $P_{\frac{c}{2}}$  per unit span are obtained by integration over the chord:

$$\Gamma = \int_{-b}^{+b} \gamma(x_1) dx_1 \quad (14)$$

$$F = \int_{-b}^{+b} \Delta p(x_1) dx_1 \quad (15)$$

$$P_{\frac{c}{2}} = \int_{-b}^{+b} x_1 \cdot \Delta p(x_1) dx_1 \quad (16)$$

The other "output" from the blade aerodynamics block in Figure 1 is the wake vortex strength. The strength of free vortices trailed and shed from a blade can be deduced by logical extrapolation of the fixed-wing "lifting line" theory. Thus, when the instantaneous bound vorticity varies along the blade span, trailed vortex strengths are given by

$$\gamma_T(r) = \frac{d\Gamma_{bw}}{dr} \quad (17)$$

where  $\gamma_T(r)$  is the strength of the trailed vortex sheet and  $\Gamma_{bw}(r)$  is the strength of the bound vortex at the spanwise location  $r$ . Similarly, for a blade with continuously changing (temporal change) bound vorticity, the shed vortex strength is given by

$$\gamma_s(r, t) = \frac{d\Gamma_{bw}(r, t)}{V_T dt} \quad (18)$$

where  $\gamma_s(r,t)$  is the strength of the shed vortex sheet as a function of spanwise position  $r$  and time  $t$ , and  $V$  is the total relative fluid velocity normal to the blade leading edge.

When the strength of the bound vortex varies both along the span and with time, the above expressions for  $\gamma_T$  and  $\gamma_S$  will represent the components of the strength of the vortex sheet in the chordwise and spanwise directions respectively.

### 1.23 Wake-Induced Velocity Relations

These relations are used for determining the "induced" velocity  $\vec{q}_Q$  at a field point  $Q$  due to a distribution of vorticity  $\vec{\Gamma}$  in a volume  $V$ . This is directly analogous to the problem of determining the magnetic induction field  $\vec{B}_Q$  at  $Q$  due to a current distribution  $\vec{J}$  in  $V$ . The latter problem has the solution given by the Biot-Savart field law:

$$\vec{B}_Q = \frac{\mu_0}{4\pi} \int_V \frac{\vec{J} \times \vec{r}}{r^3} d\tau \quad (19)$$

where  $\vec{r}$  is the vector distance from the source point to the field point. See, for example, Reference 5.

Analogously, for our induced velocities,

$$\vec{q}_Q = \frac{1}{4\pi} \int_V \frac{\vec{\Gamma} \times \vec{r}}{r^3} d\tau$$

(The  $\mu_0$  is a characteristic of the units used for the electromagnetic quantities such that  $\nabla \times \vec{B} = \mu_0 \vec{J}$ .)

If the source distribution of vorticity is over line segments as in our wake model, our formula is modified to

$$\vec{q}_Q = \frac{1}{4\pi} \int_L \Gamma \frac{d\vec{l} \times \vec{r}}{r^3} \quad (20)$$

where  $\vec{r}$  is the vector from  $d\vec{\ell}$  to  $Q$ , and  $\Gamma$  is the scalar vorticity per unit length along  $d\vec{\ell}$ , an elemental length of vortex filament in the wake. The integration is over  $L$ , which is the aggregate of all the wake filaments.

#### 1.24 Wake-Transport Relations

Kelvin's theorem of conservation of circulation (see Reference 6) states that for an ideal fluid, the substantial derivative of the circulation  $\Gamma_c = \oint_c \vec{q} \cdot d\vec{\ell}$  around a closed contour  $c$  is zero.

$$\frac{D\Gamma_c}{Dt} = 0 \quad (21)$$

Now, if  $c$  lies on the surface  $\Sigma$  of a vortex tube,

$$\Gamma_c = \oint_c \vec{q} \cdot d\vec{\ell} = \iint_{\Sigma} (\nabla \times \vec{q}) \cdot \hat{n} \, d\Sigma = 0 \quad (22)$$

using Stoke's theorem and the fact that  $\nabla \times \vec{q}$  is at right angles to the unit normal  $\hat{n}$  on the surface  $\Sigma$ . Therefore, using Kelvin's theorem, one concludes that a contour on a vortex-tube surface will always remain on a vortex-tube surface. Using two such intersecting surfaces, it is easy to see that vortex lines always travel with the fluid (Helmholtz theorem; see Reference 7).

We may consider all vorticity in the wake model to have originated from the blades. Thus, if we can calculate the positions of fluid particles released into the flow field from discrete locations on the disc\*, at all subsequent (for our purposes, discrete) instants, we will be able to predict the wake geometry (i.e., time-dependent

---

\*The "disc" here means the surface described by the blades as they rotate. Due to the pre-coning built into the blades, the steady deflection under load, and the flapping displacements, this surface will not, in general, be a plane circular surface.

positions of the wake-filament end points in Figure 15(b) ).

### 1.3 Review of Various Approaches to Handling Rotary-Wing Aerodynamics

#### 1.31 Analytical

Among existing theoretical approaches are the actuator theories, the blade element theories, and the wake theories.

a. The early actuator disc theory for a propeller assumed a uniform pressure distribution and induced velocity over the disc, and explained their interrelationship through a simple momentum transfer approach, leading to a relation like

$$T = 2\pi R^2 \rho v_i \sqrt{V_{Fs}^2 + v_i^2} \quad (23)$$

where  $T$ ,  $v_i$ , and  $V_{Fs}$  are the total thrust, the induced velocity at the disc, and the forward velocity respectively. Glauert modified this assumption of the uniform pressure distribution to one increasing linearly from the front to the rear of the rotor disc (see Reference 8). A modification due to Kinner (Reference 9) and Mangler (Reference 10) assumes an azimuthally symmetric lift distribution satisfying the requirement of a loss of lift both at the center and at the periphery of the disc.

All the actuator disc theories implicitly assume an infinite number of blades. The inherently unsteady nature of the aerodynamics associated with a finite number of blades is, therefore, ignored, as are all effects concerned with the shape of airfoil sections.

b. The blade element theories, on the other hand, consider the forces experienced by individual blades in their motion through the fluid; they are thus intimately concerned with airfoil section characteristics. The blade is divided into a number of radial elements, and airfoil properties and momentum balance are used for each element to yield the thrust and induced velocity (see Reference 11). An interesting combination of momentum and blade-element theories for forward flight

has been suggested by Wood and Hermes (Reference 12). They postulate that the instantaneous induced velocity at a point on the disc can be obtained by superposition of transient momentum theory induced velocity distributions corresponding to the number of blade passages over that point in space.

c. In contrast to the above, the early vortex wake theories represented the wake by a series of circular vortices. The geometry, however, was based on an assumed induced velocity field and on an infinite number of blades. The wake vortex theories then attempted to obtain the induced velocities with the aid of the Biot-Savart formula. Recent modifications of the vortex wake theories assume helical vortices trailed from near the blade tips and a "warped-pie" type of mesh-vortex system that is shed from the blade. These vortex wake theories may be looked upon as a modification of Prandtl's theory for a finite fixed wing.

### 1.32 Experimental

Considerable experimentation has resulted in a good deal of test data both for structural loads and aerodynamics of rotary wings. Excellent smoke-trail photographs for a model rotor in a wind tunnel were obtained by Tararine (Reference 13). Very extensive blade-load and blade-motion data were presented by Scheimann (Reference 14) and by Burpo and others (Reference 15). Much of the experimentation has been carried out primarily to gain insight, and rigid model rotors have frequently been used (e.g., Tararine). A recent water-tunnel study of rotary-wing flow visualization was carried out by Lehman (Reference 16). An interesting electromagnetic analog was reported by Gray (Reference 17).

### 1.33 Computational

There appear to be very few numerical solutions of the simultaneous equations of wake motion resulting from blade loading, vortex strength, and vortex-induced velocity as described by the Biot-Savart law. One such calculation was accomplished by Crimi (Reference 18) with an extensive iterative calculation for the time-varying flow and the vortex geometry.

Reference 2 (and its subsequent extension, Reference 19) is an example of the elaborate blade-loads programs that have been developed in recent years. Reference 19 numerically simulates most of the phenomena shown in Figure 1. (A notable exclusion is

the wake-geometry computation.) We will describe some details of the Reference 2 program in Chapter 3 of this report. Another example is the program reported in Reference 20, which compared the blade-load predictions using the rigid wake-induced velocity with similar predictions using a uniform inflow velocity at the disc for a four-bladed, fully articulated rotor.

### 1.34 Some Complicating Factors\* Encountered in the Approaches Cited

#### 1.341 Physical Aspects

As a result of the inherently unsteady aerodynamics of the rotor in forward flight, the "shed" vortices are likely to be significant, and this requires that considerable detail be retained in the wake model (see Figure 15(b)). Also, due to rotation the wake geometry is more complex than for a fixed wing with a similarly varying bound vorticity.

The flexibility of the blades, as mentioned earlier, makes unpre-scribed blade motions inevitable.

"...For example, a typical blade of a flapping, three-bladed, 25 foot radius rotor has a first bending frequency of about 2.5 times the rotational speed for operating tip speeds; by comparison, a rotating string or chain has a corresponding frequency of about 2.4 times its rotational speed. Certainly, for airloads with frequencies of third harmonic and over, the blade is quite flexible and will respond elastically. This interaction between dynamic structural deformations and airloads is the second serious physical complication in the blade airloads problem." (Reference 21)

#### 1.342 Theoretical Difficulties

Even if the equations were not coupled as regards blade motion and

---

\*Material for this section has been drawn from Reference 21.

aerodynamics, the problem is difficult to solve because of the interdependence of the wake geometry and the induced velocity. To avoid this complication, drastic assumptions have been made regarding vortex geometry. Momentum theories, which bypass wake effects completely, have been subject to other limitations. The Kinner-Mangler theory, for example, which is one of the more sophisticated actuator disc theories, ignores the nonuniformity of lift with azimuthal position.

Another disturbing factor is the questionable validity of small perturbation assumptions in linearizing the basic flow equations. For such assumptions to be valid, the downward velocity induced by the lifting surface, which from the momentum point of view is the basic source of lift, must be very small compared with forward speed. This is the case for a fixed wing and makes possible the assumption that the trailed vorticity lies on a rigid cylindrical surface through the trailing edge with generators parallel to the direction of flow. It is much less obvious that this assumption will give good results when using an "actuator disc" to represent a lifting rotor at any forward speed. Although the downward flow component near the blade tip may be small compared to the total forward velocity of the tip, there are likely to be points on the rotor where this is not the case. In any event, the "actuator disc" cannot recognize blade rotation, but only free-stream velocities, so that "perturbations" may not be small, and linearized flow equations could lead to large errors.

#### 1.3.4 Experimental and Computational Difficulties

An experimental study of blade airloads has to be very elaborate, in that (1) it is difficult to design a blade which is both aerodynamically and dynamically similar to the full scale item; (2) extensive measurements have to be made to define streamlines, tip position, oscillatory blade pressures, drag, and power; (3) elimination of tunnel wall effect is especially difficult where the load distribution over the rotor disc and unsteady effects are important.

A wake-geometry computation such as that done in Reference 18, although feasible, is lengthy even on a high-speed computer because of the time integral equations (involving unprescribed velocities) to be solved.

#### 1.4 Motivation for the Present Work

The smoke-trail photographs taken by Tararine (Reference 13) for a rigid model rotor in a wind tunnel showed significant departures

from the traditionally assumed helical tip trail, especially over the rear of the disc. Numerical results of blade-loads computations (at the Cornell Aeronautical Laboratory\*) reported by Piziali in Reference 2 suggested that a more accurate description of the wake geometry might lead to a better correlation between the computed and measured blade loads. A further modification of the Reference 2 work was performed by Chang at CAL (Reference 19), who incorporated (1) the adjustments in the pitch control settings and shaft tilt for the given flight condition (thus "representing" the pilot in the steady-state computational algorithm) and (2) torsional degrees of flexibility of the blades into the computer program. Both Reference 2 and Reference 19 used a rigid helical representation for the wake, however. The results of Reference 19

"...are not significantly closer to the measured results than those obtained in Reference 1.\*\* Therefore, it appears that, at least for these configurations, further improvement in the correlations will probably require the establishment of a better wake model and an even more complete representation of the blade motions...." (Reference 19)

Further evidence of the possible importance of wake geometry is reported in Reference 20. This comparison of the results of two blade-load computations, one using a uniform inflow and the other using a variable inflow resulting from a CAL type rigid wake, showed marked differences in the two blade-load predictions.

It was concluded that a blade-load computation using a more realistic wake-geometry input for calculating induced velocities would be worthwhile. Since an accurate wake-geometry computation (such as Reference 18) from a time-varying velocity field resulting from wake interaction, fuselage effects, and blade bound circulation would be quite extensive, a modified actuator theory approach was adopted. The approximate method reported here uses a Kinner-Mangler type actuator disc with an improved lift distribution to get an approximation to the time-averaged induced velocity field. The lift distribution is chosen so as to realistically represent the radial variation typical of helicopter rotors and to accommodate up to the

---

\*Cornell Aeronautical Laboratory, Inc., Buffalo, New York, hereafter abbreviated as CAL.

\*\*Meaning Piziali's work, Reference 2, according to our list of References.

second harmonic components of the azimuthal variation. The method then predicts the spatial positioning of individual vortices released from a finite number of blades, without any a priori assumptions regarding the wake geometry.

## CHAPTER 2

### THEORETICAL MATERIAL

#### 2.1 Theoretical Background

Kinner (Reference 9) noticed that Laplace's equation, which is the governing equation for the pressure field in case of linearized, steady, incompressible fluid flow, is separable in the ellipsoidal coordinates and that it is possible to choose the coordinate system and the harmonics in such a manner that the solution is discontinuous across a finite, flat, circular disc. Thus, he related the pressure field to the total lift developed by a circular wing. He also gave approximate values of the induced downwash on the disc. His analysis did not allow any disc-incidence angle, however, nor did he calculate the sideways induced velocities. In addition, the discontinuities Kinner dealt with yield a variation over the disc for certain combinations of these solutions that appears quite similar to the lift distribution on a typical rotor.

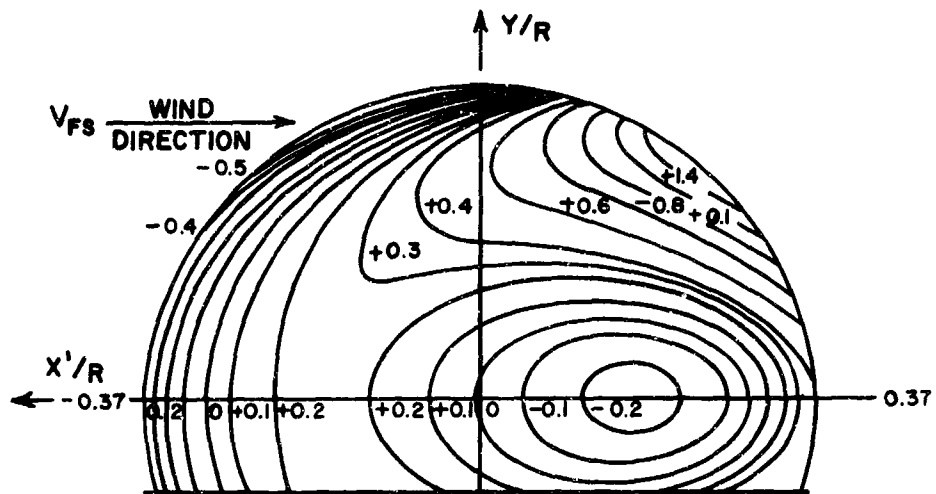
Mangler (Reference 10) modified Kinner's work to include the disc-incidence angle, but he restricted his solutions to azimuthally symmetric lift distributions. For such a restricted flight condition, he obtained numerical values of the induced downwash on the disc. Figures 3 and 4 show the distribution of the induced velocity over the disc for a disc incidence of  $0^\circ$  and  $15^\circ$  respectively. Figure 5 shows the same results as Figure 4, but they are displayed through the variation of the induced velocity along three longitudinal lines on the disc.

#### 2.2 Capsule Statement of the Work Done

In order to evaluate the importance of the details of the wake geometry, it was decided to compare the blade-load predictions from an existing blade-load program, using two different wake-geometry inputs. The program used is that\* reported in Reference 2. The two

---

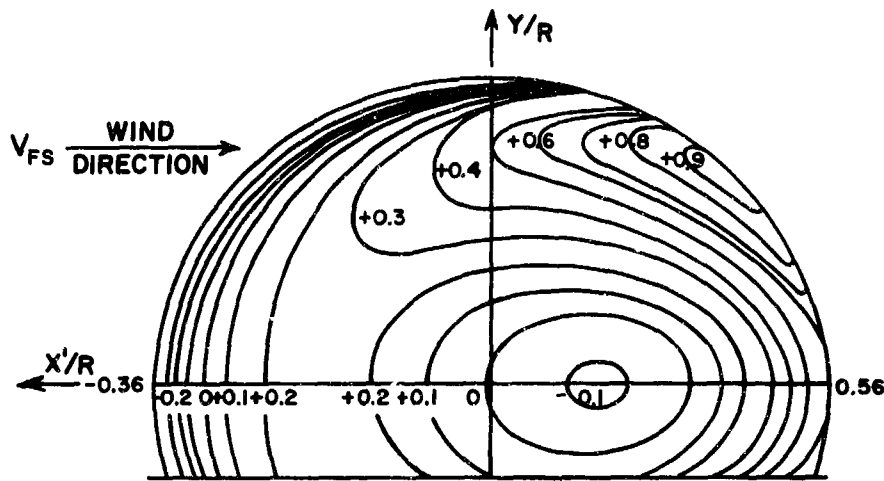
\*Referred to as BLP2 of CAL (Blade-Loads Program 2 of Cornell Aeronautical Laboratory). Some details of this program appear in Sections 3.1 and 3.2.



$$C_t \triangleq \frac{\text{Total Thrust}}{\frac{\rho}{2} \pi V_{FS}^2 R^2}$$

$\bar{w}$   $\triangleq$  induced velocity  
normal to disc

Figure 3. Induced Velocity Over Disc for Azimuthally Symmetric Lift Distribution, Expressed as Contours for  $\frac{\bar{w}}{V_{FS} C_t}$ . For Disc Incidence =  $0^\circ$ . (From Mangler, Reference 10)



$$C_t \triangleq \frac{\text{Total Thrust}}{\frac{\rho}{2} \pi V_{FS}^2 R^2}$$

$\bar{w}$   $\triangleq$  induced velocity normal to disc

Figure 4. Induced Velocity Over Disc For Azimuthally Symmetric Lift Distribution, Expressed as Contours for  $\frac{\bar{w}}{V_{FS} C_t}$ . For Disc Incidence =  $15^\circ$ . (From Mangler, Reference 10)

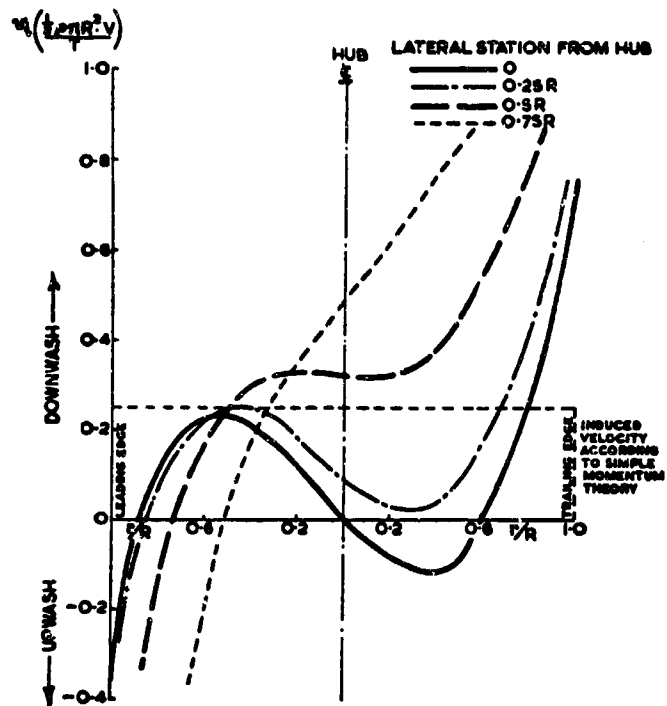


Figure 5. Induced Velocity Distribution According to Mangler and Squire. Disc Incidence =  $15^\circ$ . (From Reference 8)

wake-geometry inputs were (1) a rigid, helical wake geometry resulting from the assumption of a uniform induced velocity. (This is the type of wake geometry used in the CAL computations in Reference 2 and will be termed the CAL wake geometry.) (2) A distorted wake geometry resulting from the steady velocity field of an actuator disc with a lift distribution that includes up to the second azimuthal harmonic variations. (This wake geometry will be termed the UR wake geometry.) The steady velocity field used here includes induced velocities in all directions. Specifically, it does not ignore the sideways velocities. This is considered to be a definite advantage, since even small sideways distortions of the wake may be of importance, especially where the trailed vortex from one blade passes near the succeeding blade(s).

No changes were made in BLP2 other than to modify it to suit the IBM System 360/65 at the Computing Center of the University of Rochester\* and to modify it to interface with the UR wake computing program. The representation of rotor dynamics, blade aerodynamics, and wake-induced velocity relations was retained in its entirety.

Section 2.3 describes the theoretical scheme leading to a determination of the steady induced velocity field (used for calculating the UR wake geometry) for a given flight condition.

## 2.3 Theoretical Scheme

### 2.31 Equations of Fluid Motion

Consider a stationary, flat, circular disc, radius  $R$ , in an infinite expanse of an incompressible fluid. Establish a Cartesian coordinate system  $x y z$  such that the velocity of the fluid at an infinite distance upstream of the disc is  $-V_{\infty} \hat{x}$  at a disc-incidence angle  $\alpha$  (see Figure 6). The equations for incompressible fluid flow are

$$\text{momentum: } \frac{\partial q_i}{\partial t} + q_j q_{i,j} = -\frac{1}{\rho} p_{o,i} \quad \dots i,j = 1,2,3 \quad (24)$$

$$\text{continuity: } q_{i,i} = 0 \quad \dots i,j = 1,2,3 \quad (25)$$

---

\*Hereafter referred to as UR.

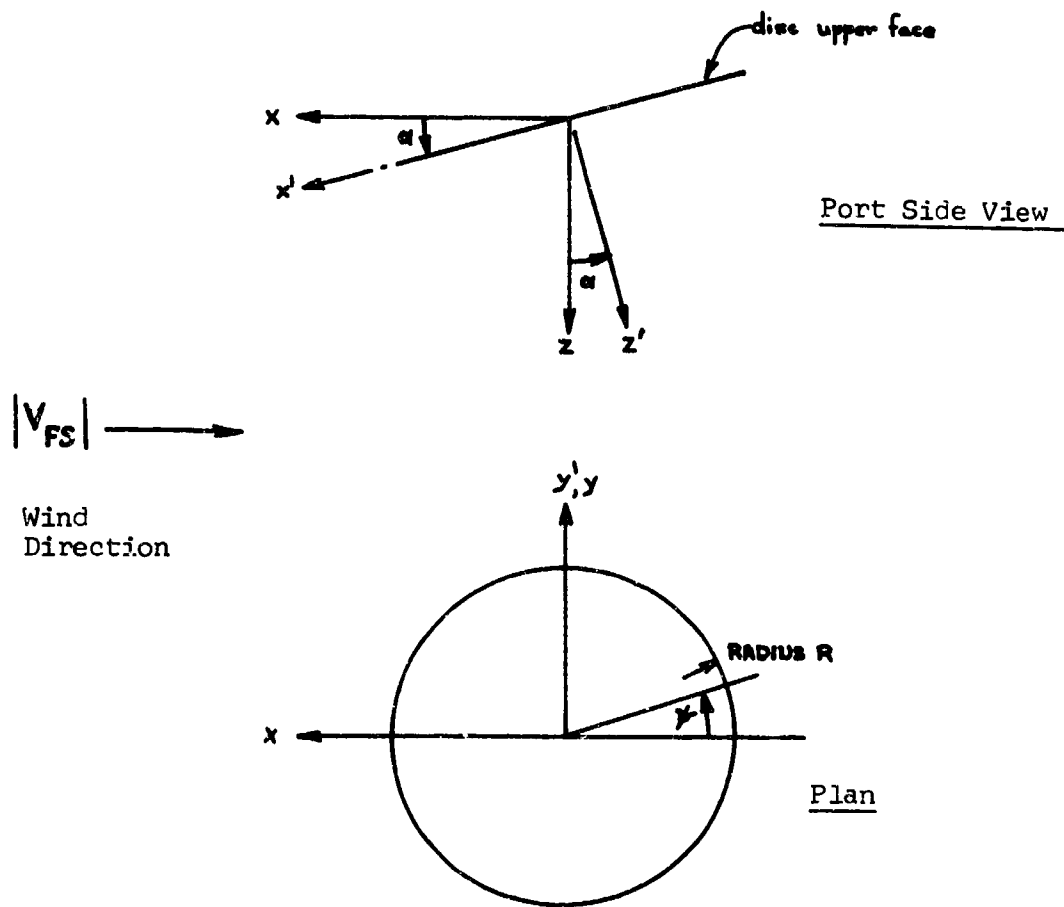


Figure 6. Cartesian Coordinate Systems  $xy'z'$  ("Wind System") and  $x'y'z'$  ("Disc System") in Dimensional Form.

where  $q_i$  are the components of the fluid velocity,  $\rho$  is the constant density of the fluid, and  $p_0$  is the pressure. For steady flow, the momentum equations become

$$q_j q_{i,j} = -\frac{1}{\rho} p_{0,i} \quad \dots i,j = 1,2,3 \quad (26)$$

Noting that the components of  $\vec{q}$  are  $(-V_{FS} + u, v, w)$ , where  $\vec{q}(u, v, w)$  is the velocity perturbation, and assuming a lightly loaded rotor, i.e., assuming

$$(u, v, w) \ll V_{FS} \quad (27)$$

allows linearizing equation (26) to

$$-V_{FS} \tilde{q}_{i,x} = -\frac{1}{\rho} p_{0,i} \quad \dots i=1,2,3 \quad (28)$$

Differentiating (28) with respect to

$$V_{FS} (\tilde{q}_{i,i})_{,x} = \frac{1}{\rho} p_{0,ii}$$

But the left-hand side of this equation vanishes as a consequence of the continuity condition (25). Hence,

$$\frac{1}{\rho} p_{0,ii} = 0 \quad (29)$$

i.e.,  $\nabla^2 p_0 = 0$

which is the governing equation for the pressure field in a steady incompressible fluid flow. Hence, the disturbance pressure field  $p$  must satisfy Laplace's equation.

## 2.32 Coordinate Transformations and Solutions of Laplace's Equation

Since we are interested in obtaining a pressure field that satisfies the boundary conditions of discontinuity across the disc, we attempt to transform Laplace's equation in 3-space to a coordinate system suitable for that purpose.

Define a Cartesian coordinate system  $x'y'z'$ , which is obtained by rotating the  $xyz$ -system through the angle  $\alpha$  about the  $y'$ -axis (see Figure 6). For convenience, let us nondimensionalize our Cartesian systems on the disc radius  $R$ , i.e., define new systems  $XY'Z$  and  $X'Y'Z'$ , such that

$$(X, Y', Z) = \frac{1}{R} (x, y', z) \quad (30)$$

and

$$(X', Y', Z') = \frac{1}{R} (x', y', z')$$

The transformations between the wind system  $XY'Z$  and the disc system  $X'Y'Z'$  are:

$$\begin{vmatrix} X \\ Y' \\ Z \end{vmatrix} = \begin{bmatrix} \cos \alpha & 0 & -\sin \alpha \\ 0 & 1 & 0 \\ \sin \alpha & 0 & \cos \alpha \end{bmatrix} \begin{vmatrix} X' \\ Y' \\ Z' \end{vmatrix} \quad (31)$$

$$\begin{vmatrix} X' \\ Y' \\ Z' \end{vmatrix} = \begin{bmatrix} \cos \alpha & 0 & \sin \alpha \\ 0 & 1 & 0 \\ -\sin \alpha & 0 & \cos \alpha \end{bmatrix} \begin{vmatrix} X \\ Y' \\ Z \end{vmatrix} \quad (32)$$

Define a curvilinear coordinate system  $\psi\eta\zeta$ , such that

$$\begin{aligned}
X' &= \sqrt{1-v^2} \sqrt{1+\eta^2} \cos \psi \\
Y' &= \sqrt{1-v^2} \sqrt{1+\eta^2} \sin \psi \\
Z' &= v\eta
\end{aligned}
\tag{33}$$

It may be noted that this  $v\eta\psi$  coordinate system will cover the entire 3-space once, if we restrict  $v$ ,  $\eta$ , and  $\psi$  (see Figure 6) to the ranges

$$\begin{aligned}
-1 &\leq v \leq +1 \\
0 &\leq \eta \leq \infty \\
0 &\leq \psi \leq 2\pi
\end{aligned}
\tag{34}$$

Figure 7 shows the  $v\eta\psi$  coordinate system viewed in the  $X'Z'$  plane (pitch plane of the helicopter). The  $v = \text{constant}$  surfaces are hyperboloids of one sheet and the  $\eta = \text{constant}$  surfaces are ellipsoids, both families of surfaces being azimuthally symmetric about the  $Z'$  axis.  $\psi$  is the azimuthal angle measured from the negative  $X'$  axis, counterclockwise looking along the plus  $Z'$  axis.  $\eta = 0$  represents the two faces of the disc. The coordinate  $v$  changes sign as one crosses the disc.

The inverse of the transformation (33) is

$$\begin{aligned}
v &= -\frac{1}{\sqrt{2}} \operatorname{sgn} Z' \cdot \sqrt{[1-(X'^2+Y'^2+Z'^2)] + \sqrt{[1-(X'^2+Y'^2+Z'^2)]^2 + 4Z'^2}} \\
\eta &= -\frac{Z'}{v} \\
\psi &= \tan^{-1}\left(\frac{Y'}{-X'}\right)
\end{aligned}
\tag{35}$$

The matrix of first partials of the Cartesian coordinates  $X', Y', Z'$  (represented by  $\xi^k$ ) with respect to the curvilinear coordinates  $v, \eta, \text{ or } \psi$  (represented by  $\zeta^k$ ) is

$$\left[ \frac{\partial \xi^i}{\partial \zeta^k} \right] = \begin{bmatrix} \mu \cos \psi \sqrt{\frac{1+\eta^2}{1-v^2}} & -\eta \cos \psi \sqrt{\frac{1-v^2}{1+\eta^2}} & \sin \psi \sqrt{(1-v^2)(1+\eta^2)} \\ -\mu \sin \psi \sqrt{\frac{1+\eta^2}{1-v^2}} & \eta \sin \psi \sqrt{\frac{1-v^2}{1+\eta^2}} & \cos \psi \sqrt{(1-v^2)(1+\eta^2)} \\ -\eta & -v & 0 \end{bmatrix}
\tag{36}$$

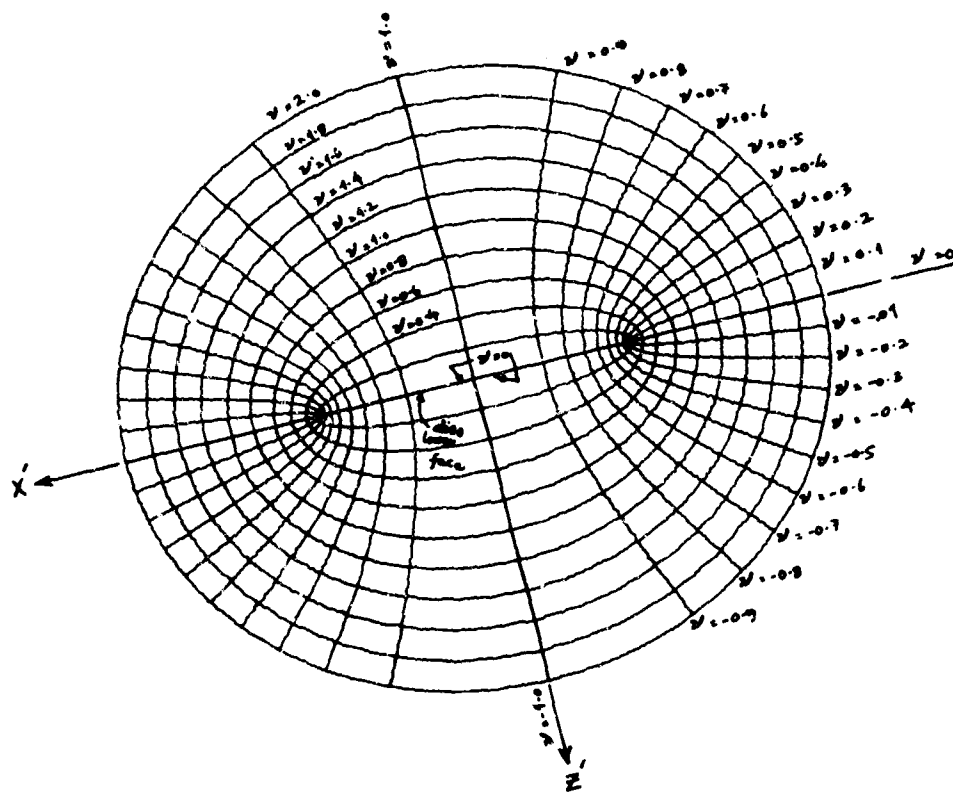


Figure 7. Ellipsoidal Coordinate System, Viewed in the  $x'z'$  Plane.

The metric tensor  $g_{ij}$  for the  $\nu\eta\psi$  system is

$$g_{ij} \triangleq \frac{\partial \xi^m}{\partial \zeta^i} \frac{\partial \xi^m}{\partial \zeta^j} = \begin{bmatrix} \frac{\nu^2 + \eta^2}{1 - \mu^2} & 0 & 0 \\ 0 & \frac{\nu^2 + \eta^2}{1 + \eta^2} & 0 \\ 0 & 0 & (1 - \nu^2)(1 + \eta^2) \end{bmatrix} \quad (37)$$

which shows that the  $\mu\eta\psi$  coordinates form an orthogonal system. This makes writing out Laplace's equation especially easy, since in orthogonal coordinates (see Reference 22),

$$\nabla^2 \phi = \frac{1}{e_1 e_2 e_3} \left[ \frac{\partial}{\partial \zeta^1} \left( \frac{e_2 e_3}{e_1} \frac{\partial \phi}{\partial \zeta^1} \right) + \frac{\partial}{\partial \zeta^2} \left( \frac{e_1 e_3}{e_2} \frac{\partial \phi}{\partial \zeta^2} \right) + \frac{\partial}{\partial \zeta^3} \left( \frac{e_1 e_2}{e_3} \frac{\partial \phi}{\partial \zeta^3} \right) \right]$$

where  $e_k \triangleq \sqrt{g_{kk}}$  (no summation).

For our ellipsoidal coordinate system, then, Laplace's equation  $\nabla^2 \phi = 0$  takes the form

$$\frac{\partial}{\partial \mu} \left[ (1 - \nu^2) \frac{\partial \phi}{\partial \nu} \right] + \frac{\partial}{\partial \eta} \left[ (1 + \eta^2) \frac{\partial \phi}{\partial \eta} \right] + \frac{\partial}{\partial \psi} \left[ \frac{\nu^2 + \eta^2}{(1 - \nu^2)(1 + \eta^2)} \frac{\partial \phi}{\partial \psi} \right] = 0 \quad (38)$$

Letting

$$\phi(\nu, \eta, \psi) = \Phi_1(\nu) \cdot \Phi_2(\eta) \cdot \Phi_3(\psi) \quad (39)$$

it is found that (38) separates into the three equations

$$\frac{d^2 \Phi_3}{d\psi^2} + m^2 \Phi_3 = 0 \quad (40)$$

$$\frac{d}{d\mu} \left[ (1 - \nu^2) \frac{d\Phi_1}{d\nu} \right] + \left[ \frac{-m^2}{1 - \nu^2} + n(n+1) \right] \Phi_1 = 0 \quad (41)$$

$$\frac{d}{d\eta} \left[ (1+\eta^2) \frac{d\bar{\Phi}_2}{d\eta} \right] + \left[ \frac{m^2}{1+\eta^2} - n(n+1) \right] \bar{\Phi}_2 = 0 \quad (42)$$

where  $m$  and  $n$  are the constants of separation. The single-valued solutions of (40) are

$$\bar{\Phi}_3(\psi) = \left[ \cos m\psi, \sin m\psi \right] \dots m = \text{integer} \quad (43)$$

Equations (41) and (42) are recognized as forms of Legendre's associated differential equation (see Reference 23), and their solutions are

$$\bar{\Phi}_1(\nu) = \left[ P_n^m(\nu), Q_n^m(\nu) \right] \quad (44)$$

$$\bar{\Phi}_2(\eta) = \left[ P_n^m(i\eta), Q_n^m(i\eta) \right] \quad (45)$$

Thus, we find that the most general single-valued solution of Laplace's equation in our ellipsoidal coordinate system is

$$\phi = \left\{ \begin{matrix} P_n^m(\nu) \\ Q_n^m(\nu) \end{matrix} \right\} \left\{ \begin{matrix} P_n^m(i\eta) \\ Q_n^m(i\eta) \end{matrix} \right\} \left\{ \begin{matrix} \cos m\psi \\ \sin m\psi \end{matrix} \right\} \quad (46)$$

where  $m$  is an integer.

### 2.33 Choice of the Pressure Field, Based on Total Thrust and Net Moments

We shall deal with the disturbance pressure in its nondimensionalized form  $P$ , normalized on twice the free-stream dynamic pressure, i.e.,

$$P \triangleq \frac{p}{\rho V_{\infty}^2} \quad (47)$$

The general solution of Laplace's equation is given by equation (46). Appendix I, which was prepared using Reference 24, shows some of the associated functions of Legendre,  $P_n^m$  and  $Q_n^m$ , and their properties. Before concluding that equation (46) is the general solution for the pressure field, we must examine it for any contradictions with the physical restrictions on the disturbance pressure  $P$ .

Thus, we notice from Appendix I that the  $Q_n^m(\mu)$  would be infinite at  $\mu = \pm 1$ , since they contain terms with denominators that vanish at  $\mu = \pm 1$ . This leads to an infinite disturbance pressure on the  $Z'$  axis. Hence, we must discard the  $Q_n^m(\mu)$  type of component from equation (44), thus reducing it to

$$\Phi_1(\nu) = P_n^m(\nu) \quad (48)$$

This form of  $\Phi_1$  eliminates disturbances of infinite magnitude along the rotor shaft axis.

Similarly, it is noted from Appendix I that  $P_n^m(i\eta) \rightarrow \infty$  as  $\eta \rightarrow \infty$ . Since this would mean an infinite disturbance at infinity, this condition must also be ruled out on physical grounds. This reduces equation (45) to

$$\Phi_2(\eta) = Q_n^m(i\eta) \quad (49)$$

Appendix I shows that (49) tends to zero as  $\eta$  tends to  $\infty$ .

Equations (39), (43), (48), and (49) are combined to obtain the general form of the disturbance pressure:

$$P = \sum_{\substack{m,n \\ m \leq n}}^{\infty} P_n^m(\nu) \cdot Q_n^m(i\eta) \cdot [C_n^m \cos m\psi + D_n^m \sin m\psi] \quad (50)$$

where  $C_n^m$  and  $D_n^m$  are arbitrary constants. From among the infinity of terms in this general form, we will retain only those terms that are necessary to simulate a reasonable lifting rotor or disc.

Since over the disc area the lift density should correspond to the difference in the pressures  $p$  just below ( $\eta=0, \nu<0$ ) and above ( $\eta=0, \nu>0$ ) the disc, we drop all combinations of  $m, n$  in (50) that result in an even  $(m+n)$ . This is because  $P_n^m(\nu)$  is an even function if  $(m+n)$  is even.

Let us set the practical requirements that (1) an integration of the lift density over the disc area should correspond to the total (steady) thrust developed by the rotor, (2) the lift density should vanish at the center and at the periphery of the disc, (3) the expression for the pressure distribution should be able to represent net pitching and rolling moments supplied by the lifting disc to the craft, (4) the pressure distribution should reasonably represent the first harmonic components of lift density as experienced by lightly loaded rotor blades, and (5) there should be some provision for simulating the second harmonic components of the blade bending moments.

#### Total Thrust

Using equation (50), the total thrust  $T$  is

$$\begin{aligned}
 T &= \int_A p \, dA - \int_A p \, dA \\
 &\quad \text{(lowerface)} \quad \text{(upperface)} \\
 &= \sum_{m,n} \rho V_{fs}^2 \left[ \int_0^{2\pi} (C_n^m \cos m\psi + \Gamma_n^m \sin m\psi) \alpha \psi \right] \cdot \left[ \int_0^R P_n^m(\nu) Q_n^m(i_0) r \, dr \right] \\
 &\quad \text{(lowerface - upperface)} \\
 &= \rho V_{fs}^2 \sum_n 2\pi C_n^0 Q_n^0(i_0) \int_0^R P_n^0(\nu) r \, dr \\
 &\quad \text{(lower-upper)}
 \end{aligned}$$

From equations (33), we find  $r^2 = R^2(1-\nu^2)$  for a point on the disc. Hence, while integrating on the disc,

$$r \, dr \Big|_0^R \Rightarrow \left[ -R^2 \nu \, d\nu \Big|_1^0 \right] - \left[ -R^2 \nu \, d\nu \Big|_0^1 \right]$$

(lower-upper)

$$\therefore T = -\rho V_{Fs}^2 \cdot 2\pi R^2 \cdot \sum_n C_n^0 Q_n^0(i_0) \int_{-1}^{+1} P_n^0(\nu) \nu d\nu$$

Noting that  $\nu \equiv P_1^0(\nu)$  and using the orthogonality relations in Appendix I, only the  $(n=1)$  term will have a nonvanishing integral, and we get

$$T = \frac{4}{3} \cdot \pi R^2 \cdot \rho V_{Fs}^2 \cdot C_1^0 \quad (51)$$

Defining a coefficient of thrust  $C_T$ ,

$$C_T \triangleq \frac{T}{\pi \rho R^4 \Omega^2} \quad (52)$$

we get

$$C_1^0 = \frac{3}{4} \frac{C_T}{\mu^2} \quad (53)$$

$\Omega$  is the rotor speed in radians per second, and  $\mu$  is called the tip-speed ratio

$$\mu \triangleq \frac{V_{Fs}}{\Omega R} \quad (54)$$

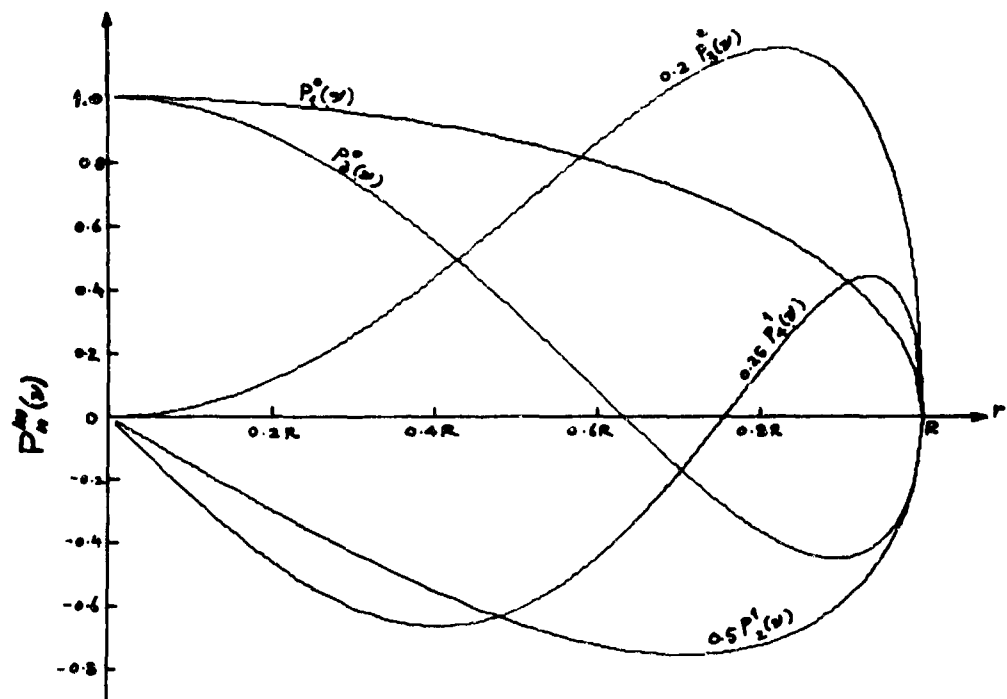
Thus, the combination  $(m=0, n=1)$  is necessary for getting a steady thrust from the pressure field.

From Figure 8, it is seen that  $P_1^0(\nu)$  does not vanish at the center of the disc, i.e., at  $\nu = \pm 1$ . In order to have a nonvanishing thrust, and still to satisfy condition (2) above, we must include the combination  $(m=0, n=1)$  along with any other combination(s) having  $(m=0)$ . Their coefficients will have to be so related that the composite lift density vanishes both at  $r=0$  and at  $r=R$ . Let us try a combination of  $(m=0, n=1)$  and  $(m=0, n=3)$ . Since  $\nu=0$  at the periphery and  $\nu = \pm 1$  at the center, we require that

$$C_1^0 \cdot P_1^0(\pm 1) \cdot Q_1^0(i_0) + C_3^0 \cdot P_3^0(\pm 1) \cdot Q_3^0(i_0) = 0$$

$$\text{and } C_1^0 \cdot P_1^0(0) \cdot Q_1^0(i_0) + C_3^0 \cdot P_3^0(0) \cdot Q_3^0(i_0) = 0$$

$$\therefore C_3^0 = \frac{3}{2} C_1^0 = \frac{9}{8} \frac{C_T}{\mu^2} \quad (55)$$



on the disc,  $\mu = \sqrt{1 - (r/R)^2}$

Figure 8.  $P_n^m(r)$  Plotted as a Function of Radius  $r$  on the Disc.

Thus, the combinations  $(m=0, n=1)$  and  $(m=0, n=3)$  can together satisfy conditions (1) and (2) on page 32 if

$$C_3^0 = \frac{3}{2} C_1^0.$$

### Rolling and Pitching Moments

Using equation (50), the rolling moment about the  $X'$  axis is

$$M_r = \rho V_{FS}^2 \sum_{m,n} Q_n^m(i\omega) \int_{r=0}^R \int_{\psi=0}^{2\pi} P_n^m(v) (C_n^m \cos m\psi + D_n^m \sin m\psi) \cdot (-r \sin \psi) \cdot r dr d\psi$$

(Lower-Upper)

Using orthogonality of the circular function over  $0 - 2\pi$

$$M_r = \rho V_{FS}^2 \sum_n Q_n^1(i\omega) \cdot D_n^1 \int_{r=0}^R P_n^1(v) \cdot (-r^2) \cdot dr \cdot \int_0^{2\pi} \sin^2 \psi d\psi$$

(Lower-Upper)

while integrating on the disc, we have

$$r^2 dr \Big|_0^R \Rightarrow \left[ -R^3 \sqrt{1-v^2} dv \Big|_{-1}^0 \right] - \left[ -R^3 \sqrt{1-v^2} dv \Big|_{+1}^0 \right]$$

$$\therefore M_r = \sum_n \rho \pi R^3 V_{FS}^2 Q_n^1(i\omega) D_n^1 \int_{-1}^{+1} P_n^1(v) \cdot \sqrt{1-v^2} dv$$

Noting that  $P_2^1(v) \equiv -3v\sqrt{1-v^2}$ , and using the orthogonality relations in Appendix I only the  $(n=2)$  term will survive integration, and we get

$$M_r = \frac{8}{3} i \cdot \pi R^3 \cdot \rho V_{FS}^2 \cdot D_2^1 \quad \text{⊕ } X' \text{ axis} \quad (56)$$

Defining a coefficient of rolling moment

$$C_{Mr} \triangleq \frac{M_r}{T \cdot R} \quad (57)$$

we get

$$D_2^1 = -\frac{5}{8}i \frac{C_{MP} \cdot C_T}{\mu^2} \quad (58)$$

A similar calculation for the pitching moment  $M_p$  leads to

$$M_p = \frac{8}{5}i \cdot \pi R^3 \cdot \rho V_{FS}^2 \cdot C_2^1 \quad \text{⊕ Y axis} \quad (59)$$

$$C_2^1 = -\frac{5}{8}i \frac{C_{MP} \cdot C_T}{\mu^2} \quad (60)$$

$$C_{MP} \triangleq \frac{M_p}{T \cdot R} \quad (61)$$

Thus, the combination ( $m=1, n=2$ ) will satisfy condition (3) on page 32.

Figure 9 shows typical plots of the steady and first two harmonic components of experimentally measured blade loads. Since the radial variation of  $P_2^1(\nu)$  in Figure 8 is quite similar to the variation of the first harmonic components in Figure 9, it was decided to retain the combination ( $m=1, n=4$ ) in equation (50). Also retained was the combination ( $m=2, n=3$ ).

Table II shows the combinations of  $m$  and  $n$  to which the steady disturbance pressure field  $P$  was restricted.

$$P = \sum_{m,n} P_n^m(\nu) \cdot Q_n^m(i\eta) \cdot [C_n^m \cos m\psi + D_n^m \sin m\psi] \quad (62)$$

#### 2.34 Choice of the Pressure Field, Based on Blade Flapping Moments

In Section 2.33 the coefficients  $C_1^0, C_2^0, C_2^1$ , and  $D_2^1$  were calculated from  $C_T, C_{MP}$ , and  $C_{MP}$ . The latter represent the "total", or integrated, effect of the disc as felt by the craft, in the form of the thrust, rolling moment, and pitching moment respectively. While this sort of a determination of the pressure field may seem

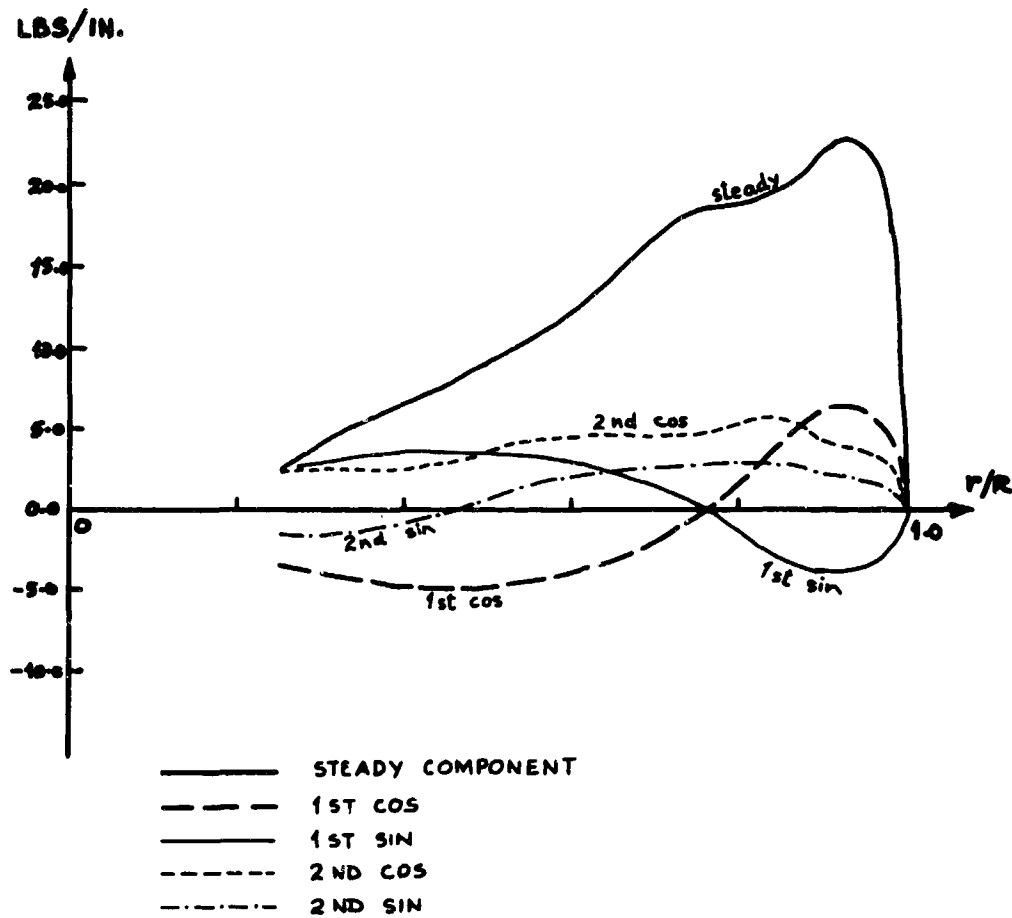


Figure 9. Typical Steady and First Two Harmonic Components of Experimental Blade Loads. (From Scheimann, Reference 14. H-34, Flight 20,  $V = 122$  Knots.)

TABLE II. THE TERMS RETAINED IN THE EXPRESSION  
(62) FOR THE DISTURBANCE PRESSURE  $P$

m	n	Remarks
0	1	This is the only term that gives rise to a non-zero total lift (but does not have zero lift density at the center of the disc).
0	3	Together with the above term, will give zero lift density at the center of the disc if $C_3^0 = \frac{3}{2} C_1^0$ .
1	2	This is the only term that will give rise to net pitching and rolling moments.
1	4	Although the net moments over the disc are zero for this term, the radial distribution of pressure due to this term is quite similar to experimentally observed pressure distributions.
2	3	To account for second harmonic variations in lift density and blade-flapping moments.

quite obvious, it certainly is not the only way to relate the pressure field to physical quantities. For a real helicopter with a finite number of blades, barring the case for which experimental measurements of blade differential pressures are available (as in case of Reference 14 and 15), it may be quite difficult to accurately determine the steady components of total thrust, rolling, and pitching moments, because of uncertainties in fuselage drag, vehicle trim, etc. It would probably be advisable, then, to be able to base the determination of the steady pressure field on some more easily (and confidently) estimable quantity. The flapwise moment on the blade could be one such quantity. Even for an experimental case, it is probably as easy, if not easier, to get measurements of the blade-flapping moments as it is to measure the differential pressures. In any event, since lift variations higher than the first harmonic do not result in any "integrated" effect at all, it is clear that expressing the  $C_n^m, D_n^m$  in terms of the instantaneous flapping moments on the blade would be helpful in simulating higher harmonic variations in lift in any actuator disc approach. This section deals with this approach.

There are two possible ways in which the coefficients  $C_n^m$  and  $D_n^m$  can be expressed in terms of the flapping moments  $M(\psi)$  experienced by the blades at their roots as they rotate:

(1) Assuming that the value  $[\rho(r, \psi) - \rho(r, \psi)]$  of the theoretical steady lift density at a point  $(r, \psi)$  on the disc is the time average of the lift supplied to the rotor when there is and is not a blade at that point, or

(2) Assuming that the  $M(\psi)$  is simply the flapping moment on a blade, when it is at the azimuthal position  $\psi$ , and subjected to the steady lift density  $[\rho(r, \psi) - \rho(r, \psi)]$  at  $(r, \psi)$ .

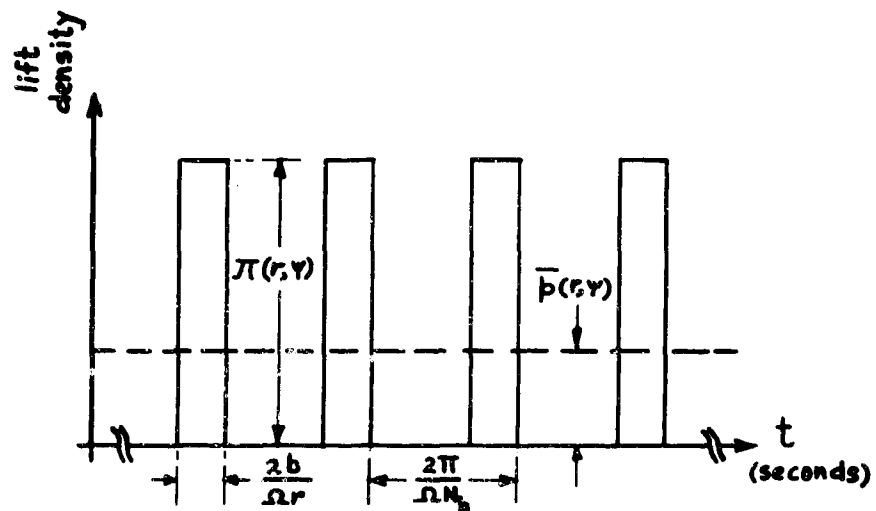
It may be noted that with assumption (1), the total momentum transferred from the fluid to the disc will equal the total momentum transferred from the fluid to the  $N_b$  blades. Assumption (2) does not satisfy this condition.

Making assumption (1), let us further assume that the time history of the blade lift density at a point  $(r, \psi)$  of the disc is a series of pulses as shown in Figure 10.  $\pi(r, \psi)$  represents the pressure difference experienced by each of the blades at  $r$  when at  $\psi$ .  $\bar{\rho}(r, \psi)$  represents the assumed steady lift density at  $(r, \psi)$ .

$$\bar{\rho}(r, \psi) = \rho(r, \psi) - \rho(r, \psi) = 2\rho(r, \psi)$$

lower
upper
lower

$N_b$  = number of blades  
 $\Omega$  = rotor speed, radians/sec  
 $b$  = blade semichord



————— assumed pulsating lift density for a finite number of blades  
 - - - - - assumed steady lift density for an actuator disc

Figure 10. Time Histories of the Lift Density at a Point  $(r, \psi)$  of the Disc.

Assumption (1) requires that the areas under the two time-history curves be equal.

$$\therefore \pi(r, \psi) = \frac{2\pi}{bN_b} \cdot r p(r, \psi)_{\text{lower}}$$

and

$$M(\psi) = \int_0^R r \cdot \pi(r, \psi) \cdot 2b \cdot dr$$

$$= \frac{4\pi}{N_b} \int_0^R r^2 p(r, \psi)_{\text{lower}} dr \quad (63)$$

Since on the disc  $r^2 = R^2(1-v^2)$ , we have  $r^2 dr \Big|_{\text{lower face}} \Rightarrow -R^3 v \sqrt{1-v^2} dv \Big|_{-1}^0$

$$\therefore M(\psi) = \frac{4\pi R^3}{N_b} \cdot \rho V_{FS}^2 \cdot \int_0^{-1} v \sqrt{1-v^2} P(r, \psi) dv. \quad (64)$$

Using expression (62) for  $P$ , we get

$$M(\psi) = -\frac{4\pi R^3}{N_b} \cdot \rho V_{FS}^2 \cdot \sum_{m,n} \left\{ [C_n^m \cos m\psi + D_n^m \sin m\psi] \cdot Q_n^m(i_0) \cdot \int_0^{-1} P_n^m(v) v \sqrt{1-v^2} dv \right\}$$

Evaluating the integrals for the five combinations of  $(m, n)$  shown in Table II, this reduces to

$$M(\psi) = -\frac{4\pi R^3}{N_b} \cdot \rho V_{FS}^2 \cdot \left\{ -\frac{\pi}{16} C_2^0 - \frac{\pi}{96} C_3^0 + \frac{4}{5} i (C_2^1 \cos \psi + D_2^1 \sin \psi) + \frac{15\pi}{4} (C_3^2 \cos 2\psi + D_3^2 \sin 2\psi) \right\}$$

Or, remembering that  $C_3^0 = \frac{3}{2} C_2^0$ , we have

$$C_2^0 = \frac{16 N_b}{5 \pi^2 \cdot \rho V_{FS}^2 \cdot R^3} M_0 \quad (65)$$

$$C_3^0 = \frac{24 N_b}{5\pi^2 \rho V_{FS}^2 \cdot R^3} \cdot M_0 \quad (66)$$

$$C_2^1 = \frac{5i N_b}{16\pi^2 \rho V_{FS}^2 \cdot R^3} \cdot M_{C1} \quad (67)$$

$$D_2^1 = \frac{5i N_b}{16\pi \rho V_{FS}^2 \cdot R^3} \cdot M_{S1} \quad (68)$$

$$C_3^2 = - \frac{N_b}{15\pi^2 \rho V_{FS}^2 \cdot R^3} \cdot M_{C2} \quad (69)$$

$$D_3^2 = - \frac{N_b}{15R^3\pi^2 \rho V_{FS}^2} \cdot M_{S2} \quad (70)$$

where  $M_0, M_{C1}, M_{S1}, M_{C2}$ , and  $M_{S2}$  are the harmonic components of  $M(\psi)$ :

$$M(\psi) = M_0 + M_{C1} \cos \psi + M_{S1} \sin \psi + M_{C2} \cos 2\psi + M_{S2} \sin 2\psi \quad (71)$$

Equations (65) through (70) relate the steady pressure field to the flapping moments resulting from the airloads on the blades, and were so used in the UR wake computations reported herein. These relations were obtained under the assumption (1) of equal average momentum transfer on page 39 .

If we choose the simpler assumption (2) on page 39 , thus ignoring the average momentum transfer requirement, we get

$$M(\psi) = \int_0^R 2p(r, \psi) \cdot r \cdot 2b \cdot dr \quad (72)$$

Since on the disc  $r^2 = R^2(1 - v^2)$  , we have  $rdr \xrightarrow{\text{lower}} -R^2 v dv \Big|_{-1}^0$

$$\therefore M(\psi) = 4bR^2 \cdot \rho V_{FS}^2 \cdot \int_0^{-1} v P(r, \psi) dv$$

Using (62) for  $\rho$ , we get

$$M(\psi) = -4bR^2 \rho V_{FS}^2 \sum_{m,n} \left\{ (C_n^m \cos m\psi + D_n^m \sin m\psi) \cdot Q_n^m(i_0) \cdot \int_0^{+1} v p_n^m(v) dv \right\}$$

Evaluating the five integrals,

$$M(\psi) = 4bR^2 \rho V_{FS}^2 \left\{ \frac{1}{3} C_1^0 + \left( \frac{5}{24} i\pi C_4^1 - \frac{3}{8} i\pi C_2^1 \right) \cos \psi \right. \\ \left. + \left( \frac{5}{24} i\pi D_4^1 - \frac{3}{8} i\pi D_2^1 \right) \sin \psi - 16C_3^2 \cos 2\psi - 16D_3^2 \sin 2\psi \right\}$$

Noting that both  $C_2^1$  and  $C_4^1$  contribute to the first harmonic cosine flapping moment, we need an additional "constraint" to determine them. Let us choose the total pitching moment  $M_p$  from equation (59) for the purpose. Similarly, equation (56) will be used to determine  $D_2^1$  and  $D_4^1$ . The results are:

$$C_1^0 = \frac{3}{4b \cdot \rho V_{FS}^2 \cdot R^2} M_0 \quad (73)$$

$$C_3^0 = \frac{9}{8b \cdot \rho V_{FS}^2 \cdot R^2} M_0 \quad (74)$$

$$C_2^1 = - \frac{5i}{8\pi \cdot \rho V_{FS}^2 \cdot R^3} M_p \quad (75)$$

$$D_2^1 = - \frac{5i}{8\pi \cdot \rho V_{FS}^2 \cdot R^3} M_p \quad (76)$$

$$C_4^1 = \frac{9}{5} C_2^1 - \frac{6i}{25\pi \cdot b \cdot \rho V_{FS}^2 \cdot R^2} M_{C1} \quad (77)$$

$$D_4^1 = \frac{9}{5} D_2^1 - \frac{6i}{25\pi \cdot b \cdot \rho V_{FS}^2 \cdot R^2} M_{S1} \quad (78)$$

$$C_3^2 = - \frac{1}{64 b \cdot \rho V_{FS}^2 \cdot R^2} M_{C2} \quad (79)$$

$$D_3^2 = - \frac{1}{64 b \cdot \rho V_{FS}^2 \cdot R^2} M_{S2} \quad (80)$$

Equations (73), (74) and (77) through (80) do not satisfy the average momentum transfer condition.

### 2.35 Induced Velocity Field

We shall deal with the induced velocity in its nondimensionalized form  $\vec{\tilde{Q}}(u, v, w)$ , normalized on the free-stream velocity  $V_{FS}$ , i.e.,

$$\vec{\tilde{Q}}(u, v, w) \triangleq \frac{1}{V_{FS}} \vec{\tilde{Q}}(u, v, w) \quad (81)$$

Using (81) and (47), equation (28) becomes

$$\tilde{Q}_{i,x} = P_i \quad \dots i = 1, 2, 3 \quad (82)$$

which is the completely dimensionless form of the linearized momentum equations. Integrating (82) and noting that all disturbances vanish at an infinite distance upstream of the disc, we get the induced velocity field

$$\tilde{Q}_i(x, y, z) = \int_{+\infty}^x P_i(\xi, y, z) d\xi \quad \dots i=1,2,3 \quad (83)$$

The subscript  $i$  represents the Cartesian "wind coordinates"  $x, y$ , and  $z$ . In order to evaluate (83), then, for a field point  $(x, y, z)$ , we must first obtain the partials  $\frac{\partial P}{\partial x}$ ,  $\frac{\partial P}{\partial y}$ , and  $\frac{\partial P}{\partial z}$  of the pressure field  $P$ , and then carry out the integration from  $\xi = +\infty$  to  $\xi = x$ . Using the chain rule for first partials,

$$\frac{\partial P}{\partial x^i} = \frac{\partial \xi^k}{\partial x^i} \cdot \frac{\partial \xi^j}{\partial \xi^k} \cdot \frac{\partial P}{\partial \xi^j} \quad \dots i, j, k = 1, 2, 3 \quad (84)$$

where  $x^m$  represent the "wind coordinates"  $(x, y, z)$

$\xi^m$  represent the "disc coordinates"  $(x', y', z')$

$\zeta^m$  represent the "ellipsoidal coordinates"  $(v, \eta, \psi)$ .

The  $\frac{\partial \xi^k}{\partial x^i}$  are available from equation (32). The  $\frac{\partial \xi^j}{\partial \zeta^k}$  are obtained by inverting the matrix of first partials  $\left[ \frac{\partial \xi^k}{\partial \zeta^j} \right]$  in equation (36):

$$\left[ \frac{\partial \xi^j}{\partial \zeta^k} \right] = \begin{bmatrix} \frac{v \cos \psi [(1-v^2)(1+\eta^2)]^{1/2}}{v^2 + \eta^2} & \frac{v \sin \psi [(1-v^2)(1+\eta^2)]^{1/2}}{v^2 + \eta^2} & \frac{-\eta(1-v^2)}{v^2 + \eta^2} \\ \frac{-\eta \cos \psi [(1-v^2)(1+\eta^2)]^{1/2}}{v^2 + \eta^2} & \frac{\eta \sin \psi [(1-v^2)(1+\eta^2)]^{1/2}}{v^2 + \eta^2} & \frac{-v(1+\eta^2)}{v^2 + \eta^2} \\ \sin \psi [(1-v^2)(1+\eta^2)]^{-1/2} & \cos \psi [(1-v^2)(1+\eta^2)]^{-1/2} & 0 \end{bmatrix} \quad (85)$$

The  $\frac{\partial P}{\partial \zeta^j}$  are obtained by using the expression (62) for  $P$  and the formulas for derivatives of Legendre's associated functions in Appendix I:

$$\frac{\partial P}{\partial v} = \sum_{m,n} Q_n^m(i\eta) \cdot [C_n^m \cos m \psi + D_n^m \sin m \psi] - \left[ (m+n) \frac{P_{n-1}^m(v)}{1-v^2} - n v \frac{P_n^m(v)}{1-v^2} \right] \quad (86)$$

$$\frac{\partial P}{\partial \eta} = \sum_{m,n} P_n^m(\nu) \cdot [C_n^m \cos m\psi + D_n^m \sin m\psi] \cdot \left[ n\eta \frac{Q_{n-1}^m(i\eta)}{1+\eta^2} + i(m+n) \frac{Q_{n-1}^m(i\eta)}{1+\eta^2} \right] \quad (87)$$

$$\frac{\partial P}{\partial \psi} = \sum_{m,n} m P_n^m(\nu) Q_{n-1}^m(i\eta) [D_n^m \cos m\psi - C_n^m \sin m\psi] \quad (88)$$

We now have all the necessary formulas for numerically integrating equations (83). Some simplification, however, is possible in case of the X-component of equation (83):

$$U(x, y, z) = \int_{-\infty}^x \frac{\partial P}{\partial \xi} d\xi \quad (89)$$

So long as the path of integration does not pass through points where  $P$  is discontinuous, evaluation of the integral on the right-hand side yields

$$U(x, y, z) = P(x, y, z) \quad (90)$$

Since the only place where the horizontal path of integration encounters a discontinuity in  $P$  is the disc surface, (90) holds for all points upstream of the disc. For a point  $(x, y, z)$  on a streamline which crosses the disc, we use the physical condition that the fluid velocity at a point on the lower face of the disc is the same as that at its image on the upper face (i.e., the actuator is permeable)\*, and evaluate the integral for  $U$  in two parts:

$$U(x, y, z) = \int_{-\infty}^x \frac{\partial P}{\partial \xi}(\xi, y, z) d\xi \quad \text{upper face} \\ \text{in the wake} \quad \text{lower face}$$

$$\text{hence, } U(x, y, z) = P(x, y, z) + P(\text{intersection point})_{\text{upper face}} - P(\text{intersection point})_{\text{lower face}} \quad (91)$$

\*Or, "no finite changes in velocity can occur in the infinitesimal time it takes a particle to cross the disc."

or, since for our disturbance pressure  $P$  of equation (62),  $P = -P_{\text{upper}} = P_{\text{lower}}$ , we get

$$U_{\text{wake}}(x, y, z) = P(x, y, z) - 2P(\text{intersection point lower face})$$

The term (intersection point) indicates the point at which the horizontal path of integration up to the field point  $(x, y, z)$  crosses the disc.

The induced velocity components  $V$  and  $W$  are evaluated numerically.

The wake geometry resulting from this steady induced velocity field is also calculated numerically, as described in Chapter 3.

## CHAPTER 3

### THE COMPUTER PROGRAM

#### 3.1 General Description

This section briefly describes the blade-loads program, BLP2 of CAL, as modified at UR. This program used to calculate blade loads based on the two different wake geometries.

The BLP2 is in two parts. Part 1 first generates the blade segment coordinates and the wake element coordinates for the given flight condition. Using these coordinates, Part 1 then calculates (using the Biot-Savart field law) the induced velocity coefficients  $S_{mkj}$  and  $T_{mki}$  appearing in equations (105) and (106),  $(m=0, 3; K=1, Nra; j=1, Nra; i=1, Na)$ . These  $S$  and  $T$  coefficients are then written in binary form on TAPE 2. Figure 11 shows the logical flow diagram for Part 1 of the unmodified CAL program.

Part 2 uses the TAPE 2 data set generated in Part 1 as input. In addition, all the dynamic properties of the blades and control inputs to the craft are supplied in Part 2. It then solves the equations of rotor dynamics, blade aerodynamics, and wake-induced effects by iteration. (The essential elements of the representation of these three phenomena in the numerical program are summarized in Sections 3.21, 3.22, and 3.23 respectively.) After achieving convergence, the blade loads and other quantities of interest (as well as their harmonic analyses) are written on TAPE 3. Figure 12 shows the major steps in the iterative procedures for solving the equations. Figure 13 shows the flow diagram for Part 2 of BLP2. It will be noticed from Figure 12 or 13 that the Part 2 procedure involves two iterations, one "inside" the other. The iterative solution of the simultaneous equations (109) in the bound circulations  $\Gamma_K$  takes place "inside" the iterative solution of the blade dynamical equations (96).

Figure 14 schematically shows the BLP2 as modified at UR. By comparison with Figure 1, it may be noted that the control settings, vehicle attitude, and motion have ceased to be unknowns. (This means that BLP2 ignores the "Pilot" and "Vehicle Dynamics" blocks in Figure 1) Similarly, the uniform induced velocity is needed if the CAL rigid wake geometry is used; and some information on the blade loads is needed if the UR wake geometry is to be computed. Since the modification to the CAL procedure is essentially the use of an alternative wake geometry, the necessary changes and/or additions to the CAL program occur in Part 1 of BLP2, as can be

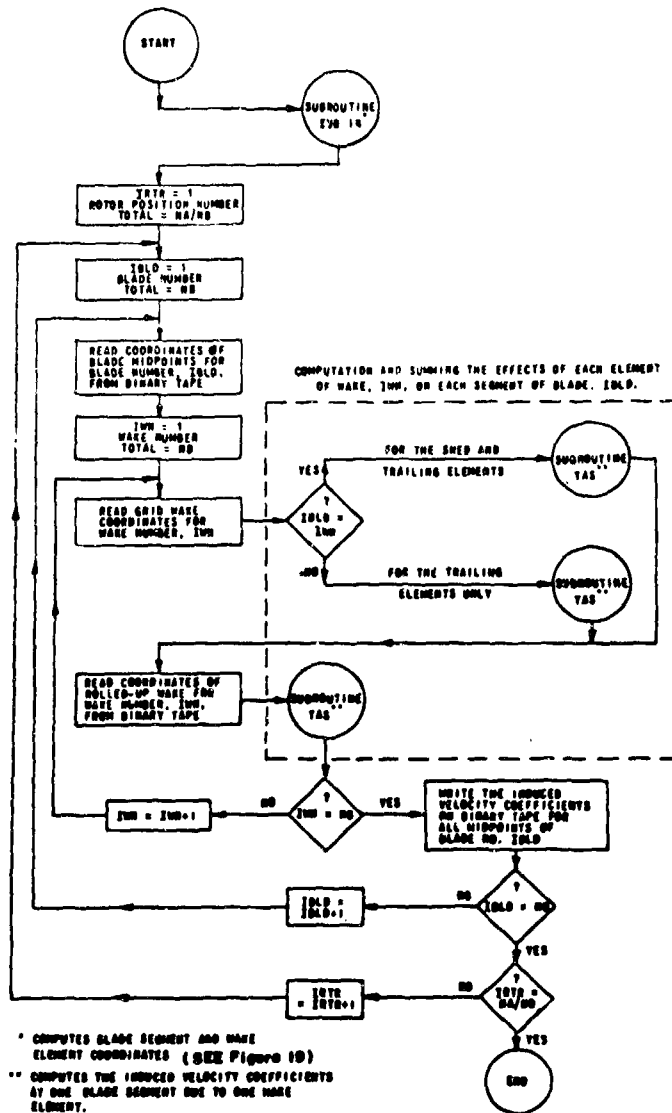


Figure 11. Flow diagram for Part 1 of BLP2. (From Reference 2)

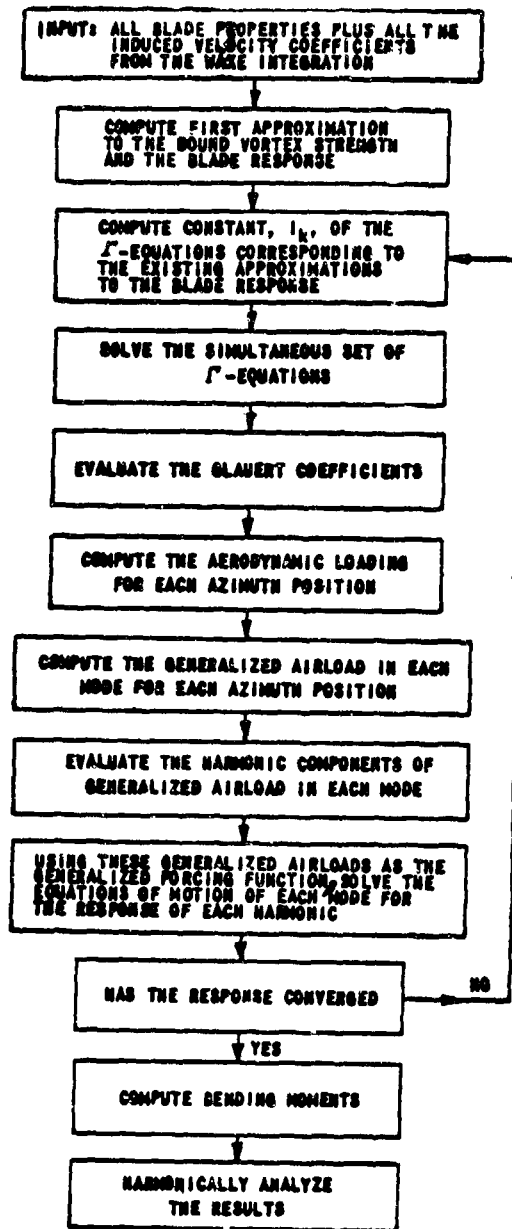


Figure 12. Major Steps in the Iterative Procedure for Solving the Equations in Part 2 of BLP2. (From Reference 2)

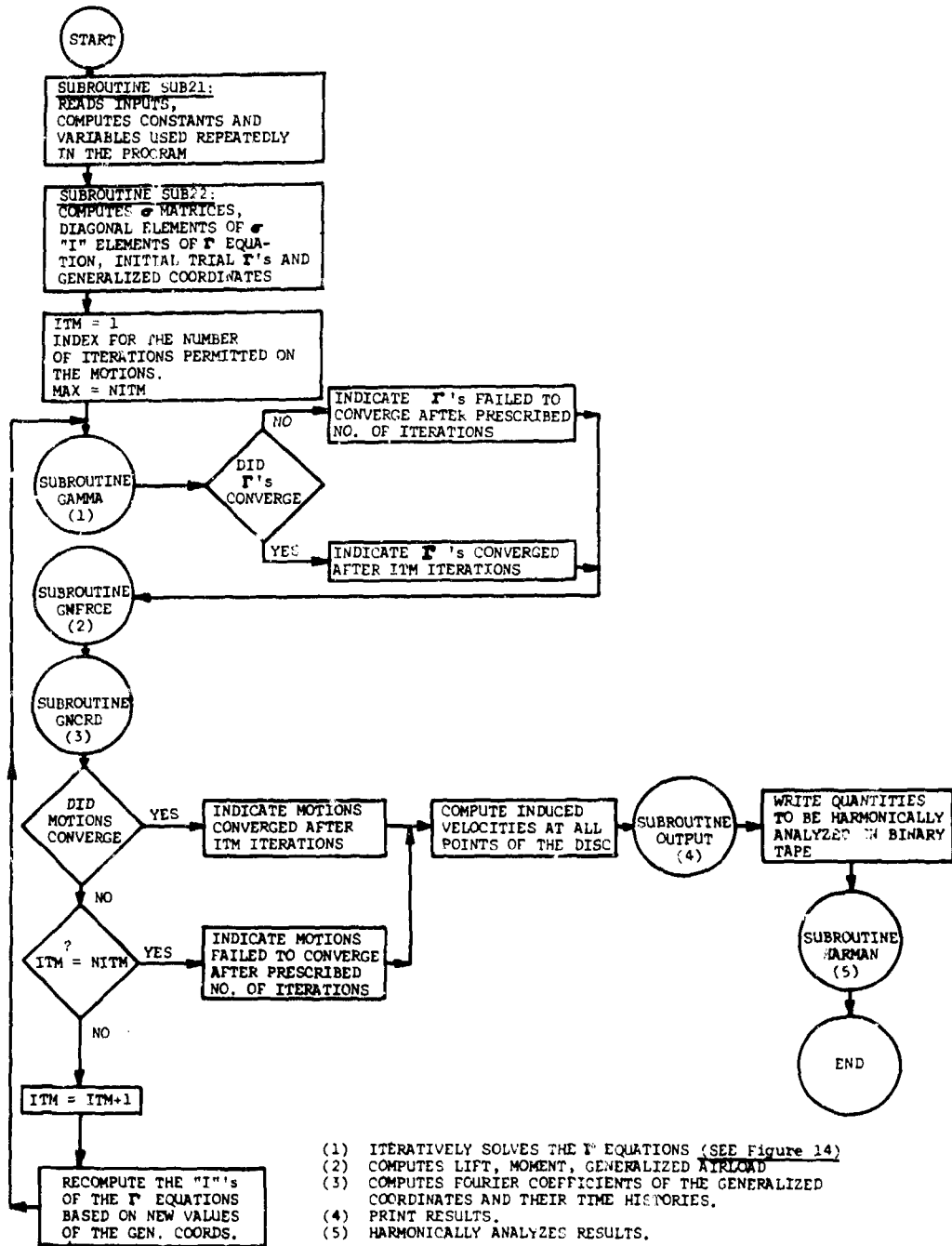
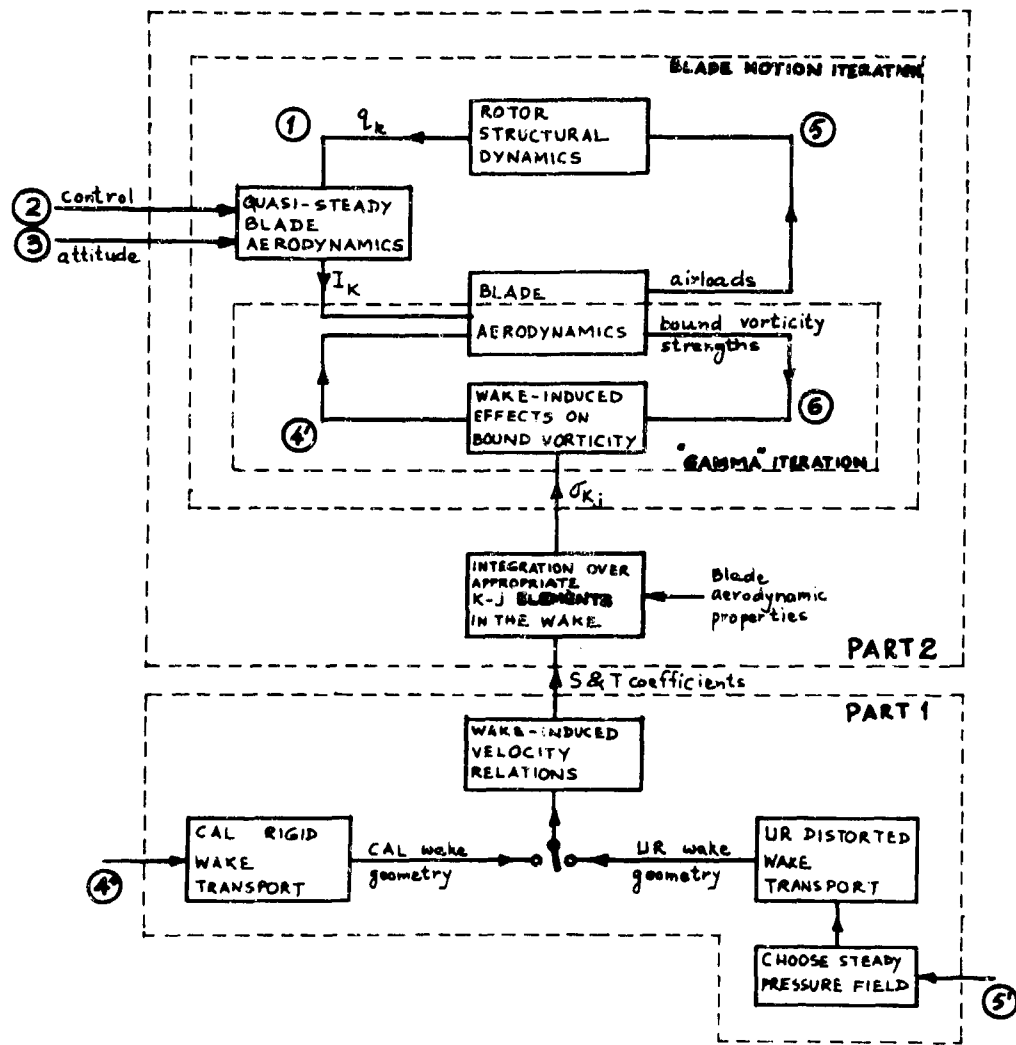


Figure 13. Flow Diagram for Part 2 of BLP2. (From Reference 2)



- ④ - Wake-induced velocity effects on bound circulation
- ⑤ - Uniform induced velocity for positioning the CAL wake
- ⑥ - Information on blade loads for choosing pressure field for calculating UR wake  
(See Figure 1 for other quantities of interest.)

Figure 14. Schematic of the Modified BLP2.

noticed from the lower right-hand portion of Figure 14. Appendix II shows the FORTRAN IV source listings for subroutine SUB14 of Part 1, as modified at UR, and for subroutines RWAKE, COEFS, STMLN, VLCTS, CHAMP, FRWRD, ADVNC, and CRSNG, which comprise the UR written wake-geometry program.

Essentially no changes were made in Part 2 of BLP2.

### 3.2 Representation of Various Physical Phenomena in the CAL Program

This section briefly describes the representation of the phenomena of rotor dynamics, blade aerodynamics, wake-induced effects, and wake transport in the original BLP2. An alternative to the CAL wake transport was added at UR, while the other three representations were left unchanged.

#### 3.21 Rotor Dynamics

For a numerical procedure in which all pertinent quantities are computed at a finite number  $N_a$  of discrete instants around the azimuth for a finite number  $N_r$  of blade radial stations, it is convenient to harmonically analyze the generalized forces  $G_k$  mentioned in Section 1.21:

$$G_k(t) = \bar{A}_{0k} + \sum_{n=1}^{N_h} (\bar{A}_{nk} \cos n\Omega t + \bar{B}_{nk} \sin n\Omega t) \quad (92)$$

...  $k = 1, N_m$

where  $N_h$  is the number of harmonics retained. (The maximum number would be  $\frac{N_a-1}{2}$ .) The components  $\bar{A}_{nk}, (\bar{A}_{nk}, \bar{B}_{nk}, n=1, N_h)$  are defined by equations (4) and (92), except that hereafter, we shall neglect the torsional displacements  $\Theta(r, t)$ , so that the aerodynamic pitching moments will not do any "work" on the blade modes, which now involve only flapping displacements. Thus,

$$\bar{A}_{nk} = \sum_{j=1}^{N_r} P_{nj} y_j^{(k)} \Delta r_j \quad (93)$$

...  $k = 1, N_m; n = 0, N_h$

$$\bar{B}_{nk} = \sum_{j=1}^{N_r} Q_{nj} y_j^{(k)} \Delta r_j$$

where:  $\Delta r_j$  is the length of the  $j$  th spanwise segment about radial position  $r_j$ ;  $y_j^{(k)}$  is the flapping displacement at  $r_j$  in the  $k$  th normal mode; and  $P_{nj}$  and  $Q_{nj}$  are the  $n$  th azimuthal cosine and sine components of the lift density  $P$  at the  $j$  th spanwise station, such that

$$P(r_j, t) = P_{0j} + \sum_{n=1}^{N_h} (P_{nj} \cos n\Omega t + Q_{nj} \sin n\Omega t) \quad (94)$$

...  $j=1, N_r$

The equations of motion (3) for the  $N_m$  modes can now be solved separately for each of the harmonic components of the steady-state response, resulting from the corresponding component of the forcing function, yielding:

$$a_{0k} = \frac{\bar{A}_{0k}}{M_k \omega_k^2} \quad \dots k=1, N_m$$

$$a_{nk} = \frac{1}{M_k} \cdot \frac{\bar{A}_{nk} (\omega_k^2 - n^2 \Omega^2) + \bar{B}_{nk} g_k \omega_k^2}{(\omega_k^2 - n^2 \Omega^2)^2 + g_k^2 \omega_k^4} \quad (95)$$

...  $n=1, N_h$

$$b_{nk} = \frac{1}{M_k} \cdot \frac{\bar{B}_{nk} (\omega_k^2 - n^2 \Omega^2) - \bar{A}_{nk} g_k \omega_k^2}{(\omega_k^2 - n^2 \Omega^2)^2 + g_k^2 \omega_k^4}$$

These define the generalized flapping displacements  $q_k$  :

$$q_k(t) = a_{0k} + \sum_{n=1}^{N_h} (a_{nk} \cos n\Omega t + b_{nk} \sin n\Omega t) \quad (96)$$

...  $k=1, N_m$

The flapping displacement and corresponding "plunging" velocity of a blade radial station can now be computed according to equation (1):

$$y_j(t) = \sum_{k=1}^{N_m} y_j^{(k)} \left[ a_{0k} + \sum_{n=1}^{N_h} (a_{nk} \cos n\Omega t + b_{nk} \sin n\Omega t) \right] \quad (97)$$

...  $j=1, N_r$

$$y_j(t) = \sum_{k=1}^{N_m} y_j^{(k)} \left[ \sum_{n=1}^{N_h} n \Omega (b_{n_k} \cos n \Omega t - a_{n_k} \sin n \Omega t) \right] \quad (98)$$

The plunging velocity affects the quasi-steady component  $I_K$  of the bound circulation, as can be seen from Figure 14.

### 3.22 Blade Aerodynamics

The blade representation of Reference 2 used trigonometric series expressions for the distributions  $\bar{\omega}(x_i)$  and  $\gamma(x_i)$  mentioned in Section 1.22:

$$\gamma_K(\theta) = 2 \left[ A_{0K} \cot \frac{\theta}{2} + \sum_{n=1}^{\infty} A_{nK} \sin n\theta \right] \quad (99)$$

...  $K = 1, N_{ra}$

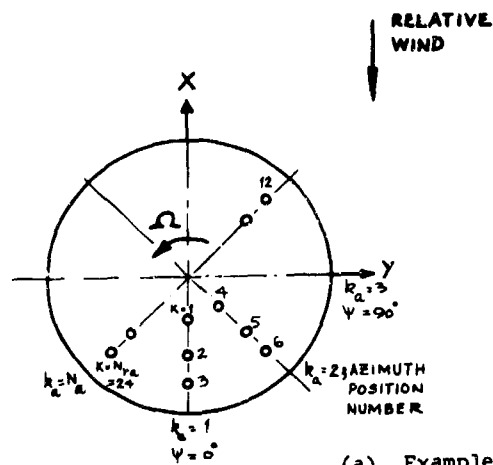
$$\bar{\omega}_K(\theta) = \bar{v}_{0K} + \sum_{n=1}^{\infty} \bar{v}_{nK} \cos n\theta \quad (100)$$

where  $\theta$  is the blade-chord based Glauert coordinate (see Figure 2(c)) defined by

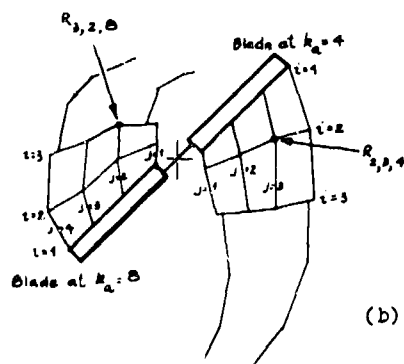
$$x_i = -b \cos \theta \quad (101)$$

The subscript  $K$  refers to the particular discrete disc point to which the  $\gamma(\theta)$ ,  $A_0$ ,  $A_n$ ,  $\bar{\omega}(\theta)$ ,  $\bar{v}_0$ ,  $\bar{v}_n$  above belong.  $K$  ranges from 1 to  $N_{ra}$ , where  $N_{ra} = N_0 \cdot N_r$ . See Figure 15(a). (Note that the vorticity distribution in equation (99) identically satisfies the Kutta-condition of equation (6).) In the numerical computations, the infinite series in equations (99) and (100) were truncated after the third term, i.e.,  $n$  ranged from 1 to 3. (It turns out that the higher harmonic components in  $\gamma_K(\theta)$  do not affect the theoretical  $T$ ,  $F$ , and  $Pc/2$  as evaluated from equations (14), (15) and (16).)

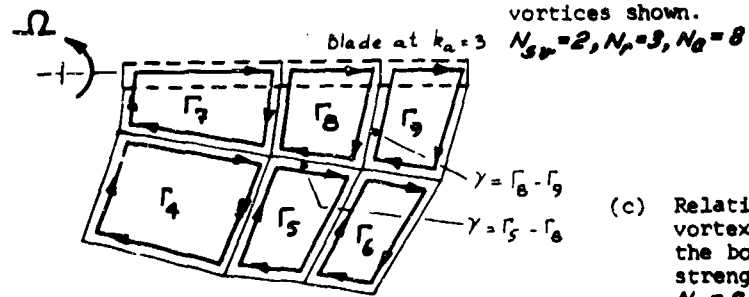
Substituting equations (99) and (100) into equation (5), the coefficients  $A_{nK}$  can be related to the components  $\bar{v}_{0K}$  of the impressed normal velocity:



(a) Example of the K-subscript notation for airload points in rotor disc when  $N_p = 3, N_a = 8$ .



(b) Wake model for two-bladed rotor. Both tip and root concentrated vortices shown.



(c) Relation between mesh-vortex strengths and the bound-vortex strengths when  $N_p = 3, N_a = 8$ .

Figure 15. K-Subscript Notation, Wake Configuration and Wake Vortex Strengths. (From Reference 2)

$$\begin{aligned}
A_{0K} &= \bar{v}_{0K} \\
A_{1K} &= -\bar{v}_{1K} \\
A_{nK} &= -\bar{v}_{nK}
\end{aligned}
\tag{102}$$

The total bound circulation is now obtained by evaluating the integral in equation (14):

$$\Gamma_K = \left( \frac{\partial C_L}{\partial \alpha} \right)_K \cdot b \cdot \left( A_{0K} + \frac{1}{2} A_{1K} \right)
\tag{103}$$

where  $\left( \frac{\partial C_L}{\partial \alpha} \right)_K$  is the measured lift curve slope for the airfoil section.

The numerical program also limits the total bound circulation  $\Gamma_K$  at disc point  $K$  to a maximum value  $\Gamma_{mK}$ , which is determined from the previously known stall angle of attack  $\alpha_{max}$  for the particular blade section:

$$\Gamma_{mK} = \left( \frac{\partial C_L}{\partial \alpha} \right)_K b_K (V_{1K} \sin \alpha_{max}) \quad \dots K=1, N_{ro}
\tag{104}$$

When the  $\Gamma_K$  as computed from equation (103) is found to exceed this  $\Gamma_{mK}$ , it is recognized that the blade is stalled at that position and the computed  $\Gamma_K$  is replaced by  $\Gamma_{mK}$ . The circulatory lift, as computed using equation (15), is augmented at the stalled segment by a cross-flow drag force.

The other "output" from the blade aerodynamics block in Figure 1 is the wake vorticity strengths. The wake configuration used in the CAL program is shown in Figure 15(b). The wake consists of a mesh wake behind each blade for  $N_{sv}$  azimuthal segments, as well as concentrated tip (and root) vortices behind these meshes. The actual locations in space of the various points in the wake model

are determined in the computations of the "wake vorticity positions"; see Figure 1. The strengths of the mesh-vortex segments are related to the bound vorticities at the  $N_{ra}$  disc points as shown in Figure 15(c). The strength of a concentrated tip (or root) vortex segment is taken to be simply the maximum value of the bound vorticity on the corresponding blade when at the appropriate azimuthal position.

### 3.23 Wake-Induced Effects

For the purposes of the numerical program, the vorticity strengths on all the filaments in the mesh wake can be expressed in terms of the  $N_{ra}$  bound vorticity strengths as shown above. Further, the wake-induced normal velocities  $\omega_K$  were needed only at the  $N_{ra}$  points on the disc in the form of components similar to the  $\bar{v}_{nK}$  in equation (100). For a given wake geometry, therefore, it was possible to evaluate coefficients  $S_{nKj}$  such that the induced normal velocity at the  $K$ th disc point due to the mesh wake is given by

$$\omega_{Ks}(\theta) = \sum_{j=1}^{N_{ra}} (S_{0Kj} + \sum_{n=1}^3 S_{nKj} \cos n\theta) \Gamma_j \quad (105)$$

...  $K=1, N_{ra}$

Similarly, for the concentrated trailed vortices part of the wake, coefficients  $T_{nKi}$  are computed such that the corresponding induced normal velocity due to the trailed wake is given by

$$\omega_{Kt}(\theta) = \sum_{i=1}^{N_a} (T_{0Ki} + \sum_{n=1}^3 T_{nKi} \cos n\theta) \bar{\Gamma}_i \quad (106)$$

...  $K=1, N_{ra}$

$\bar{\Gamma}_i$  is the maximum bound vorticity on a blade when at azimuthal position  $i$ . The induced velocity coefficients  $S_{nKj}$  and  $T_{nKi}$  are evaluated in Subroutine SUB14 of Part 1 of the CAL program.

The "impressed" normal flow component  $\bar{\omega}_K(\theta)$  is broken up into two parts: one,  $v_K(\theta)$ , resulting from all the contributing quantities on page 6 except the wake vorticity; and the other,  $\omega_K(\theta)$ , resulting exclusively from the wake vorticity. Thus,

$$\bar{\omega}_K(\theta) = v_K(\theta) + \omega_K(\theta) \quad (107)$$

...  $K=1, N_{ra}$

and

$$\omega_K(\theta) = \omega_{K_S}(\theta) + \omega_{K_T}(\theta) \quad (108)$$

Combining equations (102), (103), (107), and (108), it is possible to write

$$\Gamma_K = I_K + \sum_{j=1}^{Nra} \sigma_{Kj} T_j \quad \dots K=1, Nra \quad (109)$$

which is a set of  $Nra$  equations for the  $Nra$  unknowns  $\Gamma_K$ .  $I_K$  is the bound circulation resulting from the normal flow  $v_K$ , and  $\sigma_{Kj} T_j$  represents the bound circulation at disc point  $K$  resulting from the induced velocity due to the wake vorticity segments whose strengths depend on the bound circulation at disc point  $j$ . It may be noted that the  $I_K$  depend on the blade response, since the  $v_K$  include the blade-flapping velocities, torsional displacements, and torsional velocities. Equations (109) are solved by iteration in subroutine GAMMA of Part 1 of the CAL program.

### 3.24 Wake Transport

Representation of the wake transport in the CAL program consists of determining the positions of the points defining the mesh and trailed vortices in the wake model shown in Figure 15. The rigid-wake calculations reported in Reference 2 used the following formulas for the  $x'$ ,  $y$  and  $z'$  coordinates of the point  $R_{ijk_a}$  in the wake model, ( $i \geq 2$ ):

$$x'_{ijk_a} = -V_{FS} \cdot \frac{\Delta\psi}{\Omega} \cdot (i-1+\delta) \cdot \cos\alpha - r_j \cos[(k_a-i+\delta)\Delta\psi] - \frac{3}{2} b_j \sin[(k_a-i+\delta)\Delta\psi]$$

$$y_{ijk_a} = r_j \sin[(k_a-i+\delta)\Delta\psi] - \frac{3}{2} b_j \cos[(k_a-i+\delta)\Delta\psi] \quad (110)$$

$$z'_{ijk_a} = (V_{FS} \sin\alpha - \omega) \cdot \frac{\Delta\psi}{\Omega} \cdot (i-1-\delta) - y_{oc}(r_j) \quad \dots i \geq 2$$

where  $\Delta\psi$  is the azimuthal increment,  $\Delta\psi = \frac{2\pi}{N_a} \cdot k_a$  is the azimuthal position of the blade shedding the wake.  $b_j$  is the semichord at the blade segment end point  $j$ .  $y_{oc}(r_j)$  is the built-in coning plus steady deflection of the blade segment end points, positive upwards.  $w$  is the assumed uniform induced velocity (quantity 4" in Figure 14) over the disc.  $\delta$  is the fraction of a time interval through which the wake is advanced with respect to the true blade position  $k_a \cdot \delta$ , which is quasi-empirical, was determined in such a way that for a two-dimensional oscillating airfoil, this discrete representation of the shed wake gave results that were in "reasonable agreement" in the "reduced frequency range of interest" with the classical solution of the problem. (See Reference 2 for details of this determination of  $\delta$ .) For  $i = 1$ , the coordinates  $(x', y', z')_{ijk_a}$  are simply the points on the trailing edge of the blade at azimuthal position  $k_a$ .

It will be noticed that this wake transport ignores the displacements in the sideways direction. Also neglected is the variation, over the disc, in the induced velocity in the  $z'$  direction.

### 3.3 Algorithm for Computing the UR Wake Geometry

It can be seen from equations (110) that the point on the disc\*  $R_{ijk_a}(x', y', z')$  where the fluid particle now at the point  $R_{ijk_a}$  in the wake used to be  $(i-1+\delta)$  time intervals before the blades assumed the azimuthal position  $k_a$ , has the coordinates

$$\begin{aligned} x'_{ijk_a} &= -r_j \cos[(k_a - i + \delta)\Delta\psi] - \frac{3}{2} b_j \sin[(k_a - i + \delta)\Delta\psi] \\ y'_{ijk_a} &= r_j \sin[(k_a - i + \delta)\Delta\psi] - \frac{3}{2} b_j \cos[(k_a - i + \delta)\Delta\psi] \end{aligned} \quad (111)$$

$$z'_{ijk_a} = -y_{oc}(r_j) \quad \dots i \geq 2$$

---

\*The "disc" is not a flat surface, since blade steady deflection and built-in coning are accounted for, through  $y_{oc}$ .

The difference between the expressions (110) and (111) defines the movement of this fluid particle from  $R_{ijka}(x^0, y^0, z^0)$  to  $R(x', y, z')$ , under the influence of  $V_{FS}$  and  $\underline{w}$ , in  $(i-1-\delta)$  time intervals.

In the UR wake-geometry computations, the points of "injection",  $R_{ijka}$ , can be retained\* as in (111), but the movement under the influence of both  $V_{FS}$  and the induced velocity was computed differently, through an actual calculation of the streamlines through the injection points. The steady pressure field used for calculating the streamlines always had the pressure discontinuity on the flat disc.

### 3.31 Subroutine RWAKE

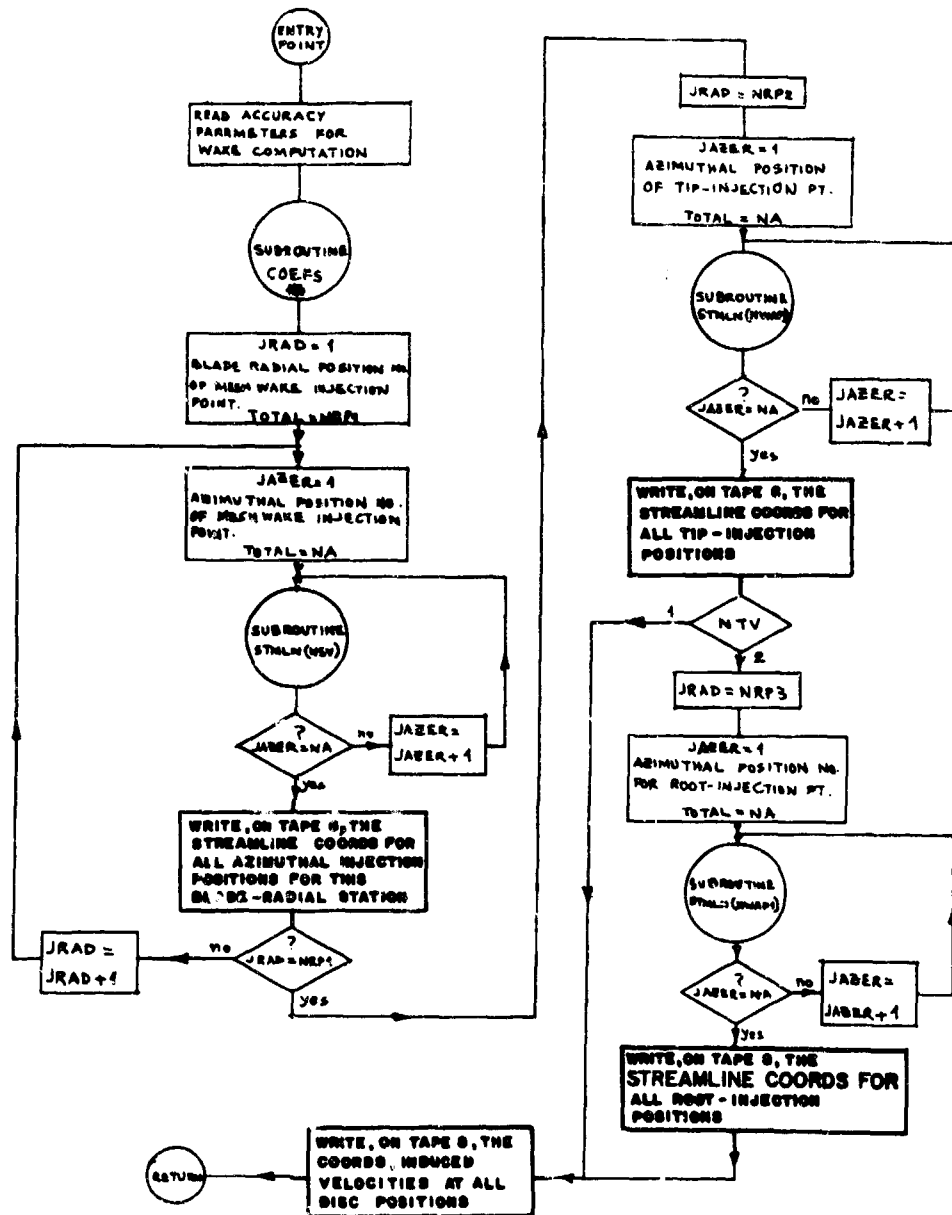
Subroutine RWAKE, which is the entry point for calculating the UR wake geometry, first chooses the steady pressure field through formulas such as those developed in Sections 2.33 and 2.34. Figure 16 shows the flow diagram for subroutine RWAKE. Table III shows the various options for the choice of the steady pressure field based on various physical quantities.

It may be noticed from Appendix I that the values of  $Q_n^m(i\eta)$  are purely imaginary quantities when  $n$  is even. The corresponding  $C_n^m$  and  $D_n^m$  also turn out to be purely imaginary quantities. ( $P_n^m(j)$  are always real.) In such cases, the quantities actually handled under QMN(J) were  $iQ_n^m$ . To offset this factor  $i$ , the corresponding quantities CMN(J) and DMN(J) in core were set equal to  $-iC_n^m$  and  $-iD_n^m$  respectively. Thus, all the computations were done in "reals", and the products CMN(J)\*QMN(J), DMN(J)\*QMN(J) always agreed with their theoretical counterparts  $C_n^m Q_n^m(i\eta)$ ,  $D_n^m Q_n^m(i\eta)$  for all J; i.e., for all combinations of  $m$  and  $n$ .

After choosing the steady pressure field, RWAKE sequentially calculates, using equations (111), the disc-injection points  $R_{ijka}$  for the mesh and trailed wake grid positions (see Figure 15(b)); it then calls subroutine STMLN, which calculates the streamline through a given disc point. At the end of RWAKE, all the wake coordinates, disc injection point coordinates, total normal velocity values at disc points, and induced velocity values at the disc points are written on TAPE8.

---

\*An option in the UR wake computation program also enables the particles to be injected on the flat disc, thus ignoring  $y_{oc}$ .



\*COEFS calculates coefficients CMN(J) and DMN(J). (See Table III)

Figure 16. Flow Diagram for Subroutine RWAKE.

TABLE III. VARIOUS OPTIONS FOR CHOOSING THE STEADY PRESSURE FIELD  $P$  THROUGH THE COEFFICIENTS  $C_n^m$  AND  $D_n^m$

$$P = \sum_{m,n} P_n^m(\psi) Q_n^m(i\eta) [C_n^m \cos m\psi + D_n^m \sin m\psi]$$

KKS	Remarks
1	Subroutine COEFS bypassed. $C_n^m$ and $D_n^m$ remain unchanged.
2	$C_n^m$ and $D_n^m$ to be read in as input to subroutine COEFS.
3	$C_n^m$ and $D_n^m$ calculated from $C_T, C_{M_r}, C_{M_p}$ and $\lambda$ . (See Section 2.33)
4	$C_n^m$ and $D_n^m$ calculated from $TT, M_p, M_r, R, V_{FS}$ and $\lambda$ . (See Section 2.33)
5	$C_n^m$ and $D_n^m$ calculated from input in the form of harmonic components of the flapping moment experienced by the blade as it rotates. (See Section 2.34) Average momentum transfer condition satisfied.
6	$C_n^m$ and $D_n^m$ calculated from input in the form of harmonic components of the blade flapping moments, plus $R, \rho, V_{FS}, b, M_r, M_p$ . Average momentum transfer condition not satisfied.
7	$C_n^m$ and $D_n^m$ calculated from $R, \rho, V_{FS}, N_b$ , plus the harmonic components of the blade flapping moments which are computed from the harmonic components of the experimentally measured lift density on instrumented blades. Average momentum transfer condition satisfied.
8	$C_n^m$ and $D_n^m$ calculated from the same inputs as 7 above, plus $M_r$ and $M_p$ . Average momentum transfer condition not satisfied.

### 3.32 Subroutine STMLN(KEND)

Subroutine STMLN(KEND) follows the fluid injected from a given disc injection point for a number (KEND-1) of time intervals, saving the coordinates of the position after each time interval. The field is assumed steady, and the particle paths and streamlines are identical. A time interval is equivalent to the rotation of a blade from one azimuthal position to the next. Thus,

$$\Delta t = \frac{2\pi}{\Omega \cdot N_a} \text{ seconds} \quad (112)$$

To nondimensionalize time, we must use a normalization that is compatible with the normalizations (30) and (81) for distance and velocity respectively. This calls for normalizing  $t$  on the time taken by  $V_{fs}$  to travel a distance  $R$ ; i.e.,

$$\Delta t = \frac{2\pi}{\Omega N_a} \cdot \frac{V_{fs}}{R} = \frac{\Delta\psi}{\mu} \quad (113)$$

where  $\Delta\psi$  is the angle (radians) between two azimuthal positions and  $\mu$  is, again, the tip-speed ratio. For accurate streamline calculations, the program has the provision for further reducing the time increment through a factor NINC. Thus, each time increment TINC is (1/NINC) times the time interval, and

$$TINC = \frac{\Delta\psi}{\mu \cdot NINC} \quad (114)$$

Equation (114) represents the "usual" time increment value. An exception is the very first interval of a streamline. (See Figure 17) For a fractional wake advance  $\delta$ , the TINC for the first NINC increments of each streamline will be  $(1-\delta)$  times that in equation (114). NINC is one of the accuracy parameters read in at the beginning of RWAKE.

Subroutine VLCTS numerically calculates the induced-velocity components  $V$  and  $W$  at a given point  $(X, Y, Z)$  by the procedure indicated in Section 2.35. XUP (the location of "infinity" upstream of the disc) and XINC (the value of the incremental length used for the numerical integration of (83)) are the accuracy parameters used in VLCTS. Both XUP and XINC are also read in at the beginning of RWAKE.

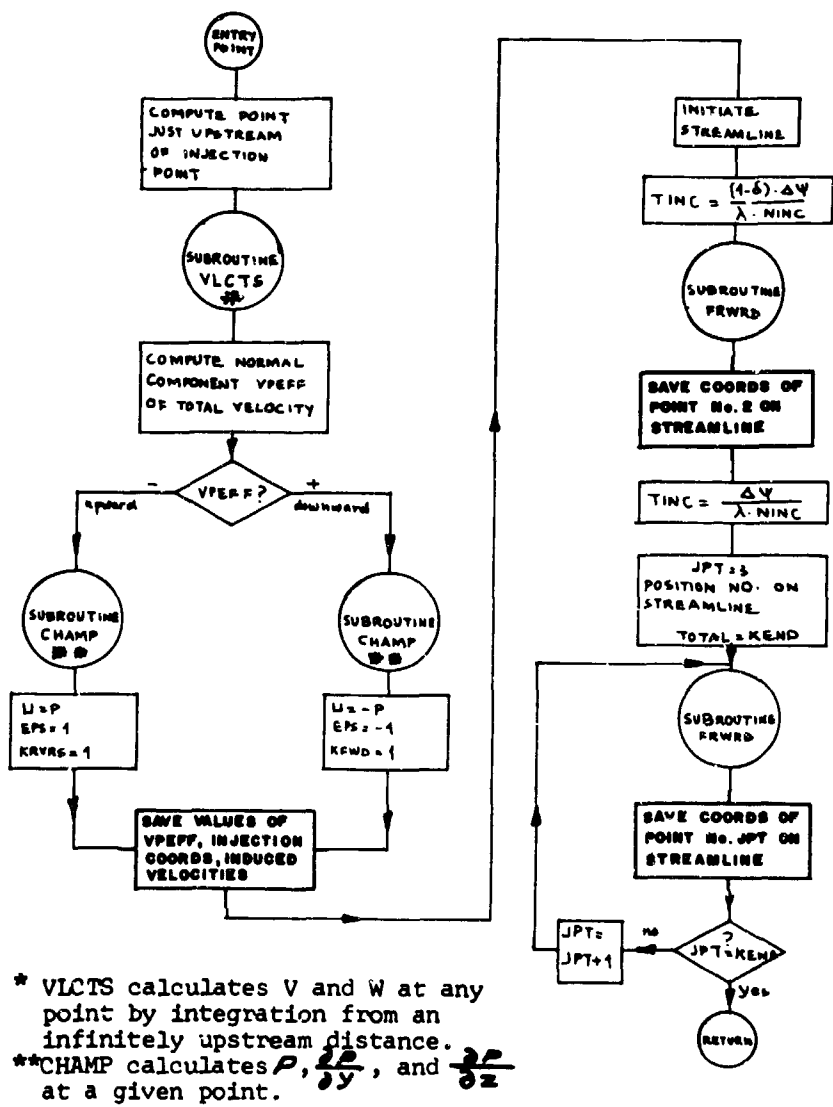


Figure 17. Flow Diagram for Subroutine STMLN(KEND).

The quantities KFWD and KRVRS appearing in Figure 17 are "counters" for the number of flat-disc crossings made by the particle being followed, in the forward (i.e., normal, or downward) and reverse (i.e., upward) directions respectively.

Subroutine CHAMP computes  $P$ ,  $\frac{\partial P}{\partial y}$ , and  $\frac{\partial P}{\partial z}$  at a given point  $(v, \eta, \psi)$ , using the formulas from Section 2.35. It may be noticed that the multiplier appearing in equation (87) for  $\frac{\partial P}{\partial \eta}$  will make the quantity real since, as explained in Section 3.31, either  $C_n^m, D_n^m$  or  $Q_{n-1}^m(i\eta)$ , but not both, will be imaginary for each value of  $n$ . The quantity handled in QMNML(J) will always be real, being equal to  $iQ_{n-1}^m(i\eta)$  if  $n$  is odd, and equal to  $Q_{n-1}^m(i\eta)$  if  $n$  is even. This leads to agreement between the products CMN(J)\*QMNML(J), DMN(J)\*QMNML(J) and their theoretical counterparts

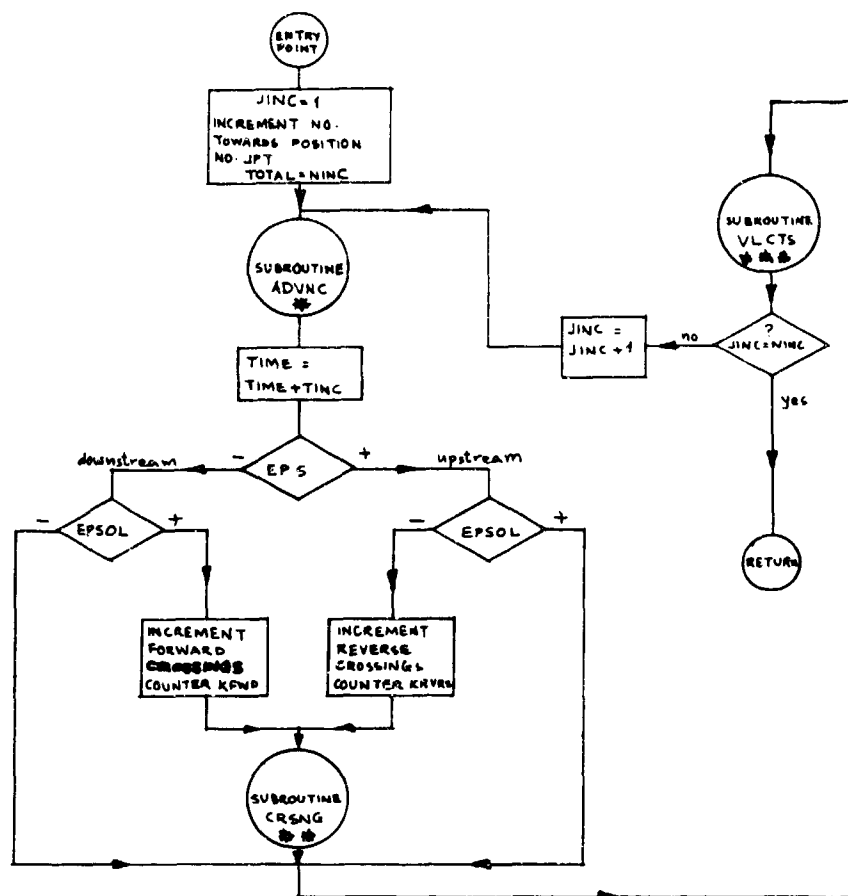
$$C_n^m Q_{n-1}^m(i\eta), D_n^m Q_{n-1}^m(i\eta) \text{ for all } J.$$

### 3.33 Subroutine FRWRD

Subroutine FRWRD, which is called in subroutine STMLN, computes the next position on the streamline by invoking the (call ADVNC - call CHAMP) cycle NINC times. Figure 18 shows the flow chart for subroutine FRWRD. Subroutine ADVNC saves the current values of coordinates, velocities, pressure, etc., and calculates the coordinates of the particle after a time increment TINC, using the current values of the velocity. If a flat-disc crossing is recognized on ADVNC-ing, FRWRD compensates for it by calling CRSNG. Subroutine CRSNG assures that the values of the velocity are continuous across the flat disc, although the pressure has a discontinuity at the flat-disc surface. This is achieved in CRSNG by first finding out the exact point of crossing, and then modifying the  $U$  component of the velocity through an operation similar to equation (91).

### 3.4 Integration With the CAL Program

It is seen from Figure 11 that the CAL wake coordinates are generated in subroutine SUB14 of Part 1 of the original BLP2. (SUB14 calls another subroutine COORD for actually computing these coordinates.) Since our modifications to the BLP2 essentially consist of generating and using an alternate wake geometry, the interfacing between the UR-written wake-computing part of the program and the BLP2 occurs in subroutine SUB14. The FORTRAN IV source listing for SUB14 appears in Appendix II. Figure 19 shows the flow diagram



\*ADVNC saves the values of various quantities and calculates coordinates of new position (after a time increment of TINC) using current velocity values.  
 \*\*CRSNG compensates for crossing of the disc, so that velocity values on either side of the disc are continuous, although pressure is not.

Figure 18. Flow Diagram for Subroutine FRWRD.



for subroutine SUB14 as modified at UR. The changes and additions to the original program are shown in dotted lines. The changes were made so as to make it possible to compute and use either of the two wake geometries. The UR wake geometry is generated (and written on TAPE8) in subroutine RWAKE. Provision was also made to make it possible to generate just the UR wake and then terminate the job. Conversely, a UR wake generated in a previous run can be directly read off TAPE8 and used for computing the induced velocity coefficients in Part 1. All these options are accomplished through an input integer variable MMSW. (See the source listing for subroutine RWAKE in Appendix II for a description of these options.)

### 3.5 Peripheral Program

Two peripheral programs had to be written in addition to the UR wake computation described in Section 3.3. These were named RWAKEPIC and RSLTSPLT. Both make extensive use of the plotter subroutines package available on the University of Rochester disc library.

RWAKEPIC reads the UR-computed wake geometry from the TAPE8 data set generated in subroutine RWAKE of Part 1 and, using the plotting routines, pictorially displays the wake geometry. Three options are available as to the type of picture produced: pictures of streamlines, instantaneous pictures of the wake generated by a finite number of blades, and progressive distortion of stream-tubes originating (from points equispaced around the azimuth) on the disc. RWAKEPIC, which is a separate main program, was found to be useful in interpreting the UR wake geometry.

RSLTSPLT, which is also a separate main program, reads the converged airloads, blade-bending moments, bound vorticity strengths, etc., from the TAPE3 data set generated toward the end of Part 2 (see page 48). Using the plotter routines, RSLTSPLT then creates curves showing the time histories as well as harmonic analyses of these converged quantities which are the results of the BLP2. RSLTSPLT was found to be helpful in comparing the blade-loads predictions resulting from a UR wake geometry with those from the CAL wake geometry and with experimentally measured blade loads.

## CHAPTER 4

### COMPUTED RESULTS AND INTERPRETATION

The UR-written wake-geometry program described in Chapter 3 was first used for calculating the induced velocity at a small number of points on a flat, lifting disc at an angle of attack of  $2.5^\circ$ . Figure 20 shows the computed  $Z$ -component of this velocity. The induced velocity is upward on a crescent-shaped area near the leading edge of the disc and on an area immediately behind the center. These results agree well with the results of Mangler's computations shown in Figures 3 and 4.

The wake-geometry program was then used to predict three wake geometries for two flight conditions of the UH-1 rotor:

- (1)  $\mu = 0.26$ . (Wake geometry computed from streamlines emanating from the flat disc, thus ignoring the steady deflections  $y_{oc}(r_j)$ . See footnote, page 61.)
- (2)  $\mu = 0.26$ . (Streamlines emanating from the steady deflected positions of the blades.)
- (3)  $\mu = 0.08$ . (Streamlines emanating from the steady deflected positions of the blades.)

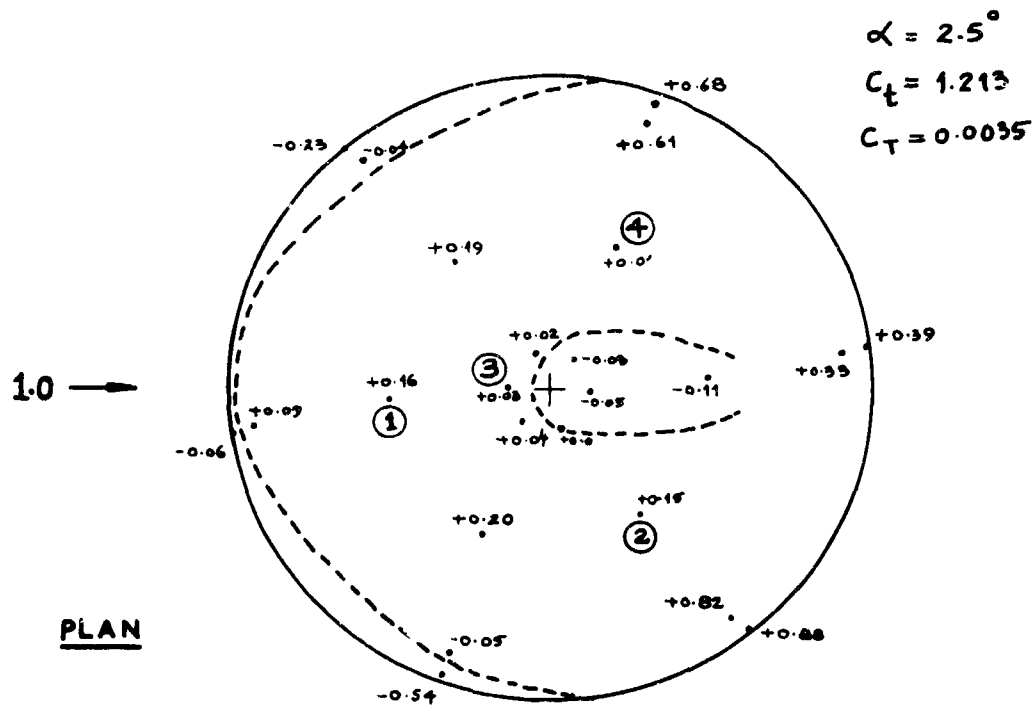
The CAL-computed values for the airloads and blade flapping moments are available (Reference 2) for these flight conditions. (These were computed using a wake geometry input calculated from a uniform downwash.) Also available are experimental measurements for the airloads and flapping moments.

The modified BLP2 was then used to obtain the blade-loads predictions resulting from the UR-computed wake geometries. Except for the wake-geometry inputs, all other inputs for these computations were identical to those in the corresponding CAL runs. Even for the wake-geometry inputs, the wake models used were the same.

#### 4.1 UH-1 at $\mu = 0.26$ (Condition 67 of Reference 15), Injection on Flat Disc

$$V_{fs} = 188 \text{ feet per second (forward speed)}$$

$$\alpha = 5.8 \text{ degrees (disc angle of attack)}$$



Contours of zero downwash are shown by dotted lines. Numbers shown in the figure are  $z$ -direction induced velocity values, positive downward, normalized on the forward velocity  $V_{FS}$ .

Comparison with Mangler's induced velocity values from Figure 3

location number	Mangler's $\frac{w}{V_{FS}}$	UR $\frac{w}{V_{FS}}$
①	0.2	0.194
②	0.24	0.182
③	0.06	0.04
④	0.34	0.24

Figure 20.  $z$ -Component of the Induced Velocity on a Lifting Disc, Using the UR Program.

$$NW = 2 \text{ (number of revolutions of wake)}$$

$$\delta = 0.7 \text{ (wake advance)}$$

The induced velocity on the disc, as computed by RWAKE, showed an upwash area near the forward edge and just behind the center of the disc. Figure 21 shows a typical instantaneous "picture" of wake trails. It is clear that the trails deviate appreciably from a skewed circular helix. Figure 22 shows streamlines starting from 90% radius on the flat disc. All the streamlines leave the disc in the downward direction, but those in the region  $|Y| > 0.8$  soon come under the influence of a tip vortex effect, the ones farther out doing so sooner. Streamlines in the  $|Y| < 0.8$  region continue downward. The result is a separation of the streamlines into two wing-tip type systems emanating from the tip areas, and a body of streamlines emanating from the inboard area of the circular wing. The "wing-tip" grouping of streamlines exhibited a tendency to go higher (and move laterally) relative to the latter group, which moves downward comparatively undisturbed by the presence of the disc. Similar separation was observed in the water-tunnel experiments reported in Reference 16. The rolling up of the tip vortices is clearly visible in Figures 23 and 24, which show the progressive distortion of an initially circular fluid contour, released from 90% radius on the flat disc, one and two rotor revolutions after release, respectively.

Figure 25 shows a comparison of the unsteady parts of the airloads (time histories), computed from this UR wake geometry, with the CAL-computed airloads and with experimentally observed values. It can be seen that the airloads predictions from the two different wake geometries are only slightly different. The UR wake airloads do not seem to suggest a decidedly better (or worse) agreement with experiment.

In Figure 21, a tip-trailed vortex is seen passing close to about the 75% radial station when the blade is at  $\psi = 75^\circ$ . The induced velocity at that station due to the nearest tip-vortex trail segment was  $-10.13 \text{ fps(CAL)}/-3.93 \text{ fps(UR)}$ . (The negative sign indicates an upward velocity, since our convention has positive  $z$  downward. See Figure 6) The induced velocity at this station due to the entire wake was  $+9.48 \text{ fps(CAL)}/+5.745 \text{ fps(UR)}$ . As compared to these, the normal component  $\frac{1}{2} \cdot \alpha_0$  due to the control input was  $92.0 \text{ fps}$  at that station. The total normal component\* was  $+43.74 \text{ fps(CAL)}/+48.60 \text{ fps(UR)}$ .

---

\*  $\bar{w}$ , normal to the blade chord. See Figure 2(a).

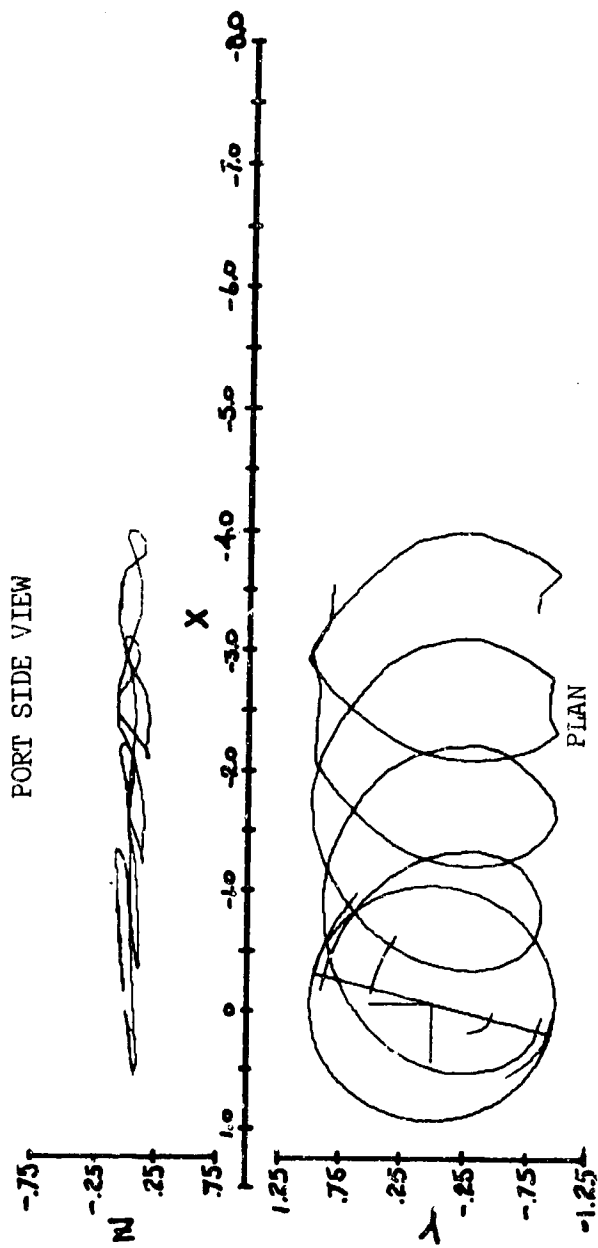


Figure 21. Typical Instantaneous Geometry of Wake Trails (UH-1,  $\mu = 0.26$ ,  $N_b = 2$ , One of the Blades at  $\psi = 75^\circ$ ).

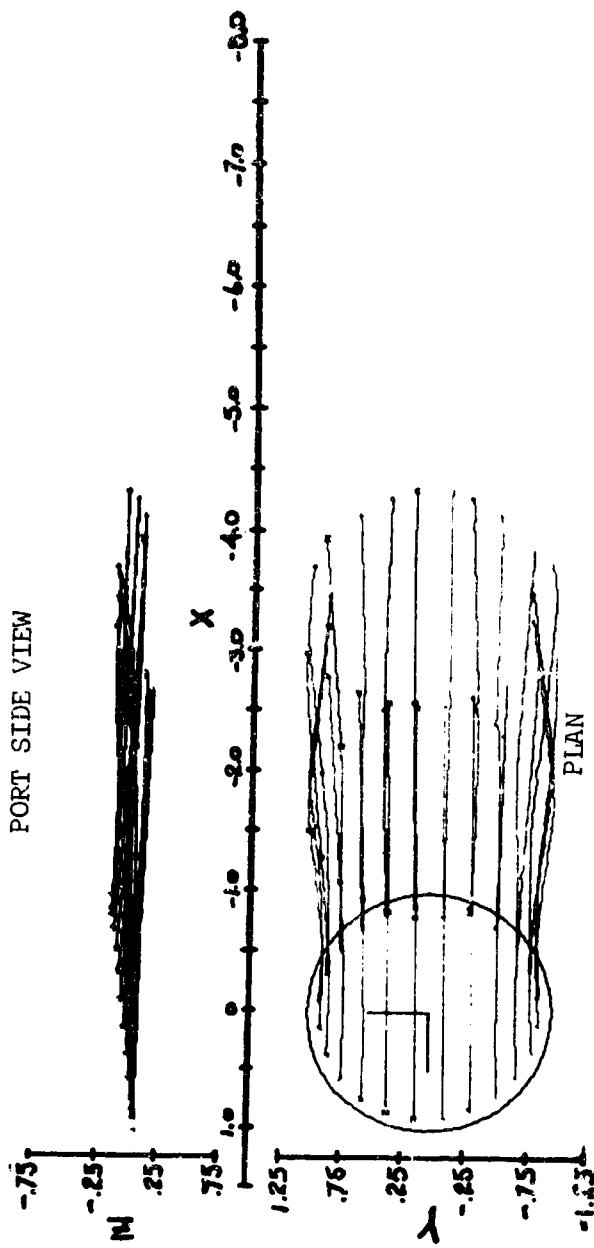


Figure 22. Geometry of Streamlines in the Steady Flow Field (UH-1,  $\mu = 0.26$ ).

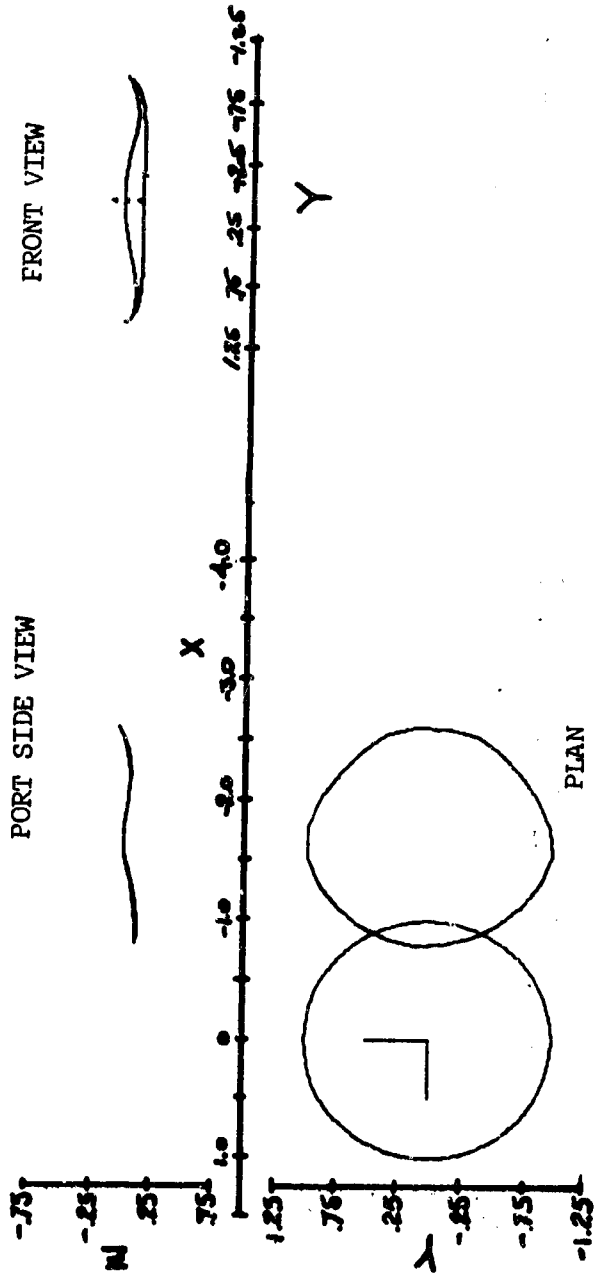


Figure 23. Three Views of a Fluid Contour, Released From 30% Radius on the Disc, One Rotor Revolution After Release (UH-1,  $\mu = 0.26$ ).

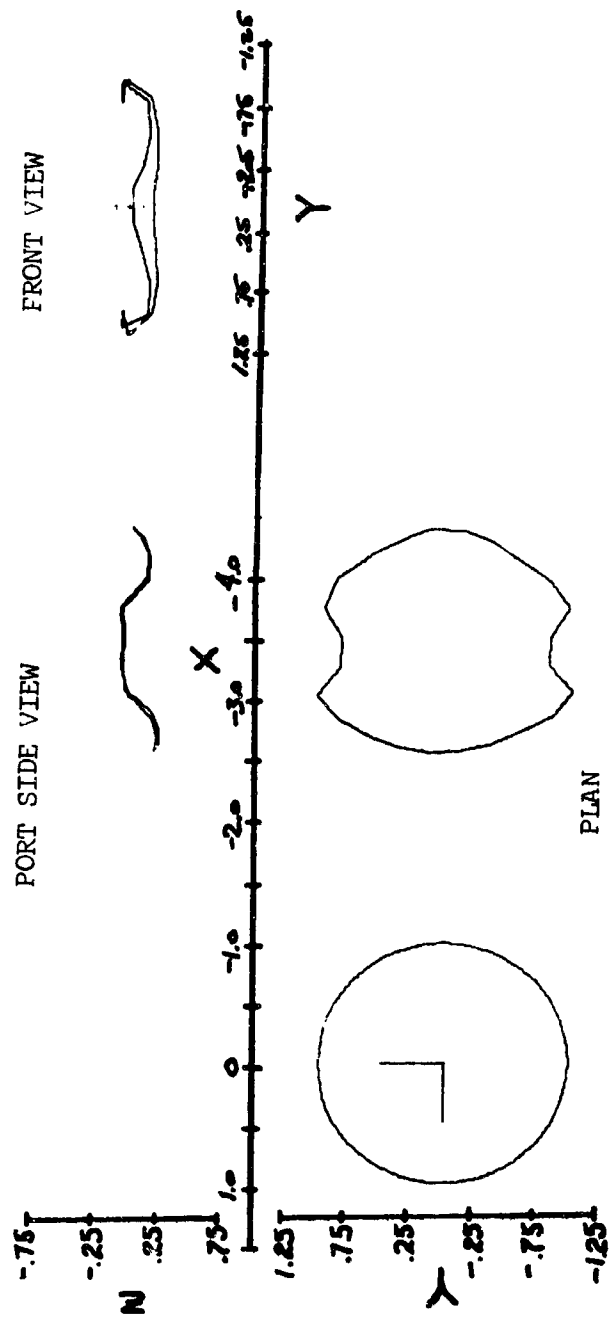


Figure 24. Three Views of a Fluid Contour, Released From 90% Radius on the Disc, Two Rotor Revolutions After Release ( $\mu = 0.26$ ).

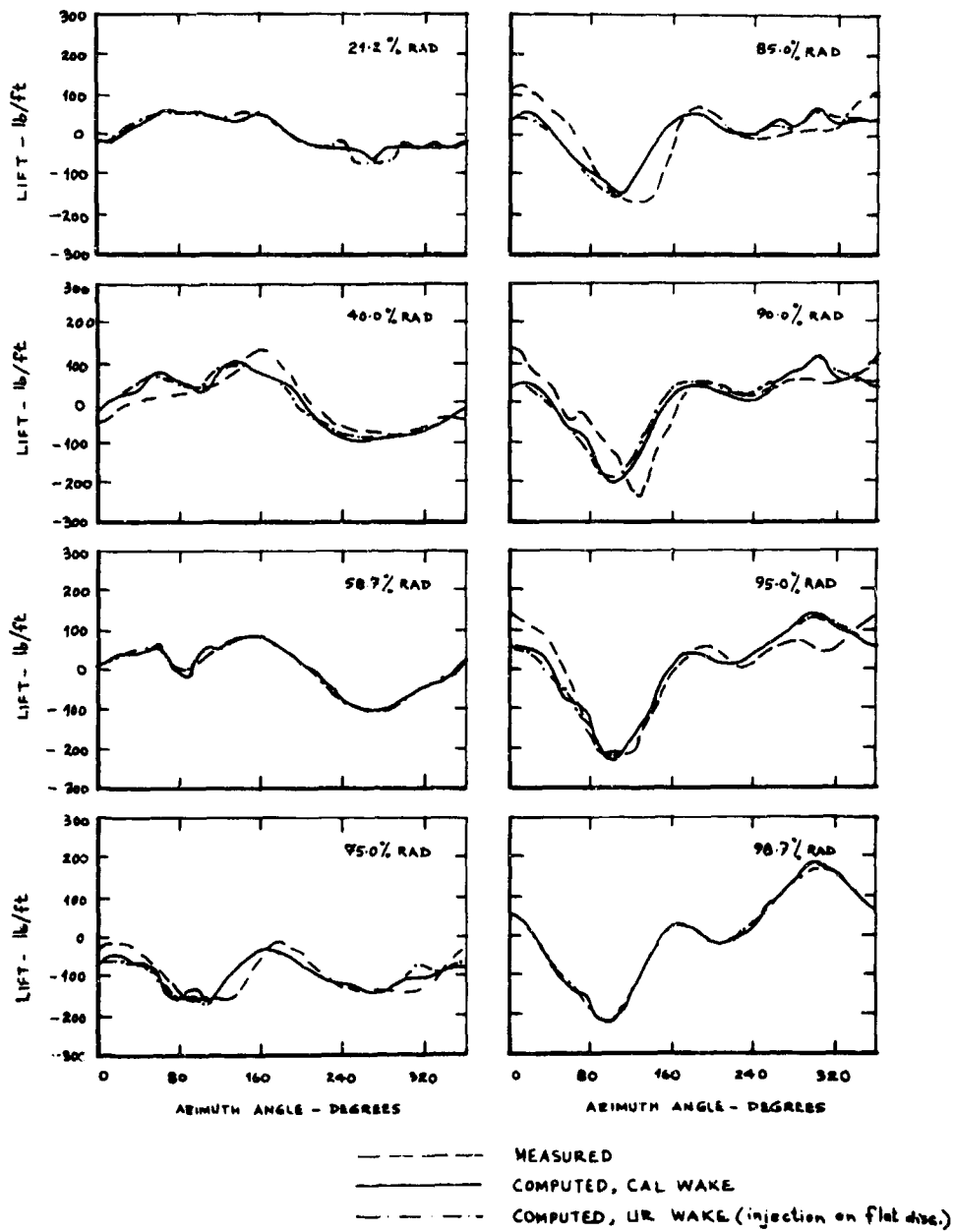


Figure 25. Time Histories of the Unsteady Parts of Measured and Computed Airloads (UH-1,  $\mu = 0.26$ ).

Conversely, at 21.2% radius and  $255^\circ$  azimuth, where significant differences between the two computed airloads are apparent in Figure 25, the induced velocity due to the three nearest segments of the tip-trail from the preceding blade is found to be  $-4.85$  fps(CAL)/ $-3.41$  fps(UR). By comparison, the induced velocity due to the entire wake is  $-25.1$  fps(CAL)/ $-9.918$  fps(UR). This difference of about 15 fps is probably due to the closeness of the mesh wake, which curls around close to the retreating blade at small radii, combined with the fact that this UR wake computation used streamlines emanating from the flat disc, thus placing the wake lower than the CAL computation which accounted for  $\gamma_{oc}$ .

The slight differences between the airload predictions from the two wake geometries are more observable at smaller radii. This is probably attributable to the smaller flapping (plunging) velocities and smaller tangential velocities (and hence smaller  $V_1 \cdot \alpha_g$  contribution) at small radii, which would make differences in the wake-induced velocity more noticeable as seen at the blade aerodynamic section. Contributions to induced velocity by specific vortex filament segments are given in Appendix III.

Figure 26 shows a comparison of harmonic breakdowns of the airloads. Figures 27 and 28 show the flapwise bending moments (time histories of unsteady parts and harmonic components, respectively) for the two computations and the experimental results.

#### 4.2 UH-1 at $\mu = 0.26$ (Condition 67 of Reference 15), Injection at Steady Deflected Positions of Blades

$V_{FS} = 188$  feet per second (forward speed)

$\alpha = 5.8$  degrees (disc angle of attack)

NW = 2 (number of revolutions of wake)

$\sigma = 0.7$  (wake advance)

The computed wake geometry for this case showed all the qualitative features of Figures 21 through 24. The tip-vortex effect, however, was delayed (i.e., became discernible farther downstream) since the streamlines, which emanated from the "coned" blade surface this time, had to travel some distance before they entered the regime influenced by the pressure discontinuity on the flat disc which is the source of the tip vortices.

When the computed geometry was used as input to BLP2, the blade motions did not converge. The iterative procedure in Part 2 exhibited a sustained-oscillations type of behavior. These iteration-to-iteration oscillations in the generalized blade displacements

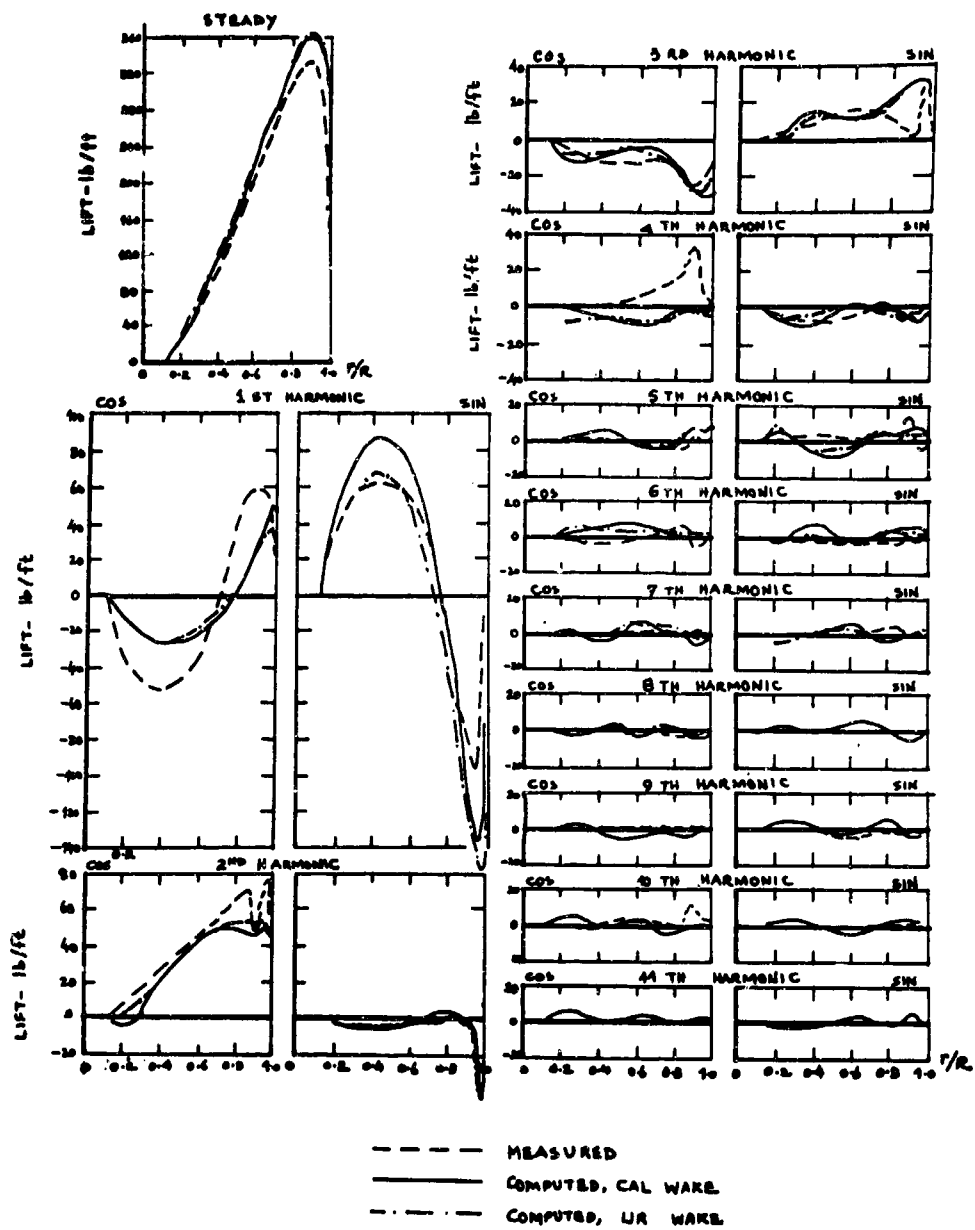


Figure 26. Harmonic Analyses of Measured and Computed Airloads (UH-1,  $\mu = 0.26$ ).

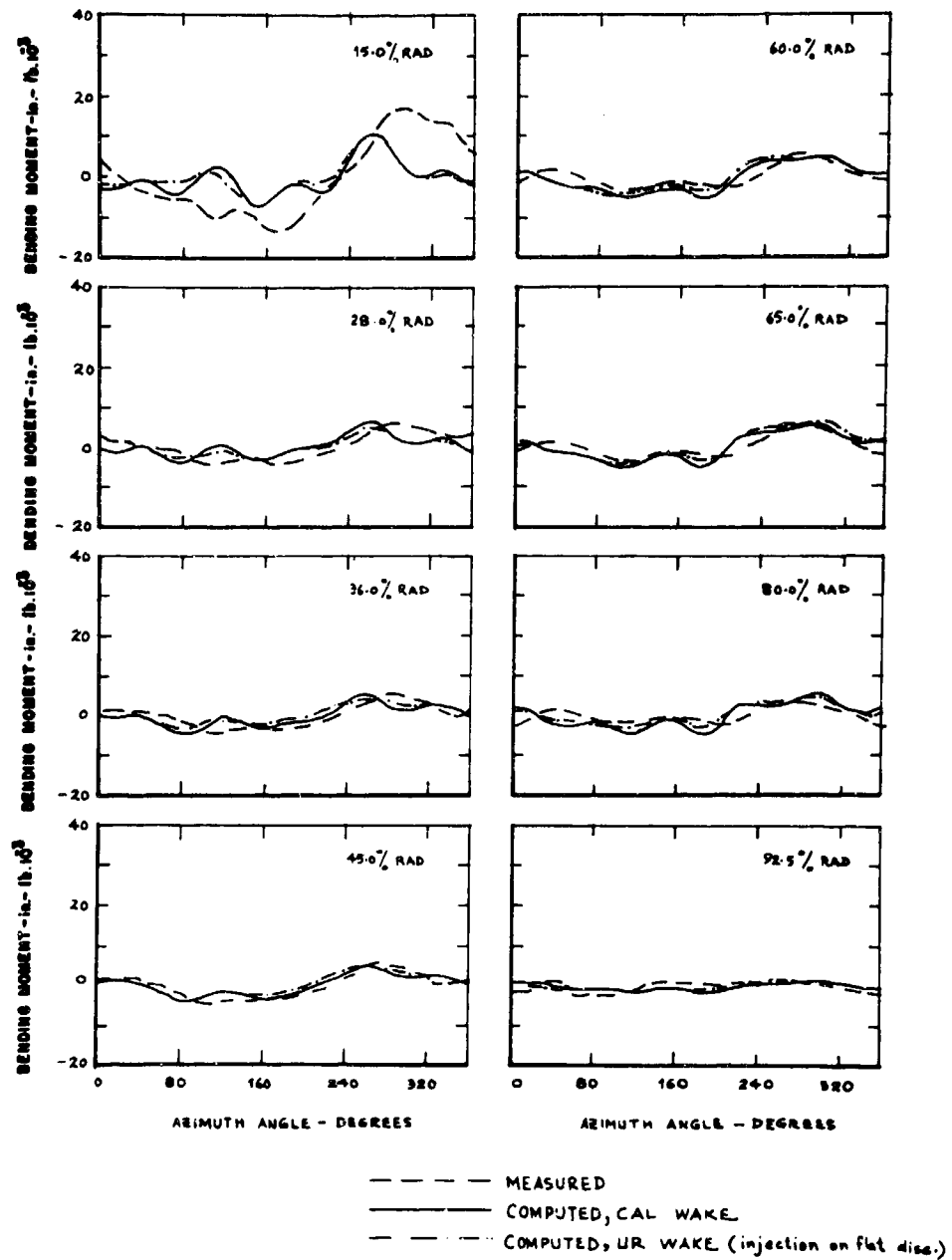


Figure 27. Time Histories of the Unsteady Parts of Measured and Computed Blade-Flapwise Bending Moments (UH-1,  $\mu = 0.26$ ).

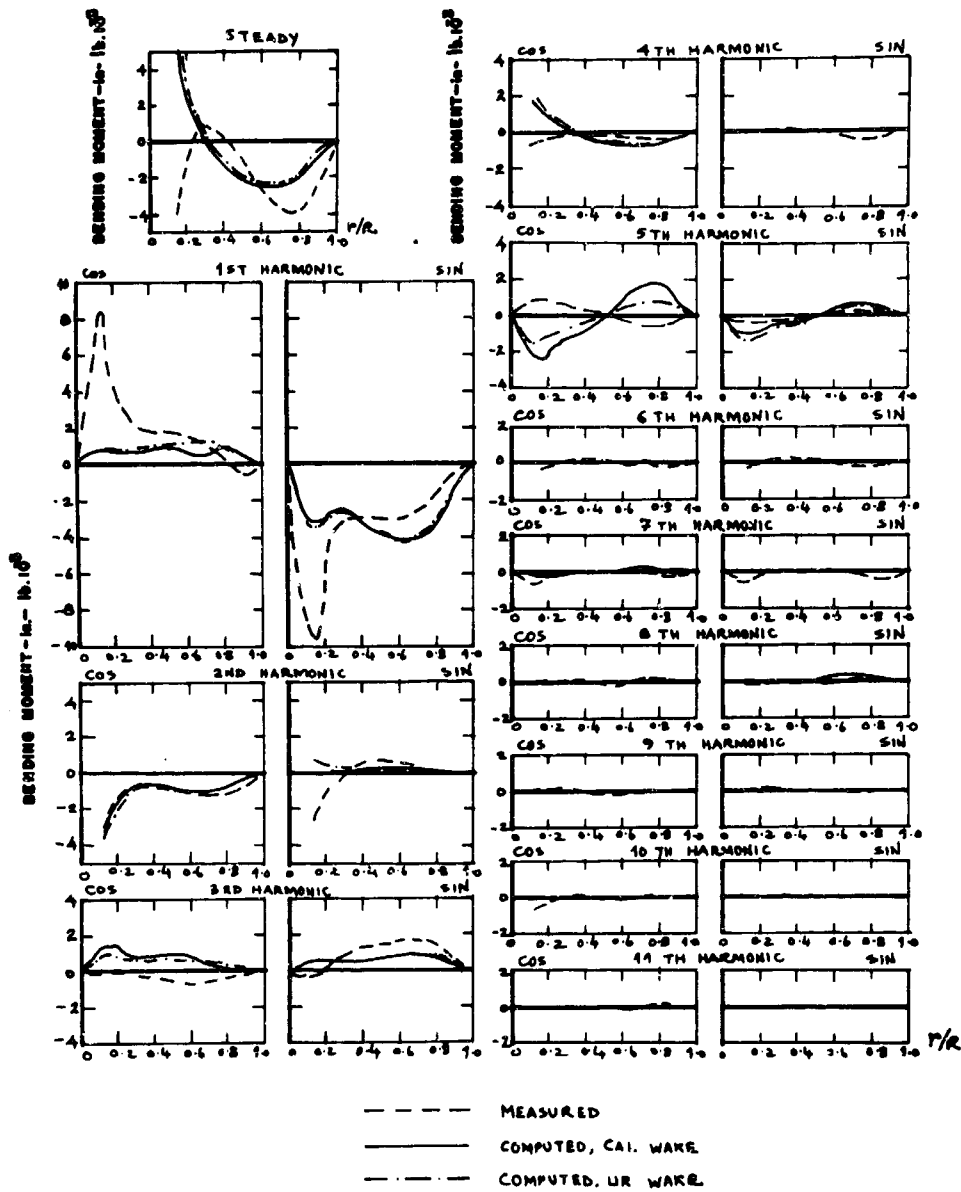


Figure 28. Harmonic Analyses of Measured and Computed Blade-Flapwise Bending Moments (UH-1,  $\mu = 0.26$ ).

were less than 1.5% for all structural modes except the highest (2nd antisymmetric), for which they were about 8.6%. The nonconverged loads, however, were found to be quite close to the CAL-computed loads. At the 255° azimuth of the 21.2% radial station, the airload prediction agreed better with the CAL-computed value than did the prediction of Section 4.1 (see Figure 25).

#### 4.3 UH-1 at $\mu = 0.08$ (Condition 65 of Reference 15), Injection at Steady Deflected Positions of Blades

$$V_{FS} = 55.1 \text{ feet per second (forward speed)}$$

$$\alpha = 2.5 \text{ degrees (disc angle of attack)}$$

$$NW = 6 \text{ (number of revolutions of wake)}$$

$$\sigma = 0.7 \text{ (wake advance)}$$

Realizing that the differences in the computed airloads for the  $\mu = 0.26$  flight condition from the two wake-geometry inputs were only slight, it was decided to carry out a similar comparison for a slower ( $\mu = 0.08$ ) flight condition. For this case, the induced velocity-to-forward speed ratio should be higher than for the faster flight case (with comparable disc loading). Airload predictions for this slower flight condition, therefore, would be expected to show more marked differences for one wake geometry as compared to the other.

During the wake-geometry computation, the downwash-to-forward speed ratio was found to be as high as 1.11 in certain regions toward the rear of the disc. This makes the entire calculation of the induced velocity field (and the resultant streamlines and wake geometry) suspect, since the theory was based on a linearization of the momentum equations. By way of comparison, the highest value of the downwash-to-forward speed ratio was about 0.12 for the  $\mu = 0.26$  flight condition. Thus, the degree of confidence in the computed wake geometry for the  $\mu = 0.08$  flight condition must be lower than for  $\mu = 0.26$ .

As expected, the upwash area of the disc was about the same as before, viz., a thin crescent near the leading edge and a small area behind the disc center. Many of the streamlines emanating from these regions started in the upward direction. (This did not happen in the  $\mu = 0.26$  case because the induced upwash, being truly a small perturbation to the fluid velocity, was more than compensated for by  $V_{FS} \cdot \sin \alpha$ , which is the normal (downward) component of the forward speed. For the  $\mu = 0.26$  case, not only was  $V_{FS}$  higher,

but  $\alpha$  was also somewhat larger,  $5.8^\circ$ , than the  $2.5^\circ$  for the  $\mu = 0.08$  flight.)

Figures 29 and 30 show typical wake trails for the  $\lambda = 0.08$  flight condition. The deviations from a helical wake are more prominent in this case because of the higher ratios of all the induced velocity components to the forward speed. Figure 31 shows the streamlines starting from 90% radius. The wing-tip phenomenon is again evident. (The upward-starting streamlines mentioned above are not noticeable in this picture because the leading edge crescent with large induced upwash was located outboard of about 92% radius, and the upwash region behind the center of the disc extended only up to about 50% radius.) This rolling-up-of-the-tip-vortex effect is more clearly seen in Figures 32 through 35, which show the progressive distortion of an originally circular fluid contour released from 90% radius, one through four rotor revolutions after release, respectively.

Figures 36 and 37 show plots of the unsteady parts of the airloads and bending moments, respectively, for  $\mu = 0.08$ . It can be seen that the airload predictions from the two different wake geometries differ significantly. The airload predictions from the UR wake seem to be in better agreement with experiment in the region around  $90^\circ$  azimuth. While the rest of the azimuthal positions show the airload histories to be qualitatively similar, the increase in higher harmonic content with the UR wake seems clear. This is emphasized in the blade response in Figure 37.

The wake-induced velocity at the 75% radius, when the blade is at  $\psi = 75^\circ$ , is found to be 14.17 fps, and the total normal velocity at that point is +55.81 fps. Thus, for this slower flight condition, the wake-induced velocity is, as expected, a more significant fraction of the normal velocity experienced at the blade section.

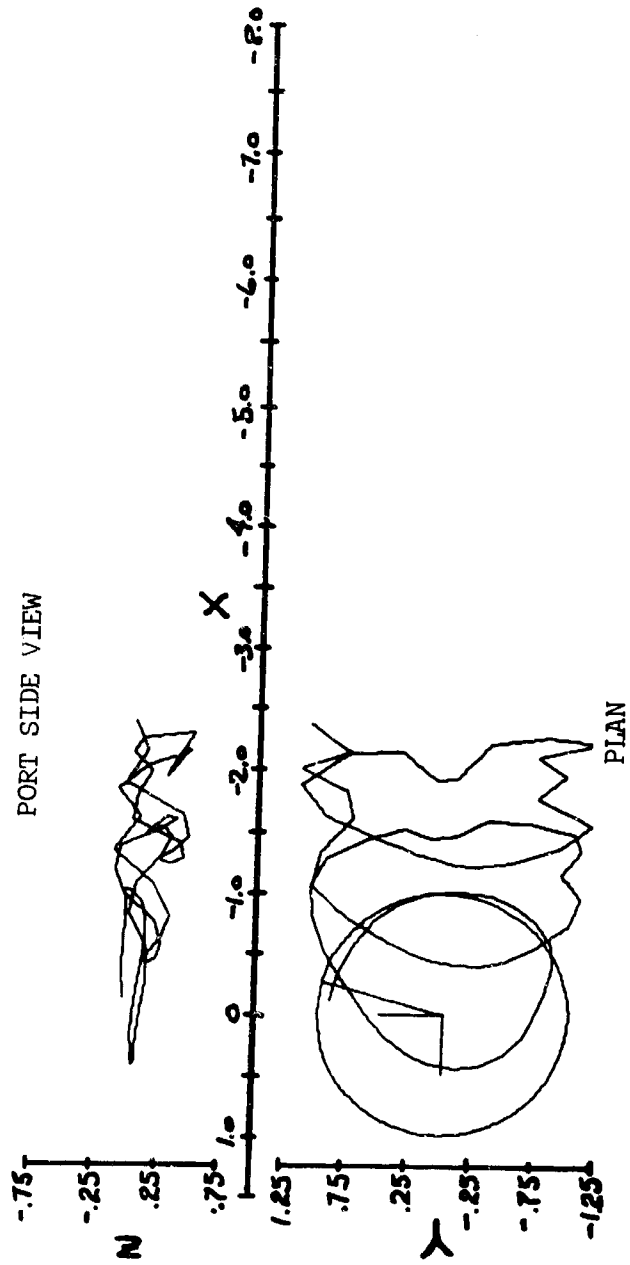


Figure 29. Typical Instantaneous Geometry of a Wake Trail (UH-1,  $\mu = 0.08$ ,  $N_b = 1$ , Blade at  $\psi = 75^\circ$ ).

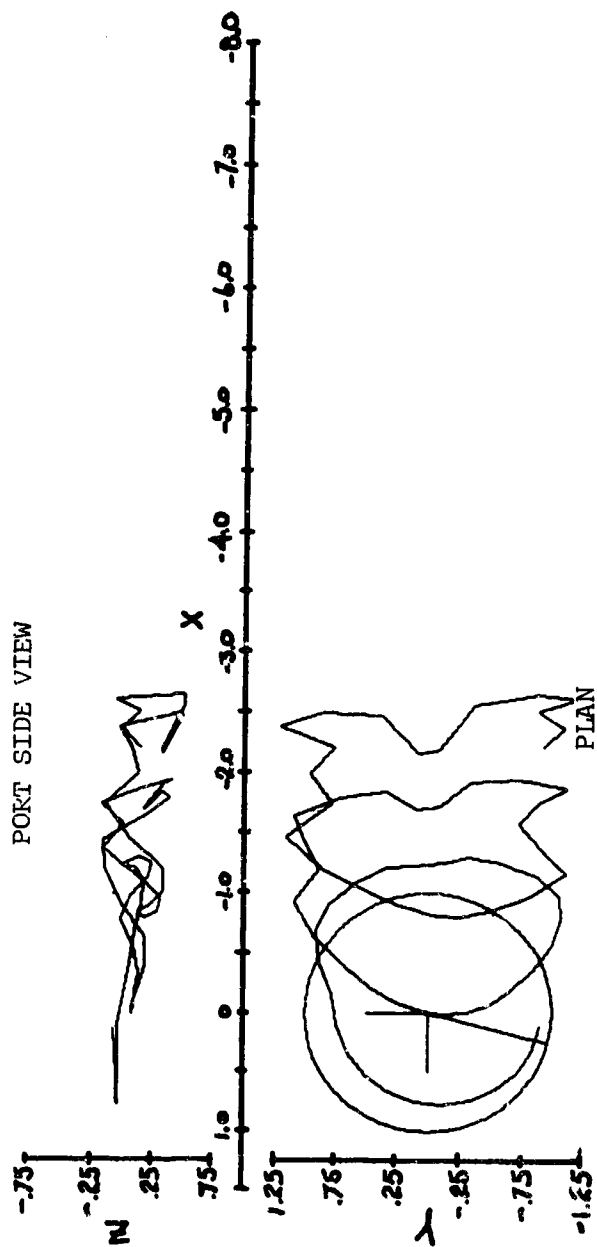


Figure 30. Typical Instantaneous Geometry of a Wake Trail (UH-1,  $\mu = 0.08$ ,  $N_b = 1$ , Blade at  $\psi = 255^\circ$ ).

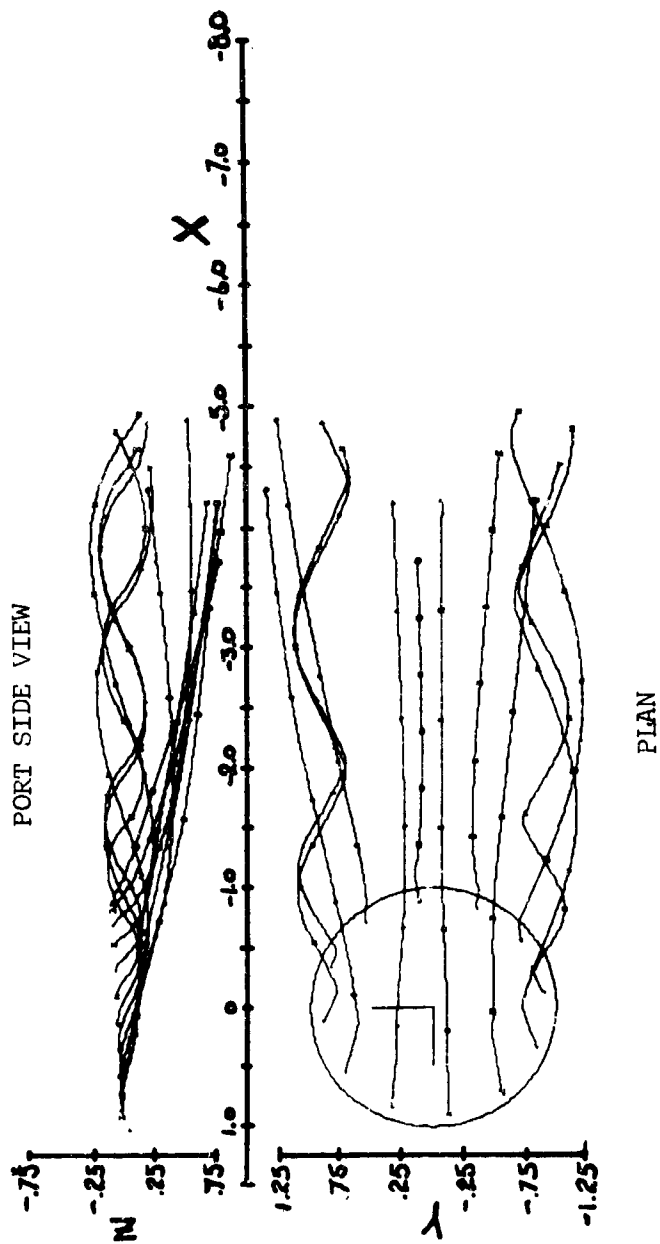


Figure 31. Geometry of Streamlines in the Steady Flow Field (UH-1,  $\mu = 0.08$ ).

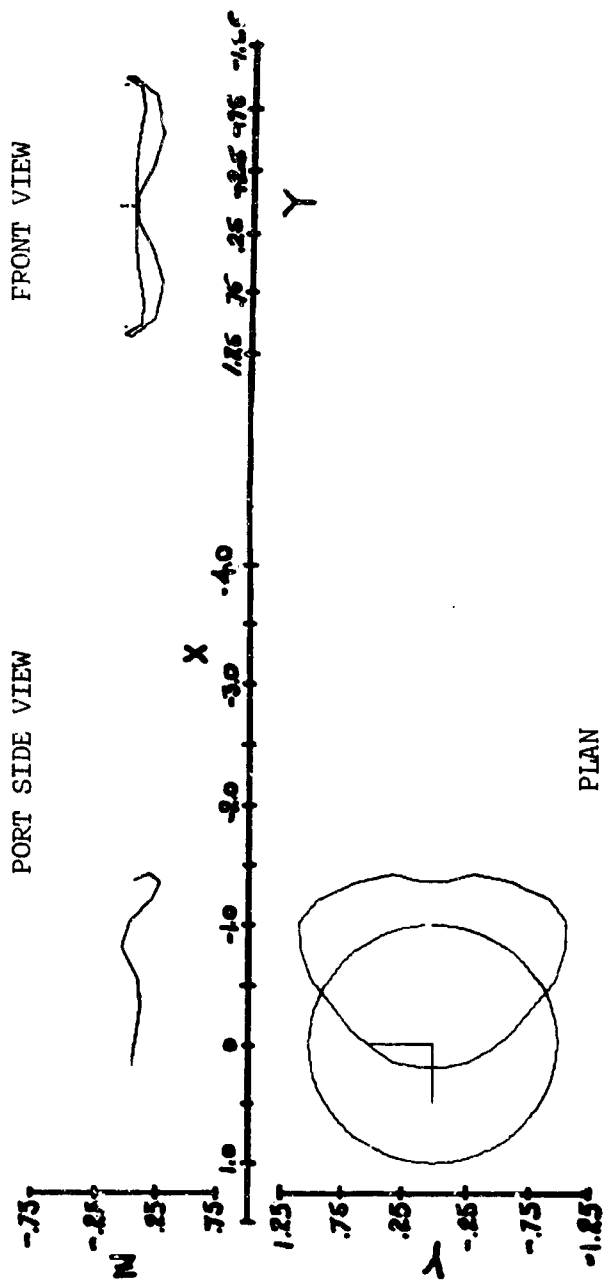


Figure 32. Three Views of a Fluid Contour, Released From 90% Radius on the Disc, One Rotor Revolution After Release (UH-1,  $\mu = 0.08$ ).

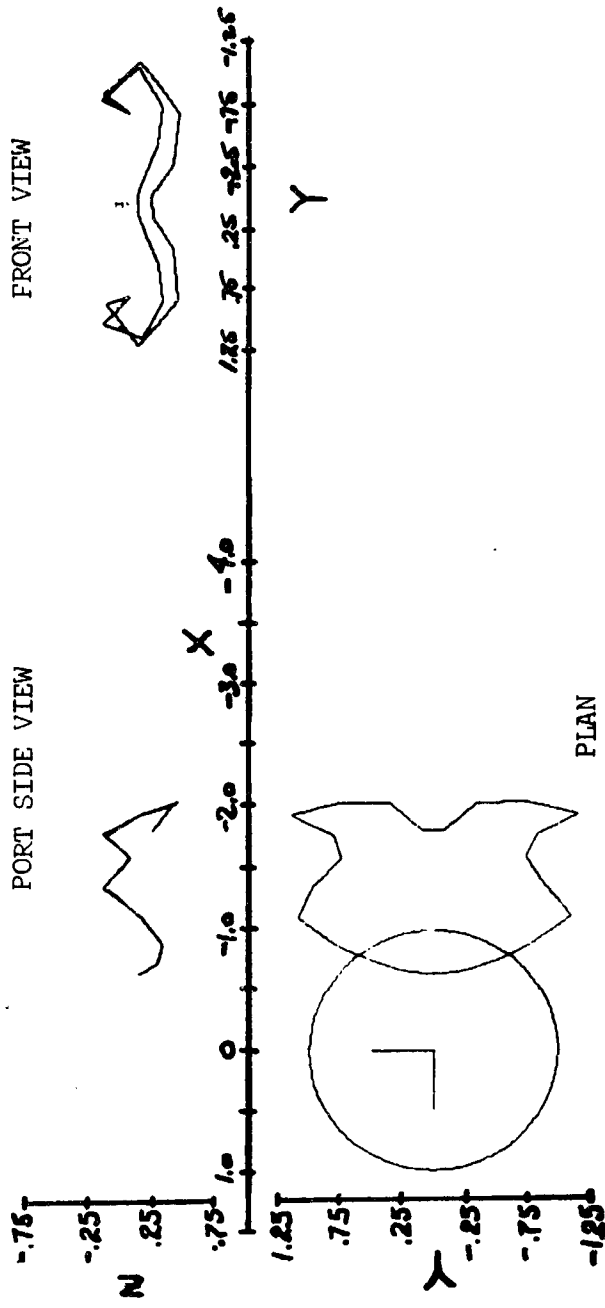


Figure 33. Three Views of a Fluid Contour, Released From 90% Radius on the Disc, Two Rotor Revolutions After Release (UH-1,  $\mu = 0.08$ ).

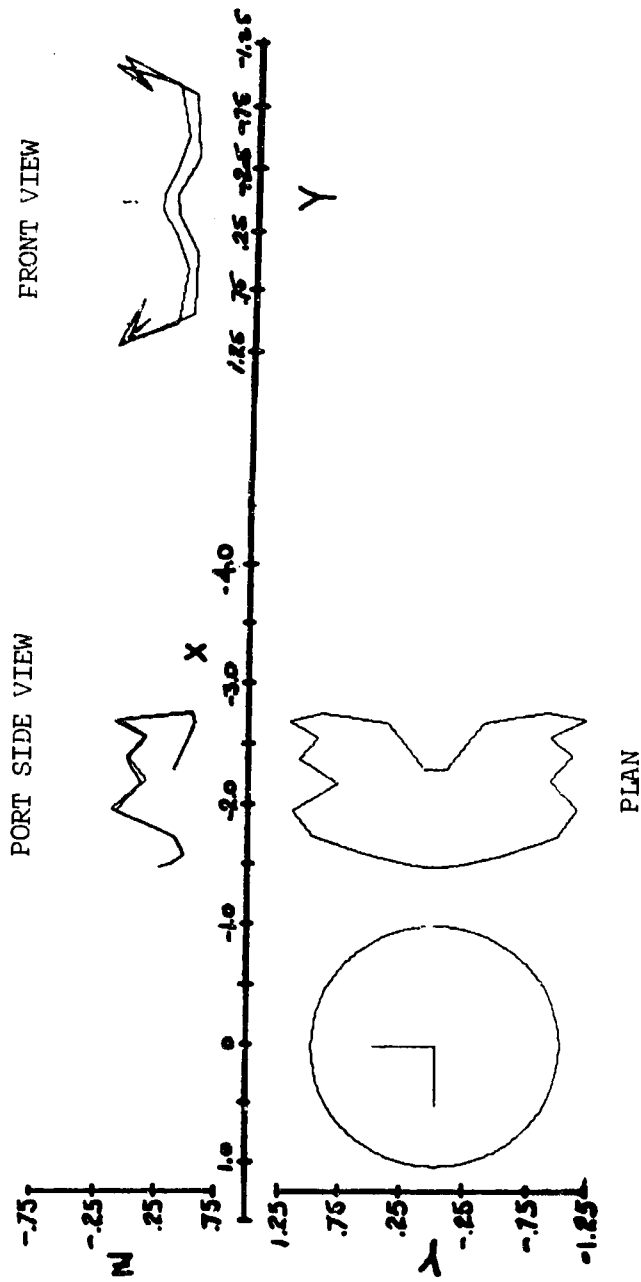


Figure 34. Three Views of a Fluid Contour, Released From 90% Radius on the Disc, Three Rotor Revolutions After Release (UH-1,  $\mu = 0.08$ ).

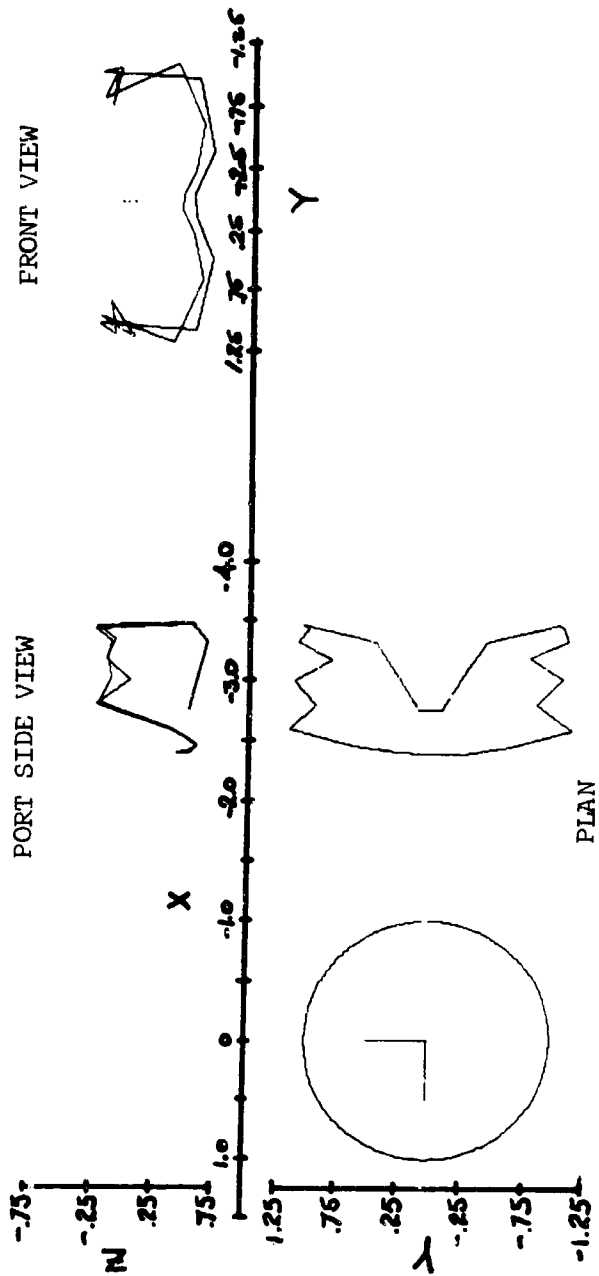


Figure 35. Three Views of a Fluid Contour, Released From 90% Radius on the Disc, Four Rotor Revolutions After Release ( $UH-1 \mu = 0.08$ ).

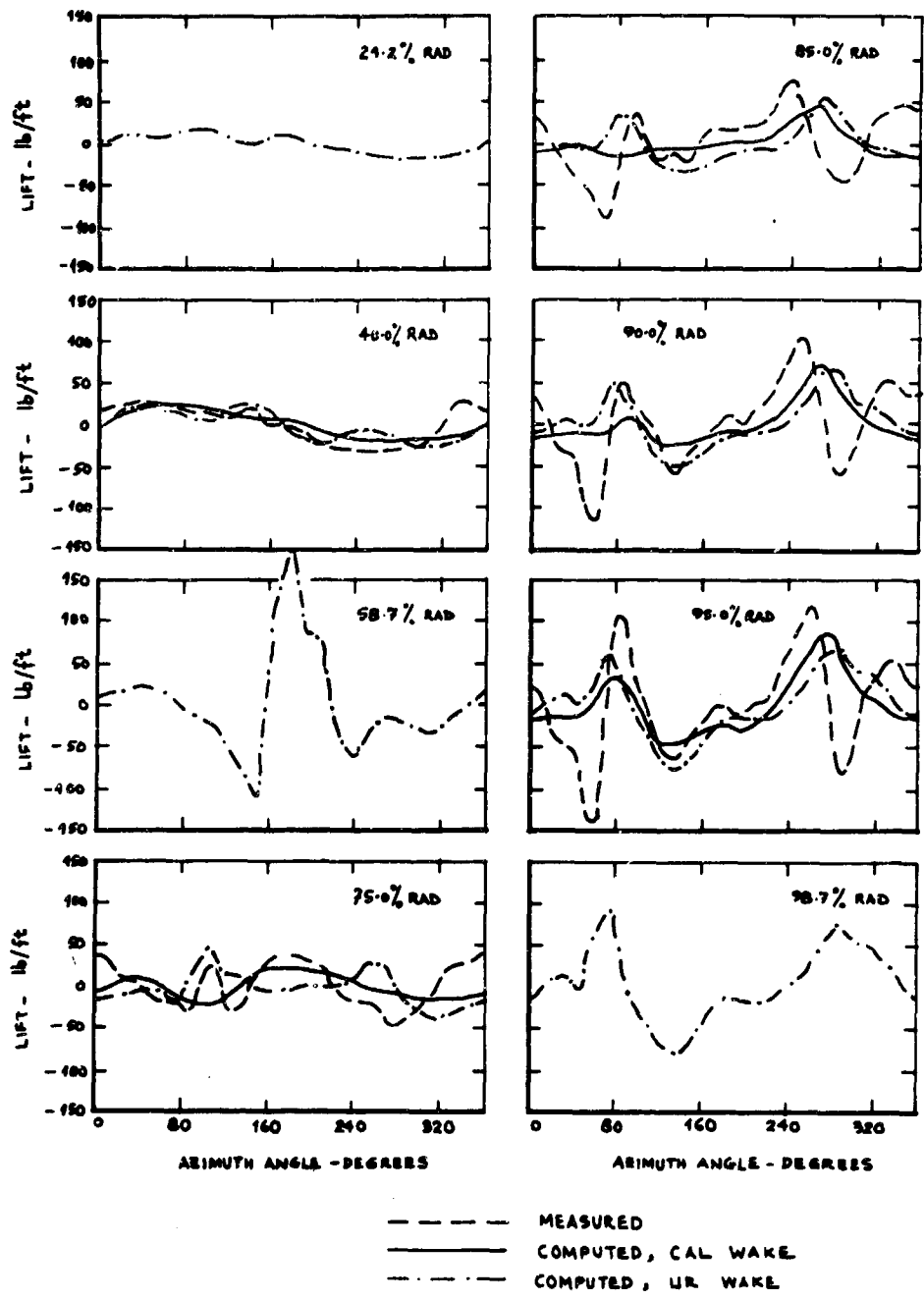


Figure 36. Time Histories of the Unsteady Parts of Measured and Computed Airloads (UH-1,  $\mu = 0.08$ ).

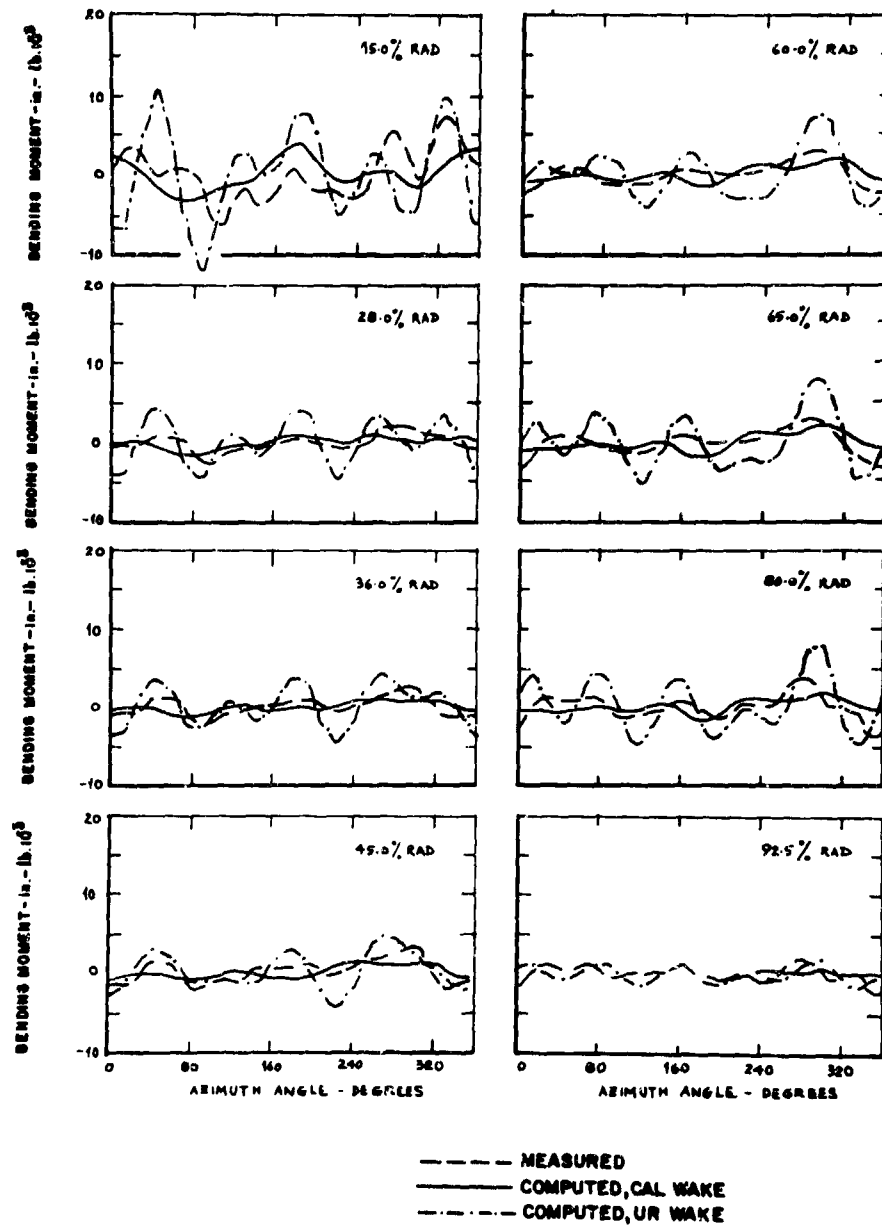


Figure 37. Time Histories of the Unsteady Parts of Measured and Computed Blade-Flapwise Bending Moments (UH-1,  $\mu = 0.08$ ).

## CHAPTER 5

### CONCLUSIONS AND POSSIBILITIES FOR FURTHER WORK

The wake-geometry computations reported in Chapter 4 show that the flow field behind a lifting actuator disc features tip vortices similar to those from a lifting wing.

The computed airloads for the  $\mu = 0.26$  flight condition of the UH-1 teetering rotor seem to be less sensitive to wake geometry than are those for the  $\mu = 0.08$  flight condition. This is indicated by the slight differences between the airload predictions resulting from two different wake geometries (CAL rigid helical wake and UR distorted wake) for the  $\mu = 0.26$  condition and by the significant differences between similar predictions for the  $\mu = 0.08$  condition. The accuracy of the UR-computed wake geometry for the slower ( $\mu = 0.08$ ) flight condition is questionable because of applying linearized equations to an inapplicable amplitude regime. Still, the airload predictions of the blade-loads program, even if this wake geometry input is considered "arbitrary", are useful in providing some insight as to the differences which will result from wake-geometry differences.

This stronger sensitivity to wake geometry in the case of a slower flight condition calls for some quantitative discussion. As suggested near the end of Chapter 4, the wake-induced velocity in the case of the  $\mu = 0.08$  condition forms a more significant fraction of the normal velocity experienced by the blades. This suggests an examination of the variation of contributions due to wake effects and those due to all other effects.

The faster flight condition certainly has larger contributions from the geometric pitch input and of the blade flapping to the total normal velocity at the blades. Thus, for example, at the 85% radial station, the collective pitch was 0.2011 rad at  $\mu = 0.26$ , as compared to 0.1209 rad at  $\mu = 0.08$ . The amplitude of the cyclic pitch input was 0.1195 rad at  $\mu = 0.26$ , as compared to 0.04 rad at  $\mu = 0.03$ . Similarly, the amplitude of the first azimuthal harmonic component of the displacement in the rigid flapping of the teetering blade (normalized on tip deflection) was 0.6096 at  $\mu = 0.26$ , as compared to 0.1830 at  $\mu = 0.08$ . At the rotor speed of 33 rad/sec, this flapping component results in a maximum flapping velocity of 20.1 fps at  $\mu = 0.26$ , as compared to 6.04 fps at  $\mu = 0.08$ .

The corresponding quasi-steady bound vorticity strength  $I_K$  comparisons (see Figure 14 and equation (109) ) for the 85% radial station are (sq ft/Sec):

steady component 331.3 ( $\mu = 0.26$ ) as compared to 249.9 ( $\mu = 0.08$ )  
 first harmonic 158.3 ( $\mu = 0.26$ ) as compared to 75.34 ( $\mu = 0.08$ )  
 second harmonic 33.2 ( $\mu = 0.26$ ) as compared to 8.9 ( $\mu = 0.08$ )  
 third harmonic 28.91 ( $\mu = 0.026$ ) as compared to 13.75 ( $\mu = 0.08$ )

These values show that in the case of the faster flight condition, the variations in the quasi-steady bound vorticity are larger. This same point is illustrated in another way in Table IV, which compares the contributions of the two terms on the right-hand side of equation (109). The ratio of the influences of the quasi-steady and wake-induced quantities on the bound vorticity is quite high for the first two harmonic variations at  $\mu = 0.26$ , but not so in the case of  $\mu = 0.08$ . For the 3rd, 4th, and 5th harmonics, the ratio is smaller at either value of  $\mu$ , because there are no cyclic variations in  $\alpha_g$  or  $V_g$  above the 1st harmonic, and the blade flapping displacements are smaller in harmonic components above the 2nd.

TABLE IV. COMPARISON OF CONTRIBUTIONS OF THE QUASI-STEADY AND WAKE-INDUCED QUANTITIES TO THE BOUND VORTICITY STRENGTH COMPONENTS AT THE 85% RADIAL STATION, UH-1, $\mu = 0.26$ AND $\mu = 0.08$		
The Ratio	$\frac{I_K}{T_K} : \frac{\sum \sigma_{Hj} \Gamma_j}{T_K}$	(See Equation (109) )
Harmonic Component	$\mu = 0.26$	$\mu = 0.08$
Steady	1.17: -0.17	1.16: -0.16
1st harmonic	1.34: -0.34	2.7: -1.7
2nd harmonic	1.25: -0.25	0.497: 0.503
3rd harmonic	1.76: -0.76	2.94: -1.94
4th harmonic	0.684: 0.316	0.157: 0.843
5th harmonic	0.204: 0.796	3.59: -2.59

As regards the amount of wake vorticity remaining close to the blades, Figures 21, 29, and 30 show how much more rapidly the distance between a given blade and the wake increases for the higher speed case. The strength of the wake vorticity, of course, also enters these considerations, but this is a more complex and less influential variable as regards the effects of forward speed.

It can therefore be concluded that the relative insensitivity of the blade loads to wake geometry in the case of the faster flight condition ( $\mu = 0.26$ ) is due mainly to (1) the wake being blown away relatively quickly and (2) a predominance of the cyclic pitch input, tangential velocity variation, and blade flapping displacements in the total time-varying aerodynamic environment at the blade sections.

It may be noted that all the computations reported here pertained to the UH-1 two-bladed teetering rotor. It would probably be worthwhile to carry out similar comparative airload computations for a fully articulated rotor such as the four-bladed Sikorsky H-34. This might facilitate comparisons of the importance of blade displacements, cyclic pitch and tangential velocity variations and wake-induced effects. Since the H-34 has four blades, there will be more wake vorticity near the disc, and hence wake geometry could be more influential than it seemed in the  $\mu = 0.25$  case for the UH-1. If this does seem worthwhile, the wake computation can be repeated using the converged blade loads to establish the time-average pressure field which is the basic input to the UR wake geometry determination.

If the UR wake-computing program is to be extensively used with the CAL BLP2, considerable saving in running time could be achieved by writing the UR wake geometry onto a temporary direct-access data set at the beginning of subroutine SUB14 (see Figure 19) and reading it from this data set instead of repeatedly reading it sequentially from TAPE8.

As alluded to earlier, a fundamental difficulty exists in the work reported here. Linearizing the equations of motion on the basis of disturbance velocities being small compared to forward speed means that the wake computations will be more reliable, for a given tip speed, at the higher advance ratios. On the other hand, since we are using an assumed steady pressure field for calculating the paths of particles which are really unsteady, sufficient time must elapse to allow an averaging of the unsteady effects to take place. Thus, the streamline positions--and the wake geometry obtained therefrom--will be most realistic (in the case of a finite number of blades) only when each vorticity element leaving the blades is subjected to the effect of a large number of blade passages. For a given number of blades and a given tip speed, this calls for a small advance ratio  $\mu$ . Put another way, the method explored here will be most accurate for a lightly loaded rotor (i.e., low thrust per disc area) with many blades at high forward speed and high tip speed. Like all other rotor vortex aerodynamic theories, the results will reflect changes in vortex strength and position only when the number of blades is sufficiently high to leave vortices close to succeeding

blades and yet low enough to keep the strength of the vortices from becoming too low. The scope of this research has not allowed definition of these limits, if in fact they exist. It has suggested, however, that wake details are important for tip speed ratios of 0.1 and below, and are unimportant at around  $\mu = 0.25$  and above.

#### LITERATURE CITED

1. Prandtl, L., and Tietjens, O. G., APPLIED HYDRO-AND-AERO-MECHANICS, Dover Publications, 1957, p. 210.
2. Piziali, R. A., A METHOD FOR PREDICTING THE AERODYNAMIC LOADS AND DYNAMIC RESPONSE OF ROTOR BLADES, Cornell Aeronautical Laboratory, Inc.; USAAVLABS Technical Report 65-74, U.S. Army Aviation Materiel Laboratories, Fort Eustis, Virginia, January 1966, AD 628583.
3. Bisplinghoff, R. L., Ashley, H., and Halfman, R. L. AERO-ELASTICITY, Addison-Wesley Publishing Co., Inc., Reading, Massachusetts, 1957, pp. 213-217.
4. Karman, Theodore von, AERODYNAMICS, McGraw-Hill Book Company, Inc., New York, 1957, p. 45.
5. Panofsky, W. K. H., and Phillips, Melba, CLASSICAL ELECTRICITY AND MAGNETISM, Addison-Wesley Publishing Company, Inc., Reading, Massachusetts, 1962, p. 125.
6. Landau, L. D., and Lifshitz, E. M., FLUID MECHANICS, Addison-Wesley Publishing Company, Inc., Reading, Massachusetts, 1959, p. 8.
7. Lamb, Horace, HYDRODYNAMICS, Dover Publications, New York, 1945, pp. 203-204.
8. Payne, P. R., HELICOPTER DYNAMICS AND AERODYNAMICS, Pitman and Sons Ltd., London 1959, Chapter 2.
9. Kinner, W. DIE KREISFORMIGE TRAGFLACHE AUF POTENTIALTHEORETISCHER GRUNDLAGE, Ingenieur-Archiv, VIII Band, 1937.
10. Mangler, K. W., CALCULATION OF THE INDUCED VELOCITY FIELD OF A ROTOR, Royal Aircraft Establishment Report, No. Aero. 2247 1948.
11. Glauert, H., AIRPLANE PROPELLERS, Aerodynamic Theory, edited by W. F. Durand, Dover Publications, New York, 1935, Chapter X Division L, Vol. IV.
12. Wood, E. R., and Hermes, M. E., ROTOR INDUCED VELOCITIES IN FORWARD FLIGHT BY MOMENTUM THEORY, presented at AIAA/AHS VTOL Research, Design, and Operations Meeting, Atlanta, Georgia, February 1969.

13. Tararine, S., EXPERIMENTAL AND THEORETICAL STUDY OF LOCAL INDUCED VELOCITIES OVER A ROTOR DISC FOR ANALYTICAL EVALUATION OF THE PRIMARY LOADS ACTING ON HELICOPTER ROTOR BLADES, European Research Office, U. S. Army Contract, October 1960.
14. Scheimann, James, A TABULATION OF HELICOPTER ROTOR-BLADE DIFFERENTIAL PRESSURES, STRESSES, AND MOTIONS AS MEASURED IN FLIGHT, NASA TMX-952, March 1964.
15. Burpo, F. B., et al, MEASUREMENT OF DYNAMIC AIRLOADS ON A FULL-SCALE SEMIRIGID ROTOR, TCREC Technical Report 62-42, December 1962.
16. Lenman, August F., MODEL STUDIES OF HELICOPTER ROTOR FLOW PATTERNS, USAAVLABS Technical Report 68-17, April 1968.
17. Gray, Robin B., EXPERIMENTAL SMOKE AND ELECTROMAGNETIC ANALOG STUDY OF INDUCED FLOW FIELD ABOUT A MODEL ROTOR IN STEADY FLIGHT WITHIN GROUND EFFECT, NASA TND-458, August 1960.
18. Crimi, Peter, PREDICTION OF ROTOR WAKE FLOWS, presented at CAL/USAAVLABS Symposium, Buffalo, New York, June 1966.
19. Chang, T. T., A METHOD FOR PREDICTING THE TRIM CONSTANTS AND THE ROTOR-BLADE LOADINGS AND RESPONSES OF A SINGLE-ROTOR HELICOPTER, Cornell Aeronautical Laboratory, Inc.; USAAVLABS Technical Report 67-71, U.S. Army Aviation Materiel Laboratories, Fort Eustis, Virginia, November 1967, AD 666802.
20. Rabbott, John P., and Paglino, Vincent M., AERODYNAMIC LOADING OF HIGH SPEED ROTORS, presented at CAL/USAAVLABS Symposium, Buffalo, New York, June 1966.
21. Loewy, Robert G., Smyers, D. J., and Gabel, R., A REVIEW OF THEORETICAL AND EXPERIMENTAL INVESTIGATIONS OF THE ROTOR AERODYNAMIC PROBLEM, Vertol Division, Boeing Airplane Company Report No. R-217, October 1960.
22. Sokolnikoff, I. S., TENSOR ANALYSIS, Second Edition, John Wiley & Sons, Inc., New York, 1964, p. 268.
23. Whittaker, E. T., and Watson, G. N., A COURSE OF MODERN ANALYSIS, Fourth Edition, Cambridge University Press, 1965, p. 324.
24. Robin, Louis, FONCTIONS SPHERIQUES DE LEGENDRE ET FONCTIONS SPHEROIDALES, Gauthier-Villars, Paris, 1957.

APPENDIX I

ASSOCIATED FUNCTIONS OF LEGENDRE AND SOME OF THEIR PROPERTIES\*

I-1 Legendre Functions of the First Kind,  $P_n(z)$

$$P_0(z) = 1$$

$$P_1(z) = z$$

$$P_2(z) = \frac{1}{2}(3z^2 - 1)$$

$$P_3(z) = \frac{z}{2}(5z^2 - 3)$$

Particular values:

$$P_n(0) = \begin{cases} \frac{(-1)^{\frac{n}{2}} (n-1)!!^{**}}{2^{\frac{n}{2}} \cdot (\frac{n}{2})!} & \dots n \text{ even} \\ 0 & \dots n \text{ odd} \end{cases}$$

$$P_n(1) = 1$$

Asymptotic values for  $|z| \rightarrow \infty$ :

$$P_n(z) \sim \frac{(2n-1)!!}{n!} z^n$$

\* Reference 24.

\*\*  $(2n-1)!! \triangleq 1 \cdot 3 \cdot 5 \cdot \dots \cdot (2n-1)$ , with  $(-1)!! \triangleq 1$ . (Schuster's notation).

I-2 Legendre Functions of the Second Kind,  $Q_n(z)$

For  $z$  outside the segment  $(-1, +1)$ :

$$Q_0(z) = \frac{1}{2} \log \frac{z+1}{z-1}$$

$$Q_1(z) = \frac{z}{2} \log \frac{z+1}{z-1} - 1$$

$$Q_2(z) = \frac{1}{4} (3z^2 - 1) \log \frac{z+1}{z-1} - \frac{3}{2} z$$

$$Q_3(z) = \frac{z}{4} (5z^2 - 3) \log \frac{z+1}{z-1} - \frac{1}{6} (15z^2 - 4)$$

For  $-1 < z < +1$ , replace  $\log \frac{z+1}{z-1}$  in the above formulas by  $\log \frac{1+z}{1-z}$ .

Particular values for  $\epsilon \rightarrow 0$  ( $\epsilon > 0$ ):

$$Q_n(1+\epsilon) \sim \frac{1}{2} \log \frac{2}{\epsilon}$$

Asymptotic values for  $|z| \rightarrow \infty$ :

$$Q_n(z) \sim \frac{n!}{(2n-1)!!} \cdot \frac{1}{z^{n+1}}$$

(Note: from the above formulas,  $Q_n(i\eta)$  take the forms:

$$Q_0(i\eta) = -i \tan^{-1} \frac{1}{\eta}$$

$$Q_1(i\eta) = \eta \tan^{-1} \frac{1}{\eta} - 1$$

$$Q_2(i\eta) = \frac{1}{2} (3\eta^2 + 1) \tan^{-1} \frac{1}{\eta} - \frac{3}{2} i\eta$$

$$Q_3(i\eta) = -\frac{7}{2} (5\eta^2 + 3) \tan^{-1} \frac{1}{\eta} + \frac{5}{2} \eta^2 + \frac{2}{3}$$

and the values on the disc ( $\eta=0$ ) are:

$$Q_1(i0) = -1$$

$$Q_3(i0) = \frac{2}{3}$$

I-3 Associated Functions of Legendre of the First Kind,  $P_n^m(z)$

For  $-1 < z < 1$  :

$$P_n^m(z) \triangleq (-1)^m (1-z^2)^{m/2} \frac{d^m P_n(z)}{dz^m} \quad (\text{Hobson's notation})$$

$$P_1^1(z) = -\sqrt{1-z^2}$$

$$P_2^1(z) = -3z\sqrt{1-z^2}$$

$$P_3^1(z) = -\frac{3}{2}z(5z^2-1)\sqrt{1-z^2}$$

$$P_4^1(z) = -\frac{5}{2}z(7z^2-3)\sqrt{1-z^2}$$

$$P_2^2(z) = 3(1-z^2)$$

$$P_3^2(z) = 15z(1-z^2)$$

For  $z$  outside the segment  $(-1, +1)$ , replace  $(-1)^m \cdot (1-z^2)^{m/2}$  in the above formulas by  $(z^2-1)^{m/2}$

Particular values:

$$P_n^m(0) = \begin{cases} (-1)^{\frac{n+m}{2}} \cdot \frac{(n+m-1)!!}{2^{\frac{n-m}{2}} \cdot (\frac{n-m}{2})!} & \dots (n-m) \text{ even} \\ 0 & \dots (n-m) \text{ odd} \end{cases}$$

For  $\epsilon \rightarrow 0 (\epsilon > 0)$ :

$$P_n^m(1-\epsilon) = (-1)^m \cdot \frac{(n+m)!}{m!(n-m)!} \cdot \left(\frac{\epsilon}{2}\right)^{m/2}$$

$$P_n^m(1+\epsilon) = \frac{(n+m)!}{m!(n-m)!} \cdot \left(\frac{\epsilon}{2}\right)^{m/2}$$

Asymptotic values for  $|z| \rightarrow \infty$ :

$$P_n^m(z) \sim \frac{(2n-1)!!}{(n-m)!} \cdot z^n$$

I-4 Associated Functions of Legendre of the Second Kind,  $Q_n^m(z)$

For  $z$  outside the segment  $(-1, +1)$ :

$$Q_n^m(z) \triangleq (z^2-1)^{m/2} \cdot \frac{d^m Q_n(z)}{dz^m}$$

$$Q_1^1(z) = \frac{1}{2} \sqrt{z^2-1} \log \frac{z+1}{z-1} - \frac{z}{\sqrt{z^2-1}}$$

$$Q_2^1(z) = \frac{3}{2} z \sqrt{z^2-1} \log \frac{z+1}{z-1} - 3 \sqrt{z^2-1} - \frac{1}{\sqrt{z^2-1}}$$

$$Q_3^1(z) = \frac{3}{4} (5z^2-1) \sqrt{z^2-1} \log \frac{z+1}{z-1} - \frac{15}{2} z \sqrt{z^2-1} - \frac{z}{\sqrt{z^2-1}}$$

$$Q_4^1(z) = \frac{5}{4} z (7z^2-3) \sqrt{z^2-1} \log \frac{z+1}{z-1} - \frac{5}{6} (21z^2-2) \sqrt{z^2-1} - \frac{1}{\sqrt{z^2-1}}$$

$$Q_2^2(z) = \frac{3}{2} (z^2-1) \log \frac{z+1}{z-1} - 3z + \frac{2z}{z^2-1}$$

$$Q_3^2(z) = \frac{15}{2} z (z^2-1) \log \frac{z+1}{z-1} - 15z^2 + 10 + \frac{2}{z^2-1}$$

For  $-1 < z < +1$ , replace the multiplicative factor  $(z^2-1)^{m/2}$  in the above formulas by  $(-1)^m (1-z^2)^{m/2}$ ; and replace  $\log \frac{z+1}{z-1}$  by  $\log \frac{1+z}{1-z}$ .

Particular values for  $\epsilon \rightarrow 0$ , ( $\epsilon > 0, m > 0$ ):

$$Q_n^m(1+\epsilon) \sim (-1)^m \cdot 2^{m/2-1} \cdot \frac{(m-1)!}{\epsilon^{m/2}}$$

Asymptotic values for  $|z| \rightarrow \infty$ :

$$Q_n^m(z) \sim (-1)^m \cdot \frac{(n+m)!}{(2n+1)!!} \cdot \frac{1}{z^{n+1}}$$

Note: From the above formulas,  $Q_n^m(i\eta)$  take the forms:

$$Q_1^1(i\eta) = \sqrt{1+\eta^2} \tan^{-1} \frac{1}{\eta} - \frac{\eta}{\sqrt{1+\eta^2}}$$

$$Q_2^1(i\eta) = 3i\eta \sqrt{1+\eta^2} \tan^{-1} \frac{1}{\eta} - 3i\sqrt{1+\eta^2} + \frac{i}{\sqrt{1+\eta^2}}$$

$$Q_3^1(i\eta) = -\frac{3}{2}(5\eta^2+1)\sqrt{1+\eta^2} \tan^{-1} \frac{1}{\eta} + \frac{15}{2}\eta \sqrt{1+\eta^2} - \frac{\eta}{\sqrt{1+\eta^2}}$$

$$Q_4^1(i\eta) = -\frac{5}{2}i\eta(7\eta^2+3)\sqrt{1+\eta^2} \tan^{-1} \frac{1}{\eta} + \frac{5}{6}i(21\eta^2+2)\sqrt{1+\eta^2} + \frac{i}{\sqrt{1+\eta^2}}$$

$$Q_2^2(i\eta) = 3i(1+\eta^2) \tan^{-1} \frac{1}{\eta} - 3i\eta - \frac{2i\eta}{1+\eta^2}$$

$$Q_3^2(i\eta) = -15\eta(1+\eta^2) \tan^{-1} \frac{1}{\eta} + 15\eta^2 + 10 - \frac{2}{1+\eta^2}$$

and the values on the disc ( $\eta = 0$ ) are:

$$Q_2^1(i0) = -2i$$

$$Q_4^1(i0) = \frac{8}{3}i$$

$$Q_3^2(i0) = 8$$

I-5 Some Properties of the Associated Functions of Legendre,  
 $P_n^m(z)$  and  $Q_n^m(z)$

$$P_n^m(-z) = (-1)^{m+n} P_n^m(z)$$

$$Q_n^m(-z) = (-1)^{m+n+1} Q_n^m(z)$$

Orthogonality

$$\int_0^1 P_n^m(z) P_{n'}^m(z) dz = 0 \quad \text{for } n \neq n'$$

$$\int_0^1 P_n^m(z) P_n^{m'}(z) \frac{dz}{1-z^2} = 0 \quad \text{for } m \neq m'$$

Normalization

$$\int_0^1 [P_n^m(z)]^2 dz = \frac{1}{2} \int_{-1}^1 [P_n^m(z)]^2 dz = \frac{1}{2n+1} \cdot \frac{(n+m)!}{(n-m)!}$$

$$\int_0^1 [P_n^m(z)]^2 \frac{dz}{1-z^2} = \frac{1}{2} \int_{-1}^1 [P_n^m(z)]^2 \frac{dz}{1-z^2} = \frac{1}{2m} \cdot \frac{(n+m)!}{(n-m)!}$$

Differentiation

$$\frac{dP_n^m(z)}{dz} = \frac{nz}{z^2-1} P_n^m(z) - \frac{n+m}{z^2-1} P_{n-1}^m(z)$$

For  $z$  outside the segment  $(-1, +1)$ ,

$$\frac{dQ_n^m(z)}{dz} = \frac{nz}{z^2-1} Q_n^m(z) - \frac{n+m}{z^2-1} Q_{n-1}^m(z)$$

$$\therefore \frac{dQ_n^m(i\eta)}{d\eta} = \frac{n\eta}{1+\eta^2} Q_n^m(i\eta) + \frac{(n+m)i}{1+\eta^2} Q_{n-1}^m(i\eta)$$

APPENDIX II

FORTRAN IV SOURCE LISTINGS

	<u>Page</u>
Subroutine SUB14 (as modified at UR) . . . . .	107
Subroutine RWAKE . . . . .	118
Subroutine COEFS . . . . .	127
Subroutine STMLN . . . . .	137
Subroutine VLCTS . . . . .	145
Subroutine CHAMP . . . . .	150
Subroutine FRWRD . . . . .	155
Subroutine ADVNC . . . . .	159
Subroutine CRSNG . . . . .	162
Subroutine VAREMT . . . . .	166
Mainprog RWAKEPIC . . . . .	167
Mainprog RSLTSPLT . . . . .	180

\* \* \* \* \*  
 \* SUBROUTINE SUB14 \*  
 \* (AS MODIFIED AT U R) \*  
 \* \* \* \* \*

\*\*\*SUB14

SUBROUTINE SUB14

DIMENSION DUMMY(2500)

DIMENSION RE(11),SCE(11),SIDF(11),WZ(11),NC(4,11),WS(4,11),A(250)  
 1,SCM2(10),SCE15(11),SILFM(10),GNPSI(4,25),SNPSI(4,25),M(275)  
 DIMENSION UMNZO(6)

ADTNBYUR

COMMON

RM(10) ,SCM(10) ,AB(250) ,  
 XI(151,11) ,ETA(151,11) ,  
 XM(10) ,YM(10) ,ZM(10) ,  
 DX(10) ,DY(10) ,SGDR(10) ,  
 SZ(10,250) ,SI(10,250) ,  
 S3(10,250) ,TZ(10,25) ,  
 T2(10,25) ,T3(10,25) ,  
 CPSI(25) ,SPSI(25)

COMMON

WMEAN ,MKAUV ,ILSTRT,IAZ ,NRPL ,NTV ,DLTV ,ULRV ,  
 DELX ,VFSAT ,DT ,DSTRT ,NA ,I ,IB ,  
 JB ,KT ,ZNIS ,ZN2S ,ZNS3 ,FPI ,AM ,  
 AN ,BM ,BN ,CC1 ,CC4 ,CC7 ,CC10 ,  
 RA ,KB ,AA5 ,AA3 ,XVZ ,XV1 ,XV3 ,  
 IRTR ,IBN ,IMN ,IST2 ,DMPRAD,IVZ ,TV1 ,TV2 ,  
 TV3 ,SVZ ,SV1 ,SV2 ,SV3 ,KAZ ,ISW4 ,  
 ESW5 ,KA ,DPRUD ,NB ,NR ,NSV ,NRA ,  
 NMAP1 ,FNA ,PI ,TPI ,ZNL ,NAUB ,  
 UMEGR ,KTRAD ,BLDRAD,AZER ,ZNL ,ZNS ,VF ,  
 XONTM ,ISW3 ,ISWT

COMMON

XUOFR(25,151),YUOFR(25,151),ZUOFR(25,151),VNRML(12,25)  
 ADTNBYUR

```

COMMON      EM(6),EN(6),QMNZ(6),PMN(6),QMN(6),CPN(6),DMN(6)      AUTNBYUR
COMMON      DPMN(6),ULMN(6),PMN1(6),GMN1(6),RUMNO(4),TITLE(14)    AUTNBYUR
COMMON      FMT3(12),XDISK(12,25),YDISK(12,25),ZDISK(12,25),FMT4(12)AUTNBYUR
COMMON      UDISK(12,25),VDISK(12,25),WDISK(12,25),IISW,JJSW      ADTNBYUR
COMMON      KASH,LL,M,MSSH,M,SM,XINJN,YINJN,ZINJN,JRAD,JZER,JPTSL  ADTNBYUR
COMMON      AR,LIH,LOUT,LTAP2,LTAP4,LTAP8,IHRCL,IMNCL,ISCOL      ADTNBYUR
COMMON      XUP,XMAX,JINC,BLUG,FINC,PSIND,TINC,JMAX,AMUD,PSIO     ADTNBYUR
COMMON      PSIO,AMU,ATA,PSI,EPS,X,Y,Z,XP,ZP,RP,UVEL,VVEL,MVEL,P,I ADTNBYUR
COMMON      TIME,JPT,JINC,KTAG,KFMD,KRVS,DPDY,DPOZ                ADTNBYUR
COMMON      MEPSUL,PULD,UULD,VOLD,WOLD,TOLD,TIMOL,KULE            ADTNBYUR
COMMON      XULU,YULD,ZOLL,XPULD,ZPOLU,AMUOL,ATAOL,PSIOL,EPSOL    ADTNBYUR
COMMON      XSAVE,YSAVE,ZSAVE,USAVE,VSAVE,WSAVE,AMUSV,ATASV,PSISV ADTNBYUR
COMMON      EPSSV,PSAVE,MEPSV,NW,MEPS,RNDM,ALDEG,ALPHA,COSAL,SINAL ADTNBYUR

```

```

EQUIVALENCE (SZ,DUMMY)

```

```

EQUIVALENCE ( DUMMY(1),RE), ( DUMMY(12),SCE), ( DUMMY(23),STDFE),
1 ( DUMMY(34),WZ), ( DUMMY(45),WC), ( DUMMY(89),WS),
2 ( DUMMY(133),A), ( DUMMY(383),SCM2), ( DUMMY(393),SCE15),
3 ( DUMMY(404),STDFM), ( DUMMY(414),CNPSI),
4 ( DUMMY(514),SNPSI), ( DUMMY(614),W)
EQUIVALENCE (OR,BLURAD),(VF,VFS),(AT,ALDEG),(ATR,ALPHA)
EQUIVALENCE (AMUD,AMUC),(QMNZO(1),QMNZO(1)),(PSIO,PSIO)

```

```

COMMON      REMIND 2      AUTNBYUR
COMMON      REMIND 4      RMVDBYUR
COMMON      READ(5,5) ISW1,ISW2,ISW3,ISW4,ISW5,ISWT      RMVDBYUR
COMMON      FORMAT(14) ISW1,ISW2,ISW3,ISW4,ISW5,ISWT,KKSW,LLSW,MMSW,NNSW ADTNBYUR
COMMON      REAG(5,5) ISW1,ISW2,ISW3,ISW4,ISW5,ISWT,KKSW,LLSW,MMSW,NNSW ADTNBYUR
COMMON      FORMAT(1214)
10 READ(5,15) VA,VB,VR,NSV,NTV,NW,IDSRT,WKADY,DLRV,DLTV,WMEAN,VF,
15 FORMAT(14/16E12.4)

```

```

COMMON      WRITE(6,62) ISW1,ISW2,ISW3,ISW4,ISW5,ISWT,NA,NS,NR,NSV,NTV,NW,
COMMON      WRITE(6,62) ISW1,ISW2,ISW3,ISW4,ISW5,ISWT,KKSW,LLSW,MMSW,NNSW,

```



```

45 READ(5,35)(STDFF(J),J=1,NRPI)
WRITE(6,82)(STDFF(J),J=1,NRPI)
82 FORMAT(/IX,17HSTDFF(J),J=1,NRPI/IX,(15F8.3))

50 READ(5,35)(WZ(J),J=1,NRPI)
86 WRITE(6,88)(WZ(J),J=1,NRPI)
88 FORMAT(/IX,14HWZ(J),J=1,NRPI/IX,(15F8.3))
55 READ(5,35)(WC(N,J),J=1,NRPI),N=1,4)
92 WRITE(6,93)(WC(N,J),J=1,NRPI),N=1,4)
93 FORMAT(/IX,23HWC(N,J),J=1,NRPI),N=1,4)
READ(5,35)(WS(N,J),J=1,NRPI),N=1,4)
98 WRITE(6,101)(WS(N,J),J=1,NRPI),N=1,4)
101 FORMAT(/IX,23HWS(N,J),J=1,NRPI),N=1,4/IX,(11F8.3))

```

```

IF (CWA.EQ.U.U) WRITE(6,104) (A(KD),KD=1,NRA)
104 FORMAT(1HU,14HA(KD),KD=1,NRA/IH,(11F8.3))
NSV = NSV + 1

```

```

NADJ=NA/ND
FNA = FLOAT(NA)
MKAMI=MKADV-1.0
GSTKT=FLOAT(IDSTRT)-1.0-MKADV
NMAP1=NW*NA+1
PI=3.14159265
TPI=2.0*PI
FPI=4.0*PI
AFR = AT* PI/180.0
COSAL=COS(ALPHA)
SINAL=SIN(ALPHA)
LPSI=TPI/FNA
UMEGR=DEGA*TP I/60.0
GT=LPSI/UMEGR
VFSAT = VF * SIN(AIK)

```

\*\*\*\*\*CWA

AUTNBYSUR  
AUTNBYSUR

```
DELX = VF* COS(ATR)*DT  
RTRAG=RE(I)  
BLDRAD=RE(NRPI)
```

C

```
DO 169 J=1, NR  
JPI=J+1  
RM(J)=(RE(J)+RE(JPI))/2.0  
SCM(J)=(SCE(J)+SCE(JPI))/2.0  
SCDR(J) = SCM(J)/(RE(JPI) - RE(J))  
SCMD2(J)=SCM(J)/2.0  
STDFM(J)=(STDFE(J)+STDFE(JPI))/2.0
```

169 CONTINUE

```
DO 171 J=1, NRPI  
SCE15(J)=1.5*SCE(J)
```

171 CONTINUE

C

```
174 DO 194 KA=1, NA  
KDT=(KA-1)*NR  
LO 190 J=1, NR  
KD=KDT+J
```

```
AB(KD)=A(KD)*SCM(J)
```

190 CONTINUE

194 CONTINUE

C

```
DO 243 KA=1, NA
```

```
XC=(FLOAT(KA)+KAMI)/FNA
```

204 DO 241 N=1, 4

```
ARG = ( AMOD( ( FLOAT(N)* XC), 1.0) ) * TPI
```

222 CNPSI(N,KA)=COS(ARG)

```
SNPSI(N,KA)=SIN(ARG)
```

```
IF (ABS(CNPSI(N,KA)) .LE. 0.010) CNPSI(N,KA) = 0.0
```

```
IF (ABS(SNPSI(N,KA)) .LE. 0.010) SNPSI(N,KA) = 0.0
```

241 CONTINUE

243 CONTINUE

C





```

IWR = 1
340 DO 436 IBN=1,NB
C   AZ POSITION NO OF THIS BLADE.
   KA= ITR+(IRN-1)*NADK
344 DO 350 KT=1,NK
   XM(KT)=RM(KT)*CPSI(KA)+SCM2(KT)*SPSI(KA)
   YM(KT)=RM(KT)*SPSI(KA)-SCM2(KT)*CPSI(KA)
   ZM(KT)=STDFM(KT)
   LX(KT)=-SCM(KT)*SPSI(KA)
   DY(KT)=SCM(KT)*CPSI(KA)
350 CONTINUE
C
352 WRITE(4)(XM(KT),YM(KT),ZM(KT),DX(KT),DY(KT),KT=1,NR)
C
353 IF(ISM2) 382,354,382
354 WRITE(6,384) ITR,IBN,(XM(KT),YM(KT),ZM(KT),DX(KT),DY(KT),KT=1,NR)
384   FORMAT(15HOROTOR POS. NO.13/41X,9HBLADE NO.12,27H MIDCHD. COORLS.
      1, LX, AND DY/(10E12.4))
C
356 DO 410 IWN=1,NH
C
C   PRESENT AZ POSITION NO. OF BLADE WHICH IS GENERATING THIS WAKE IWN.
   IAZ= ITR+(IWN-1)*NADK
360 DO 366 J=1,NRPI
   XI(I,J)=RE(J)*CPSI(IAZ)+SCB15(J)*SPSI(IAZ)
   ETA(I,J)=RE(J)*SPSI(IAZ)-SCB15(J)*CPSI(IAZ)
   ZETA(I,J)=STDFE(J)
366 CONTINUE
C
370 GO TO (370,509,509,509),MMSH
C
C   CALL COORD(2,NSV,1,NRPI)
   GO TO 510

```

\*\*\*\*ISM2

\*\*\*\*MFSW  
AUTNBYUR

AUTNBYUR





```

402 WRITE(6,404)I,N,NV,((XI(I,J),ETA(I,J),ZETA(I,J),J=1,NTV),
11=N,V,NWAPI)
404 FORMAT(1HU          47X,31HTRL. VTX. COURDS. OF BLADE NO. I3,3X,
14HNIV=I3/I3,(9F14.4))
C 410 CONTINUE
C
IWR1 = 2
GG TO 434
C 420 DO 430 IMN=1,NB
READ(2) ((XI(I,J),ETA(I,J),ZETA(I,J),I=1,NSV),J=1,NRPI)
WRITE(4)((XI(I,J),ETA(I,J),ZETA(I,J),I=1,NSV),J=1,NKPI)
READ(2) ((XI(I,J),ETA(I,J),ZETA(I,J),I=NSV,NWAPI),J=1,NTV)
WRITE(4)((XI(I,J),ETA(I,J),ZETA(I,J),I=NSV,NWAPI),J=1,NTV)
430 CONTINUE
434 REMIND 2
436 CONTINUE
450 CONTINUE
C
REMIND 4
REMIND 2
RETURN
END

```

\*\*\*SUP14

```

C      * * * * *
C      * SUBROUTINE RWAKE *
C      * * * * *
C
C COMMENT      SUBROUTINE RWAKE STARTS HERE.
C
C      ***RWAKE
C
C SEQUENTIALLY GENERATES THE ARRAYS XUOFR(JAZER,JPTSL),
C XUOFR(JAZER,JPTSL) AND ZUOFR(JAZER,JPTSL) ; FOR THE NUMBER
C NMBRDS(=NR+1+NTV) RADIAL STATIONS.
C WRITES THIS INFO. ON TAPE8. ALSO WRITES XDISK,YDISK,ZDISK,UDISK,
C VDISK,AND WDISK AT ALL DISK POINTS ((JRAD,JAZER),JRAD=1,NMBRDS),
C JAZER=1,NA) ON TAPE8.
C
C XUOFR(JAZER,JPTSL) IS THE X-COORDINATE OF POSITION NO. JPTSL ON THE
C STREAMLINE, I.E., THIS PARTICLE WAS SHED FROM THE PARTICULAR RADIAL
C POSITION WHEN THE SHEEDING BLADE WAS AT AZIMUTHAL POSITION NO. JAZER.
C THAT WAS (JPTSL-L-BLUG) TIME INTERVALS BEFORE THIS PARTICLE REACHED
C THIS POSITION.
C
C THIS SUBROUTINE WILL BE CALLED ONLY IF MMSM = 3 OR 4.
C
C      M O D E   O P T I O N S
C
C KCSW  1  SUBROUTINE COEFS BYPASSED THIS TIME. THE VALUES OF THE
C          COEFFICIENTS CMN(J) AND DMN(J) REMAIN THE SAME AS FOR THE
C          PREVIOUS PASS.
C      2  CMN(J) AND DMN(J) SUPPLIED AS INPUT.
C      3  C01,C03,C12,D12 COMPUTED FROM CT,CMR,CMP.
C      4  C01,C03,C12,D12 COMPUTED FROM DR,RHG,VFS,IT,ROLMG,P1MG.
C      5  C01,C03,C12,D12,C23,D23 COMPUTED FROM DR,RHO,VFS,FPMZC,FPACI

```

C FPM2, FPM2, FPM2. (AVERAGE MOMENTUM CONDITION SATISFIED.)  
 C C01, C03, C12, D12, C14, D14, C23, D23 COMPUTED FROM DR, RHU, VFS, RC,  
 C PIMOM, ROLMO, FPM20, FPM21, FPM22, FPM23, FPM24, FPM25, FPM26, FPM27, FPM28, FPM29, FPM30,  
 C ( AVERAGE MOMENTUM CONDITION NOT SATISFIED.)  
 C C01, C03, C12, D12, C14, D14, C23, D23 COMPUTED FROM DR, RHU, VFS AND THE  
 C STEADY, FIRST HARMONIC AND SECOND HARMONIC COMPONENTS OF THE  
 C SPANWISE LIFT DENSITY (IN LBMT/IN ) AT 40, 75, 85, 90 AND 95  
 C PER CENT RADIUS. APPLICABLE FOR HU-1.  
 C ( AVERAGE MOMENTUM CONDITION SATISFIED.)  
 C C01, C03, C12, D12, C14, D14, C23, D23 COMPUTED FROM DR, RHU, VFS, RC,  
 C PIMOM, ROLMO AND THE LIFT DENSITY COMPONENTS IN 7 ABOVE.  
 C APPLICABLE FOR HU-1.  
 C ( AVERAGE MOMENTUM CONDITION NOT SATISFIED.)  
 C CURNELL WAKE GEOMETRY USED IN THIS RUN.  
 C U OF R WAKE GEOMETRY, WHICH WAS GENERATED IN A PREVIOUS RUN,  
 C WAS USED IN THIS RUN. HENCE SUBROUTINE WAKE WAS NOT CALLED.  
 C SUBROUTINE COORD WAS NEVER CALLED IN THIS RUN.  
 C U OF R WAKE GEOMETRY WAS GENERATED. JOB WAS TERMINATED ON  
 C RETURN FROM SUBROUTINE WAKE. THUS, GENERATION OF THE LIFT  
 C DATASET WAS THE SOLE PURPOSE OF THIS RUN.  
 C U OF R WAKE GEOMETRY WAS GENERATED AND USED IN THIS RUN.  
 C HENCE, SUBROUTINE WAKE WAS CALLED. SUBROUTINE COORD WAS  
 C NEVER CALLED IN THIS RUN.  
 C VELOCITIES AT POINTS IN THE WAKE WERE COMPUTED USING THE  
 C INCORRECT FORMULA, WHICH IGNORED THE UX AND OY DISPLACEMENTS.  
 C STREAMLINES WERE INITIATED FROM THE FLAT DISK, THUS IGNORING  
 C THE STEADY DEFLECTIONS STDFF(J).  
 C AN INTEGRATION FROM 'INFINITY' WAS PERFORMED EACH TIME THE  
 C VELOCITIES AT A POINT IN THE WAKE WERE COMPUTED.  
 C STREAMLINES WERE INITIATED FROM THE FLAT DISK, THUS IGNORING  
 C THE STEADY DEFLECTIONS STDFF(J).  
 C STREAMLINES WERE INITIATED FROM ABOVE THE FLAT DISK WHICH IS  
 C STILL THE PRESSURE-DISCONTINUITY SURFACE. THUS, THE STEADY  
 C DEFLECTIONS STDFF(J) OF THE BLADES WERE ACCOUNTED FOR.

MMSW

NNSW

C ( ANSWERS ONLY IF THE U OF R MAKE GEOMETRY IS COMPUTED ;  
 C I.E., ONLY IF MMSW = 3 OR 4. )  
 C  
 C  
 C

C SUBROUTINE KWANK  
 C  
 C \*\*SOURCE

C DIMENSION DUMPY(2500)  
 C  
 C DIMENSION RL(11),SCE(11),SIDEF(11),WZ(11),WC(4,11),KS(4,11),A(250)  
 C ,SC(2(10),SCE15(11),STDFK(10),CNPSI(4,25),SNPSI(4,25),M(275)  
 C DIMENSION QMNZO(6)

C COMMON RM(10) ,SCM(10) ,AB(250) ,  
 C XI(151,11) ,ETA(151,11) ,  
 C XM(10) ,YM(10) ,ZM(10) ,  
 C UX(10) ,UY(10) ,SCDR(10) ,  
 C SZ(10,250) ,S1(10,250) ,S2(10,250) ,  
 C S3(10,250) ,T2(10,25) ,T1(10,25) ,  
 C T2(10,25) ,T3(10,25) ,FMT(12) ,  
 C LPSI(25) ,SPSI(25) ,

C COMMON NMEAN ,WKADV ,IDSTRT,IAZ ,NRPI ,NTV ,DLTV ,DLRV ,  
 C LELA ,VFESAT ,DT ,USTRT ,NA ,I ,J ,IB ,  
 C JB ,KT ,ZNIS ,ZM2S ,ZM3S ,FPI ,AL ,AM ,  
 C AV ,BL ,BM ,BN ,CC1 ,CC4 ,CC7 ,CC10 ,  
 C RA ,RB ,AA5 ,AA6 ,XVZ ,XVI ,XV2 ,XV3 ,  
 C IRTK ,IBN ,IMN ,IST2 ,DMPRAD ,TVZ ,TV1 ,TV2 ,  
 C TV3 ,SV7 ,SV1 ,SV2 ,SV3 ,KAZ ,KA3 ,KSW4 ,  
 C ISW3 ,KA ,DPRDS ,NB ,NR ,NSV ,NRA ,  
 C NMAP1 ,FVA ,PI ,IPI ,ZNI ,ZNS ,ZNF ,  
 C OMEGR ,RTKAL ,BLDKAU ,AZER ,ISW3 ,ISW1 ,VF ,  
 C XNFTM

COMMON XUPFR(25,151),YUJFR(25,151),ZUFR(25,151),VNRML(12,25)  
 COMMON EM(6),QNZ(6),PMN(6),QMN(6),CMN(6),DMN(6)  
 COMMON DPMN(6),QMN(6),PMNM(6),QNM(6),RUNNO(4),TITLE(14)  
 COMMON FMT3(12),XDTSK(12,25),YDTSK(12,25),ZDTSK(12,25),FMT4(12)  
 COMMON ULTSK(12,25),VDTSK(12,25),WDTSK(12,25),IISW,JJSW  
 COMMON KKSX,LLSW,MHSH,NNSW,XINJN,YINJN,ZINJN,JRAD,JAZER,JPTSL  
 COMMON AK,LR,LJPT,LTAP2,LTAP4,LTAP8,IHR0L,IMN0L,ISG0L  
 COMMON XUP,XMAX,NINC,BLJLG,FINC,PSIND,TINC,JMAX,AMUO,PSIO  
 COMMON PSIDU,AMU,ATA,PSI,EPS,X,Y,Z,XP,ZP,RP,UVEL,VVEL,WVEL,P,T  
 COMMON TIME,JPT,JINC,KTAG,KFWD,KRVS,DPDY,DPDZ  
 COMMON MAPSOL,POLD,UBLD,VOLD,HOLD,TOLD,TIMOL,KOLD  
 COMMON XCLB,YOLD,ZOLD,XPOLD,ZPOLD,AMUOL,ATAOL,PSIOL,EPSOL  
 COMMON XSAVE,YSAVE,ZSAVE,USAVE,VSAVE,WSAVE,AMUSV,ATASV,PSISV  
 COMMON EPSSV,PSAVE,MEPSV,NW,MEPS,RNDM,ALDEG,ALPHA,COSAL,SINAL

EQUIVALENCE (SZ,DUMPY)

EQUIVALENCE ( DUMMY(1),RE), ( DUMMY(12),SCE), ( DUMMY(23),STDFE),  
 1 ( DUMMY(34),WZ), ( DUMMY(45),MC), ( DUMMY(89),WS),  
 2 ( DUMMY(133),A), ( DUMMY(383),SCMD2), ( DUMMY(393),SCE15),  
 3 ( DUMMY(404),STDFM), ( DUMMY(414),CNPSI),  
 4 ( DUMMY(514),SNPSI), ( DUMMY(614),M)  
 EQUIVALENCE (DR,BLDRAD),(VF,VFS),(AT,ALDEG),(ATR,ALPHA)  
 EQUIVALENCE (AMUO,AMUO),(CMNZU(1),QMNZO(1)),(PSIO,PSIO)

EM(1)=0.  
 EM(2)=0.  
 EM(3)=1.  
 EM(4)=1.  
 EM(5)=2.  
 EM(6)=0.

FN(1)=1.

```
EN(2)=3.  
EN(3)=2.  
EN(4)=4.  
FN(5)=3.  
EN(6)=0.
```

C

```
QMNZO(1)=-1.  
QMNZO(2)=2./3.  
QMNZO(3)=2.  
QMNZO(4)=-8./3.  
QMNZO(5)=8.  
QMNZO(6)=0.
```

C

C

C

C

NING IS THE NUMBER OF INCREMENTS PER AZIMUTHAL POSITION.

122

```
1201 READ(5,1201)XUP,XMAX,NINC,BLDLG,XQNTM  
1201 FORMAT(IX,F4.1,6X,F4.1,6X,I3,7X,F5.3,7X,F7.4)
```

C

```
AR=VFS/(DR*OMEGR)  
RN=FLOAT(NB)  
FNINC=FLOAT(NINC)  
PSIND=360./(FNA*FNINC)  
TINC=AK*PI/(FNA*FNINC)  
JMAX=((XUP+1.)/TINC)+FLOAT(N*API)*FNINC)*1.25
```

C

```
1202 WRITE(6,1202)XUP,XMAX,NINC,BLDLG,XQNTM,AR,PSIND,TINC,JMAX,ALDEG,  
1 ALPHA  
1202 FORMAT(///IX,' INPUTS FOR SUBROUTINE RMAKE'///6H XUP = ,F4.1,10X,  
1 7H XMAX = ,F4.1,10X,6HNINC = ,I3,10X,8HBLDLG = ,F5.3,  
1 10X,8HXQNTM = ,F7.4//5H AR = ,  
1 11.8,10X,8HPSIND = ,F10.7,10X,7HTINC = ,E15.8,10X,7HJMAX = ,  
1 14//6H ALDEG = ,F10.5,10X,7HALPHA = ,E15.8)  
1203 FORMAT(1H1)
```

```

C      CALL COEFS
C
C      REMIND 6
C
C      WRITE(8) RUNNO, TITLE, NA, NB, NR, NRPI, NW, NSV, NIV, AR, ALDEG, DR, VFS,
1      BLDLG, XUP, NINC, DLTV, DLRV, (RE(I), SCE15(I), I=L, NRPI)
C
C      DO 1204 JJRAD=L, NRPI
C      JRAD=JJRAD
C      RNDM= (SORT(RF(JRAD)*RF(JRAD)+SCE15(JRAD)*SCE15(JRAD)))/DR
C      IF (RNDM.GT.0.99) RNDM=0.99
C      AMUD=-SORT(1.-RNDM*RNDM)
C      DELTG=-ATAH(SCE15(JRAD)/RE(JRAD))
C
C      DO 1207 JJAZER=L, NA
C      JAZER=JJAZER
C
C      PSID=(TPI*(FLOAT(JAZER-1)+BLDLG)/FNA)+DELTG
1208 IF (PI-ABS(PSID))1209, 1210, 1210
1209 PSID=PSID*(1.-((PI/ABS(PSID))))
C      GO TO 1208
1210 CONTINUE
C      XP=-RNDM*COS(PSID)
C      Y=RNDM*SIN(PSID)
C      GO TO (1211, 1211, 1211, 1212), NNSW
1211 ZP=-0.1E-3
C      GO TO 1223
1212 ZP=-STDFE(JRAD)/DR
1223 CONTINUE
C      KKEND=NSV
C      CALL STMLN(KKEND)
C      GO TO 1207
1207 CONTINUE
C

```

\*\*\*\*\*NSW

```

WRITE(8) ((XUDFR(KAZER,KPTSL),YUDFR(KAZER,KPTSL),
1      ZUDFR(KAZER,KPTSL),KAZER=1,NA),KPTSL=1,NSV)
C 1214 CONTINUE
C
C      TIP INJECTIONS
C
      JRAU=NR+Z
      XNDX=(SQRT((RE(NRPI)-DLTV)*(RE(NRPI)-DLTV))+(SCE15(NRPI)*
1      SCE15(NRPI)))/DR
      IF(RNDM.GT.0.99) KNDM=0.99
      AMUO=-SQRT(1.-RNDM)*RNDM
      DELTG=-ATA/(SCE15(NRPI)/(RE(NRPI)-DLTV))
      GO TO 1213 JJAZER=1,NA
      JAZER=JJAZER
      PSIG=(TPI*(FLJAT(JAZER-1)+6LDLG)/FNA)+DELTLG
1214 IF(PI-ABS(PSIG))1215,1216,1216
1215 PSIG=PSIG*(1.-(PI/ABS(PSIG)))
      GO TO 1214
1216 CONTINUE
      XP=-RNDM*COS(PSIG)
      Y=RNDM*SIN(PSIG)
      GO TO (1224,1224,1229),NMSW
1224 ZP=-0.1E-3
      GO TO 1230
1229 ZP=-STDFE(NRPI)/DK
1230 CONTINUE
      KKEND=N*API
      CALL STMEN(KKEND)
1213 CONTINUE
C
WRITE(8) ((XUDFR(KAZER,KPTSL),YUDFR(KAZER,KPTSL),
1      ZUDFR(KAZER,KPTSL),KAZER=1,NA),KPTSL=1,NWAPI)
C
C

```

\*\*\*\*\*NSW

\*\*\*\*\*TV

```

C      GO TC (1218,1217),NTV
C      ROOT I,J,ECTIONS
C
1217  JRAU=NR+3
      RNDM=(SQRT((RE(1)+ILRV)*(RE(1)+DLRV))+(SCE15(1)*SCE15(1)))/DR
      AMJU=-SQRT(1.-RNDM*RNDM)
      DELTU=-ATAI(SCE15(1))/(RE(1)+DLRV)
      DO 1219 JJAZER=L,NA
      JAZER=JJAZER
      PSIG=(TPI*(FLJAT(JAZER-1)+BLDLG)/FNA)+DELTU
1222  IF(PI-ABS(PSIG))1220,1221,1221
1220  PSIG=PSIG*(1.-((PI/ABS(PSIG))))
      GO TO 1222
1221  CONTINUE
      XP=-KNDY*COS(PSIG)
      Y=RNDM*SIN(PSIG)
      GO TO (1233,1233,1231),NNSA
1233  ZP=-0.1E-3
      GO TO 1232
1231  ZP=-STDFE(1)/DR
1232  CONTINUE
      KKEND=NHAPI
      CALL STMLN(KKEND)
1219  CONTINUE
C
      *RIIE(8) ((KUFR(KAZER,KPTSL),YUFR(KAZER,KPTSL),
      I      ZUFR(KAZER,KPTSL),KAZER=1,NA),KPTSL=1,NHAPI)
C
1218  CONTINUE
C      NMBROS=NRPI+NTV
C      CALL VARFMT(20H(/(
      I      ,20,F4F3) ,20,NRPI,20HE12.4))

```

\*\*\*\*\*SW

```

CALL VARFMT(20H(//
1  ,20,FMT4)
,20,NMBRDS,20HE11.3))
C
WRITE(6,1225)NMBRDS,NA
1225 FORMAT(1H1////' DISTRIBUTION OF UVEL ON THE DISK.((UDISK(KRAD,KAZ
LER),KRAD=1,' ,12,' ),KAZER=1,' ,12,' ),'////)
WRITE(6,FMT4) ((UDISK(KRAD,KAZER),KRAD=1,NMBRDS),KAZER=1,NA)
WRITE(6,1226)NMBRDS,NA
1226 FORMAT(1H1////' DISTRIBUTION OF VVEL ON THE DISK.((VDISK(KRAD,KAZ
LER),KRAD=1,' ,12,' ),KAZER=1,' ,12,' ),'////)
WRITE(6,FMT4) ((VDISK(KRAD,KAZER),KRAD=1,NMBRDS),KAZER=1,NA)
WRITE(6,1227)NMBRDS,NA
1227 FORMAT(1H1////' DISTRIBUTION OF HVEL ON THE DISK.((WDISK(KRAD,KAZ
LER),KRAD=1,' ,12,' ),KAZER=1,' ,12,' ),'////)
WRITE(6,FMT4) ((WDISK(KRAD,KAZER),KRAD=1,NMBRDS),KAZER=1,NA)
WRITE(6,1228)NMBRDS,NA
1228 FORMAT(1H1////' DISTRIBUTION OF VNRML ON THE DISK.((VNRML(KRAD,KA
ZER),KRAD=1,' ,12,' ),KAZER=1,' ,12,' ),'////)
WRITE(6,FMT4) ((VNRML(KRAD,KAZER),KRAD=1,NMBRDS),KAZER=1,NA)
WRITE(8) ((UDISK(KRAD,KAZER),VDISK(KRAD,KAZER),
1  VDISK(KRAD,KAZER),UDISK(KRAD,KAZER),
2  VDISK(KRAD,KAZER),WDISK(KRAD,KAZER),
3  VNRML(KRAD,KAZER),KRAD=1,NMBRDS),KAZER=1,NA)

```

```

END FILE 8
RETURN 8
RETURN
END

```

\*\*\*KRWAKE

C \* \* \* \* \*  
 C \* SUBROUTINE COEFS \*  
 C \* \* \* \* \*

\*\*\*COEFS

SUBROUTINE COEFS  
 DIMENSION PZ0(26),PCI(26),PSI(26),PC2(26),PS2(26)  
 DIMENSION M(6),RNDMG(26),RNDMS(26),BILD(2000)  
 DIMENSION DJMHY(2500)

C DIMENSION RE(11),SCE(11),STDFE(11),MZ(11),WC(4,11),MS(4,11),A(250)  
 1,SCMD2(10),SCE15(11),STDFM(10),CNPSI(4,25),SNPSI(4,25),M(275)  
 DIMENSION QMNZO(6)

C COMMON RM(10) ,SCM(10) ,AB(250)  
 1 XI(151,11) ,ETA(151,11) ,ZETA(151,11) ,  
 2 XM(10) ,YM(10) ,ZM(10) ,  
 3 DX(10) ,DY(10) ,SCDR(10) ,  
 4 SZ(10,250) ,SI(10,250) ,S2(10,250) ,  
 5 S3(10,250) ,TZ(10,25) ,TI(10,25) ,  
 6 T2(10,25) ,T3(10,25) ,FMT(12) ,  
 7 CPSI(25) ,SPSI(25)

C COMMON WMEAN ,WKADV ,IUSTRT,IAZ ,NRPI ,NTV ,DLTV ,  
 1 DELX ,VFSAT ,DT ,DSRT ,NA ,I ,IB ,  
 2 JB ,KT ,ZMS ,ZNS ,ZNS3 ,FPI ,AM ,  
 3 AN ,BL ,BM ,BN ,CC1 ,CC4 ,CC7 ,CC10 ,  
 4 RA ,KB ,AA5 ,AA6 ,AVZ ,XV1 ,XV2 ,XV3 ,  
 5 ITR ,IBV ,IWN ,IST2 ,UMPRAD ,TVZ ,TV1 ,TV2 ,  
 6 TV3 ,SVZ ,SV1 ,SV2 ,SV3 ,KAZ ,KAZ ,KAZ ,  
 7 ISW3 ,KA ,DPRDS ,NB ,NR ,NSV ,NSV ,NSV ,  
 8 MWAP1 ,FNA ,PI ,TPI ,ZNI ,ZNI ,ZNI ,  
 9 OMEGR ,RTRAD ,BLDRAD ,AZER ,ISW3 ,ISWT ,ZNI ,  
 COMMON XJNTM ,DLRV ,  
 COMMON XUOFR(25,151),YUOFR(25,151),ZUOFR(25,151) ,VNRML(12,25)



748 FORMAT(IH+, 6SX, I2, '. THIS HAPPENED AT THE BEGINNING OF COEFS.'//)

746 CONTINUE

C

LT=U.  
LMR=0.  
LMP=U.  
RHC=U.  
IT=0.  
RULMO=0.  
PIMOM=0.  
FPMZO=0.  
FPMC1=0.  
FPPS1=U.  
FPMC2=0.  
FPM52=0.  
HC=U.  
P40ZU=0.  
P40C1=0.  
P40S1=0.  
P40C2=0.  
P40S2=0.  
P75C1=U.  
P75S1=0.  
P75C2=0.  
P75S2=U.  
P85C1=0.  
P85S1=0.  
P85C2=0.  
P85S2=0.  
P90Z0=0.  
P90C1=0.  
P90S1=0.  
P90C2=0.

```
P9052=0.  
P95ZU=0.  
P95C1=0.  
P95S1=0.  
P95C2=0.  
P95S2=0.
```

C

```
GO 712 I=1,6  
CMN(I)=0.  
CMN(I)=0.  
M(I)=EM(I)+0.05  
NN(I)=EN(I)+0.05
```

712 CONTINUE

C

```
GO TO (722,704,705,706,707,708,709,710,733,734,735,736,737,738,739  
1 ,740),KKS
```

\*\*\*\*KKS

C

```
704 DO 719 I=1,6  
719 READ(5,702) CMN(I),LMN(I)  
702 FORMAT(16X,E10.3,16X,E10.3)  
WRITE(6,711)
```

711 FORMAT(1X,55HCOEFFICIENTS CMN(I) AND DMN(I) WERE SUPPLIED AS INPUT  
1 //)

GO TO 701

C

```
705 READ(5,721) CI,CMR,UMP  
721 FORMAT(13X,F10.3,10X,E10.3,10X,E10.3)  
WRITE(6,713)
```

713 FORMAT(1X,51HTHE FOLLOWING COEFFICIENTS WERE SUPPLIED AS INPUT  
1 //)

```
715 WRITE(6,714)CI,CMR,UMP  
714 FORMAT(10X,3HCF= ,E10.3,20X,4HCMR= ,E10.3,20X,4HUMP= ,E10.3//1X,  
1 14HTHESE LEAD TO //)
```

```
CMN(1)=0.75*CI/(AR*AR)  
CMN(2)=1.125*CI/(AR*AR)
```

```

CMN(3)=-0.625*CMP*CT/(AR*AR)
DMN(3)=-0.625*CHR*CT/(AR*AR)
GO TO 701

C
706 READ(5,716)RHO,TT,ROLMO,PIMOM
716 FORMAT(19X,19.3,10X,3(4X,E10.3))
WRITE(6,717)UR,RHO,VFS,TT,ROLMO,PIMOM
717 FORMAT(1X,4)THE FOLLOWING QUANTITIES WERE SUPPLIED AS INPUT //
1 IX,3HDR= ,F6.2,11H FT, RHO= ,E9.3,18H SLUGS/CFT, VFS= ,
2 F5.1,11H FPS, TT= ,E10.3,14H LBS, ROLMO= ,E10.3,
3 15H LBFT, PIMOM= ,E10.3,5H LBFT ///IX,14H THESE LEAD TO ///
4 )
CT=TT*AR*AR/(3.141593*RHO*DR*DR*VFS*VFS)
CHR=ROLMO/(TT*DR)
CMP=PIMOM/(TT*DR)
GO TO 715

C
707 READ(5,723)RHO,FPMZ0,FPMC1,FPMZ1,FPMC2,FPMZ2
723 FORMAT(19X,E9.3/11X,E15.8/11X,E15.8,15X,E15.8/11X,E15.8,15X,E15.8)
WRITE(6,724)DR,RHO,VFS
724 FORMAT(1X,4)THE FOLLOWING QUANTITIES WERE SUPPLIED AS INPUT //
1 IX,3HDR= ,F6.2,11H FT, RHO= ,E9.3,18H SLUGS/CFT, VFS= ,
2 F5.1,4H FPS///
31 WRITE(6,730)FPMZ0,FPMC1,FPMZ1,FPMC2,FPMZ2
730 FORMAT(1X,31H STEADY FLAPPING MOMENT= ,E15.8,5H LBFT/
1 IX,31H FIRST COSINE FLAPPING MOMENT= ,E15.8,5H LBFT/
2 IX,31H FIRST SINE FLAPPING MOMENT= ,E15.8,5H LBFT/
3 IX,31H SECOND COSINE FLAPPING MOMENT= ,E15.8,5H LBFT/
4 IX,31H SECOND SINE FLAPPING MOMENT= ,E15.8,5H LBFT///
5 IX,14H THESE LEAD TO ///)
CMN(1)=16.*BN*FPMZ0/(5.*9.8696044*RHO*VFS*VFS*DR*DR)
CMN(2)=1.5*CMN(1)
CMN(3)=5.*H.*FPMC1/(16.*3.1415927*RHO*VFS*VFS*DR*DR)
DMN(3)=5.*HY*FPMZ1/(16.*3.1415927*RHO*VFS*VFS*DR*DR)
CMN(5)=-B.*FPMC2/(15.*9.8696044*RHO*VFS*VFS*DR*DR)

```



```

2 1X,6HP40C2= ,E10.3,18HLBS/IN, / P40S2= ,E10.3,7HLBS/IN /
3 1X,6HP75Z0= ,E10.3,7HLBS/IN, / P75S1= ,E10.3,7HLBS/IN /
4 1X,6HP75C1= ,E10.3,18HLBS/IN, / P75S2= ,E10.3,7HLBS/IN /
5 1X,6HP75C2= ,E10.3,18HLBS/IN, / P85S1= ,E10.3,7HLBS/IN /
6 1X,6HP85Z0= ,E10.3,7HLBS/IN, / P85S2= ,E10.3,7HLBS/IN /
7 1X,6HP85C1= ,E10.3,18HLBS/IN, / P90S1= ,E10.3,7HLBS/IN /
8 1X,6HP85C2= ,E10.3,18HLBS/IN, / P90S2= ,E10.3,7HLBS/IN /
9 1X,6HP90Z0= ,E10.3,7HLBS/IN, / P95S1= ,E10.3,7HLBS/IN /
10 1X,6HP90C1= ,E10.3,18HLBS/IN, / P95S2= ,E10.3,7HLBS/IN /
11 1X,6HP90C2= ,E10.3,18HLBS/IN, /
12 1X,6HP95Z0= ,E10.3,7HLBS/IN, /
13 1X,6HP95C1= ,E10.3,18HLBS/IN, /
14 1X,6HP95C2= ,E10.3,18HLBS/IN, /
15 1X,14HTHESE LEAD TO ///
16 FPMZ0=12.*DX*DR*(0.126672*P40Z0+0.162078*P75Z0+0.0628125*P85Z0
17 +0.045*P70Z0+0.0475*P95Z0)
18 FPMC1=12.*DX*DR*(0.126672*P40C1+0.162078*P75C1+0.0628125*P85C1
19 +0.045*P90C1+0.0475*P95C1)
20 FPM51=12.*DX*DR*(0.126672*P40S1+0.162078*P75S1+0.0628125*P85S1
21 +0.045*P90S1+0.0475*P95S1)
22 FPMC2=12.*DX*DR*(0.126672*P40C2+0.162078*P75C2+0.0628125*P85C2
23 +0.045*P90C2+0.0475*P95C2)
24 FPM52=12.*DX*DR*(0.126672*P40S2+0.162078*P75S2+0.0628125*P85S2
25 +0.045*P90S2+0.0475*P95S2)
26 GO TO 731

C
710 READ(5,728)RHU,BC,PIMOM,ROLMO,
1 P40Z0,P40C1,P40S1,P40C2,P40S2,P75Z0,P75C1,P75S1,P75C2,P75S2,
2 P85Z0,P85C1,P85S1,P85C2,P85S2,P90Z0,P90C1,P90S1,P90C2,P90S2,
3 P95Z0,P95C1,P95S1,P95C2,P95S2
718 FORMAT(19X,E9.3,14X,F5.3,7X,E10.3,6X,E10.3 /
1 (11X,E15.8/11X,F15.8,15X,E15.8/11X,E15.8,15X,E15.8))
WRITE(6,726)DR,RHU,VFS,BC,PIMOM,ROLMO
WRITE(6,732)
1 P40Z0,P40C1,P40S1,P40C2,P40S2,P75Z0,P75C1,P75S1,P75C2,P75S2,

```

```

2 P85Z0,P85C1,P85S1,P85C2,P85S2,P90Z0,P90C1,P90S1,P90C2,P90S2,
3 P95Z0,P95C1,P95S1,P95C2,P95S2
FPM/O=12.*DR*DR*(0.126672*P40Z0+0.162078*P75Z0+0.0628125*P85Z0
1 +0.045*P90Z0+0.0475*P95Z0)
FPMC1=12.*DR*DR*(0.126672*P40C1+0.162078*P75C1+0.0628125*P85C1
1 +0.045*P90C1+0.0475*P95C1)
FPMJ1=12.*DR*DR*(0.126672*P40S1+0.162078*P75S1+0.0628125*P85S1
1 +0.045*P90S1+0.0475*P95S1)
FPMC2=12.*DR*DR*(0.126672*P40C2+0.162078*P75C2+0.0628125*P85C2
1 +0.045*P90C2+0.0475*P95C2)
FPMJ2=12.*DR*DR*(0.126672*P40S2+0.162078*P75S2+0.0628125*P85S2
1 +0.045*P90S2+0.0475*P95S2)
GO TO 729

```

C  
C

```

733 CONTINUE
734 CONTINUE
735 CONTINUE
736 CONTINUE
737 CONTINUE
738 CONTINUE
739 CONTINUE
740 CONTINUE

```

WRITE(6,718)KKS

```

718 FORMAT('H1//' CALLED EXIT IN CUEFS BECAUSE KKS EXCEEDS RANGE.
CURRENT VALUE OF KKS = ',I4)
CALL EXIT

```

C  
C

```

701 IF(KSIGN.LT.0) GO TO 744

```

C

```

X0=5.
X1=11.5
X2=18.
Y1=9.5

```

```

Y2=4.5
Y1P=Y1-4.
Y2P=Y2-4.
GO 741 I=1,26
AIMI=FLOAT(I-1)
RNDMC(I)=Y1-(4.*AIMI/25.)
RNDMS(I)=Y2-(4.*AIMI/25.)
AMUZO=-SORT(1.-(AIMI*AIMI/625.))
PMN(1)=AMUZO.
PMN(2)=AMUZO*(5.*AMUZO*AMUZO-3.)/2.
PMN(3)=-3.*AMUZO*SORT(1.-AMUZO*AMUZO)
PMN(4)=-2.5*AMUZO*(7.*AMUZO*AMUZO-3.)*SORT(1.-AMUZO*AMUZO)
PMN(5)=15.*AMUZO*(1.-AMUZO*AMUZO)
PZO(I)=(CMN(1)*PMN(1)*QPNZO(I)+CMN(2)*PMN(2)*QMNZO(2))*2.
PCL(I)=(CMN(3)*PMN(3)*QMNZO(3)+CMN(4)*PMN(4)*QMNZO(4))*2.
PSI(I)=(DMN(3)*PMN(3)*QMNZO(3)+DMN(4)*PMN(4)*QMNZO(4))*2.
PC2(I)=CMN(5)*PMN(5)*QMNZO(5)*2.
PS2(I)=DMN(5)*PMN(5)*QMNZO(5)*2.
CALL SCALE(PZO,26,5.,PZUMN,SCLZO,1)
CALL SCALE(PCL,26,5.,PCLMN,SCLCL,1)
CALL SCALE(PSI,26,5.,PSIMN,SCLSI,1)
CALL SCALE(PC2,26,5.,PC2MN,SCLC2,1)
CALL SCALE(PS2,26,5.,PS2MN,SCLS2,1)
WRITE(6,743)PZOMN,SCLZO,PCLMN,SCLCL,PSIMN,SCLSI,PC2MN,SCLC2,
I PS2MN,SCLS2
743 FORMAT(//IUX,15HPRESSURE PLOTS ,//5(I5X,E10.3,IUX,E10.3)///)
GO 742 I=1,26
PZO(I)=PZO(I)+X0
PCL(I)=PCL(I)+X1
PSI(I)=PSI(I)+X1
PC2(I)=PC2(I)+X2
PS2(I)=PS2(I)+X2
CALL AXIS(X0,Y1,4HRNDM,-4,4.,270.,0.,0.25)
CALL AXIS(X0,Y1P,20HAZIMUTUALLY CONSTANT,-20,5.,0.,PZOMN,SCLZO)
CALL LINE(PZO,RVDMC,26,1,5,1)

```

NOT REPRODUCIBLE

```
CALL AXIS(X1,Y1,4HRNDM,-4,4,270,0,0,0.25)
CALL AXIS(X1,Y1P,12HFIRST COSINE,-12,5,0,0,PL1MN,SCLC1)
CALL LINE(PL1,RJDMC,26,1,5,2)
CALL AXIS(X1,Y2,4HRNDM,-4,4,270,0,0,0.25)
CALL AXIS(X1,Y2P,12HFIRST SINE,-10,5,0,0,PS1MN,SCLS1)
CALL LINE(PS1,RJDMC,26,1,5,4)
CALL AXIS(X2,Y1,4HRNDM,-4,4,270,0,0,0.25)
CALL AXIS(X2,Y1P,12HSECOND COSINE,-13,5,0,0,PC2MN,SCLC2)
CALL LINE(PL2,RJDMC,26,1,5,3)
CALL AXIS(X2,Y2,4HRNDM,-4,4,270,0,0,0.25)
CALL AXIS(X2,Y2P,12HSECOND SINE,-11,5,0,0,PS2MN,SCLS2)
CALL LINE(PS2,RJDMC,26,1,5,5)
Y0=Y1P-3.
Y1=Y0-0.6
Y2=Y1-0.6
Y2P=Y2-0.3
CALL SYMBOL(X0,Y0,0.21,RUN40,0,0,16)
CALL SYMBOL(X0,Y1,0.14,47HCOMPONENTS OF PRESSURE-DIFFERENTIAL ON 1
1HF WISK,0,47)
CALL SYMBOL(X0,Y2,0.14,32H NONDIMENSIONALIZED ON TWICE THE,0,32)
CALL SYMBOL(X0,Y2P,0.14,30H FREE-STREAM DYNAMIC PRESSURE,0,30)
CALL PLOT(30,0,0,-3)
C 744 CONTINUE
C
C 720 I=1,0
720 WRITE(6,703) M(I),NN(I),I,PMN(I),M(I),NN(I),I,DMN(I)
703 FORMAT(10X,1HC,21I,1H=,4HC,MN(I,2H)=,E10.3,10X,1HD,21I,1H=,
1 4HDMN(I,2H)=,E10.3)
722 RETURN
END
```

\*\*\*COEFS

```

* * * * *
* SUBROUTINE SIMLN *
* * * * *

```

\*\*\*SIMLN

SUBROUTINE SIMLN(KEND)

DIMENSION DUMMY(2500)

DIMENSION RE(11),SCE(11),STOFE(11),STOFE(11),WZ(11),MC(4,11),MS(4,11),A(250)  
 1,SCMD2(10),SCE15(11),STLFM(10),CNPSI(4,25),SNPSI(4,25),M(275)

DIMENSION QPNZ(6)

COMMON RM(10) ,SCM(10) ,AB(250)  
 1 XI(151,11) ,CTA(151,11) ,  
 2 XM(10) ,YM(10) ,ZM(10) ,  
 3 UX(10) ,UY(10) ,SCDR(10) ,  
 4 SZ(10,250) ,SI(10,250) ,S2(10,250) ,  
 5 S3(10,250) ,TZ(10,25) ,T1(10,25) ,  
 6 T2(10,25) ,T3(10,25) ,FMT(12) ,  
 7 LPSI(25) ,SPSI(25)

COMMON WMEAN ,WKADV ,IUSTRT,IAZ ,NRPI ,NTV ,DLTV ,DLRV ,  
 1 DELX ,VFSAF ,DT ,USTRT ,NA ,J ,IB ,  
 2 JH ,KT ,ZN15 ,ZN25 ,ZN35 ,FPI ,AL ,AM ,  
 3 AV ,DL ,BF ,BN ,CCI ,CC4 ,CC7 ,CC10 ,  
 4 RA ,RB ,AA5 ,AA6 ,XVZ ,XV1 ,XV2 ,XV3 ,  
 5 IRTK ,IBN ,IWN ,IST2 ,DMPRAD ,IVZ ,TV1 ,TV2 ,  
 6 TV3 ,SVZ ,SV1 ,SV2 ,SV3 ,KAZ ,KA3 ,ISM4 ,  
 7 ISW5 ,KA ,DPRD5 ,NB ,NK ,NSV ,NSA ,NRA ,  
 8 NMAP1 ,FVA ,PI ,TPI ,ZNI ,ZN2 ,ZN3 ,VF ,  
 9 OMEGR ,RTRAD ,HLDRAD ,AZER ,ISW3 ,ISWT

COMMON XUNTM  
 COMMON XUOPR(25,151),YUJFR(25,151),ZUOFR(25,151),VNRML(12,25)  
 COMMON EM(6),EV(6),QMNZ(6),PMNZ(6),QMN(6),CMN(6),QMN(6),QMN(6)  
 COMMON DPMJ(6),DQMN(6),PMNMI(6),QMNMI(6),RUNNO(4),TITLE(14)

```

COMMON      FMT3(12),XDISK(12,25),YDISK(12,25),ZDISK(12,25),FMT4(12)
COMMON      UDISK(12,25),VDISK(12,25),WDISK(12,25),IISK,JJSH
COMMON      KSW,LLSW,MMSW,NNSW,XINJN,YINJN,ZINJN,JRAD,JZER,JPTSL
COMMON      AX,LIN,LOUT,LTAP2,LTAP4,LTAP8,IHRUL,IMNCL,ISGGL
COMMON      XUP,XMAX,NINC,BLDLG,FNINC,PSIND,TINC,JMAX,AMUO,PSIO
COMMON      P>IUD,AMU,ATA,PSI,EPS,X,Y,Z,XP,ZP,RP,UVEL,WVEL,P,T
COMMON      TIME,JPT,JINC,KTAG,KFWD,KRVR,DPDY,DPDZ
COMMON      MEPSOL,POLD,WOLD,WOLD,TOLD,TIMOL,KOLD
COMMON      XULD,YULD,ZULD,XPULD,ZPULD,AMUOL,ATAOL,PSIOL,EPSOL
COMMON      XSAVE,YSAVE,ZSAVE,USAVE,VSAVE,WSAVE,AMUSV,ATASV,PSISV
COMMON      FPSSV,PSAVE,MEPSV,NW,MEPS,RNDM,ALDEG,ALPHA,COSAL,SINAL

```

```

EQUIVALENCE (SZ,DUMMY)

```

```

EQUIVALENCE ( DUMMY(1),RE), (DUMMY(12),SCE), (DUMMY(23),STDFE),
1          ( DUMMY(34),WZ), (DUMMY(45),WC), (DUMMY(89),WS),
2          ( DUMMY(133),A), (DUMMY(383),SCMD2), (DUMMY(393),SCE15),
3          ( DUMMY(404),STDFM), (DUMMY(414),CNPSI),
4          ( DUMMY(514),SMPST), (DUMMY(614),W)
EQUIVALENCE (UR,BLURAD),(VF,VFS),(AT,ALDEG),(ATR,ALPHA)
EQUIVALENCE (AMUO,AYUO),(QMNZO(1),QMNZO(1)),(PSIG,PSIO)

```

```

PSIUD=PSIO*180./PI

```

```

TRANSFORMATION FROM DISK COORDINATES TO WIND COORDINATES      EQ 31
X=XP#COSAL-ZP#SINAL
Z=XP#SINAL+ZP#COSAL

```

```

TRANSFORMATION FROM DISK COORDINATES TO ELLIPSOIDAL COORDINATES      EQ 35
EPS=-SIGN(1.-ZP)
PSI=ATAN2(Y,-XP)
ABCU=1.-XP*XP-Y*Y-ZP*ZP
RTABCD=SQRT(ABCD*ABCD+4.*ZP*ZP)

```

```

IF ((ABCD+RTABCD).GT.0.) GO TO 7777
AMU=0.
ATA=SQRT(-ADCD)
WRITE(6,1)XP,Y,ZP,ADCD,RTABCD,AMU,ATA
1  FORMAT(/' /*(ABCD+RTABCD).LE.0. VALUES ARE:',7E12.4,' IN STMLN1*/'
/ )
GO TO 6666
7777 AMU=0.70710*7812*EPS*SQRT(ABCD+RTABCD)
6666 MEPS=1.05*EPS
C
XINJN=X
YINJN=Y
ZINJN=Z
X=XUP
KOLD=0
P=0.
POLD=0.
FPSOL=1.
UVEL=0.
VVEL=0.
WVEL=0.
T=0.
TIME=0.
JPT=0
KTAG=0
KFWD=0
KRVS=0
C
C
TSMLN=60.*TIMER(1,1)
WRITE(6,1402)JRAL,JAZER,TSMLN,RNUM,PSIOD,XINJN,YINJN,ZINJN,X
1402 FORMAT(I11,15HSTREAMLINE CALCULATIONS FOR JRAL=,13,9H JAZER=,
9 13,5X,'STARTED AT RMAKE CLOCK=',F7.2,' SECONDS.',
1 ///IX,10H RNDM=,F6.4,7H PSIOD=,F7.2,7H XINJN=,E10.3,

```

```

1  /H YINJN= ,E10.3,7H ZINJN= ,E10.3,11H XUPSTREAM= ,E10.3,3X,1H)
2  ///1X,15HJPI JNC KTG EPS ,8X,1HT,9X,4HTIME,10X,1HX,11X,1HY,
3  11X,1HZ,11X,1HP,10X,4HVEL,8X,4HVEL,8X,4HVEL///)
C
C
C  OBTAIN POINT JUST UPSTREAM OF INJECTION POINT.
C
C  X=XINJN+0.1E-2
C
C  CALL VLCTS
C
C  VVEL=VVEL-(0.1E-2)*LEPDY
C  *VEL=HVEL-(0.1E-2)*LEPDZ
C
C
C  OBTAIN STARTING POINT FOR THE STREAMLINE.
C
C  VPEFF=(1.-UVEL)*SINAL+HVEL*COSAL
C  VWRML(JRAD,JAZER)=VPEFF
C  IF(VPEFF)1418,1419,1420
C  1418 WRITE(6 ,1421)VPEFF
C  1421 FORMAT(' THE VELOCITY AT THIS INJECTION POINT HAS A NET NORMAL CO
C      MPONENT DIRECTED UPWARDS. VPEFF=',E12.4///)
C
C  TRANSFORMATION FROM WIND COORDINATES TO DISK COORDINATES      EQ 32
C  XP=X*COSAL+Z*SINAL
C  ZP=-X*SINAL+Z*COSAL
C
C  TRANSFORMATION FROM DISK COORDINATES TO ELLIPSOIDAL COORDINATES  EQ 35
C  EPS=-SIGN(1.,ZP)
C  PSI=ATAN2(Y,-AP)
C  ABCD=1.-XP*XP-Y*Y-ZP*ZP
C  NTABCD=ABS(ABCD*ABCD+4.*ZP*ZP)
C  IF((ABCD+NTABCD).GT.0.) GO TO 2222
C  ANU=0.

```

```

ATA=SQRT(-A*CU)
WRITE(6,2)XP,Y,ZP,ALCD,RTABCD,AMU,ATA
2  FORMAT(/' *(ABCD+RTABCD).LE.O. VALUES ARE:',7E12.4,' IN STMLN2*'/)
1  (/)
      GO TO 1111
2222 AMU=0.70710.7812*EPS*SQRT(ABCD+RTABCD)
      ATA=-ZP/AMU
1111 EPS=1.05*EPS
C
      CALL CHAMP
      LEVEL=P
      FPS=1.
      MEPS=1
      GO TO (1401,1401,1423),NMSW
1401 KRVS=KRVS+1
      GO TO 1423
1411 WRITE(6,1422)
1422 FORMAT(/' NOTICE. VPEFF AT THIS DISK POINT IS ZERO.'//)
1426 CONTINUE
C
C
      TRANSFORMATION FROM WIND COORDINATES TO DISK COORDINATES
      XP=X*CSAL+Z*SEAL
      ZP=-X*SINAL+Z*CSAL
C
C
      TRANSFORMATION FROM DISK COORDINATES TO ELLIPSOIDAL COORDINATES
      EPS=-SIGN(1.,ZP)
      PSI=ATAN2(Y,-XP)
      ABCU=1.-XP*XP-Y*Y-ZP*ZP
      RTABCD=SQRT(ABCU*ABCD+4.*ZP*ZP)
      IF((ABCD+RTABCD).GT.O.) GO TO 3333
      AMU=0.
      ATA=SQRT(-ABCU)
      WRITE(6,3)XP,Y,ZP,ABCD,RTABCD,AMU,ATA
3  FORMAT(/' *(ABCD+RTABCD).LE.O. VALUES ARE:',7E12.4,' IN STMLN3*'/)
1  (/)

```

\*\*\*\*\*NMSW

EU 32

EU 35

141

```

GO TO 4444
3333 AMU=0.7071067812*EPS*SQRT(ABCD+RTABCD)
ATA=-ZP/AMU
4444 MEPS=1.05*EPS
C
CALL CHAMP
C
GO TO (1403,1403,1403,1404),NMS*
1403 UVEL=-P
EPS=-1.
MEPS=-1
KFWD=KFWD+1
GO TO 1423
1404 UVEL=P
EPS=1.
MEPS=1
C
1423 PULU=P
JPT=1
JINC=NINC
TIME=0.
KTAG=1
C
WRITE(6,1412)
1412 FORMAT(//IX,1A,1D,40X,HEEELRE'S THE ..... STREAMLINE ...)
WRITE(6,1417)
1417 FORMAT(1H+,40X, ' '///)
X=XINJN
WRITE(6,1408)JPT,JINC,KTAG,MEPS,T,TIME,X,Y,Z,P,UVEL,VVEL,WVEL
1408 FORMAT(IX,2I3,1A,11,2X,12,1X,9E12.4)
C
XUOFR(JAZER,1)=X
YUOFR(JAZER,1)=Y
ZUOFR(JAZER,1)=Z
C

```

\*\*\*\*\*NSW

```

XDISK(JRAD,JAZER)=X
YDISK(JRAD,JAZER)=Y
ZDISK(JRAD,JAZER)=Z
JDISK(JRAD,JAZER)=UVEL
VDISK(JRAD,JAZER)=VVEL
WDISK(JRAD,JAZER)=WVEL

C   I INC=(1.-BLD LG)*AR*TPI/(FNA*FNINC)
    JPT=2
C   CALL FRWRD
C   XUOFR(JAZER,2)=X
    YUOFR(JAZER,2)=Y
    ZUOFR(JAZER,2)=Z
C   T INC=AR*TPI/(FNA*FNINC)
    IF(KEND-3)1413,1414,1414
C   1414 GO 1415 JJPT=3,KEND
    JPT=JJPT
C   CALL FRWRD
C   XUOFR(JAZER,JPT)=X
    YUOFR(JAZER,JPT)=Y
    ZUOFR(JAZER,JPT)=Z
C   1415 CONTINUE
    1413 TSM LN=60.*TIMCK(1,1)
    WRITE(6,1416)JRAD,JAZER,TSM LN,KFWD,KRVR S
    1416 FORMAT(IX////36H STREAMLINE CALCULATIONS FOR JRAD= ,13,
    1 2H JAZER= ,13,5X, ENDED AT RWAKE CLOCK = ,F7.2,0 SECONDS. //
    2 0 KFWD = ,12,5X, KRVR S = ,12,0.0)

```

\*\*\*STMLN

RETURN  
END

C \* \* \* \* \*  
 C \* SUBROUTINE VLCTS \*  
 C \* \* \* \* \*

\*\*\*VLCTS

SUBROUTINE VLCTS

DIMENSION DUMAY(2500)

DIMENSION RE(11),SCE(11),SUFJE(11),WZ(11),WC(4,11),WS(4,11),A(250)  
 1,SCM2(10),SCEL5(11),STCFM(10),CNPSI(4,25),SNPSI(4,25),M(275)  
 DIMENSION QANZU(6)

COMMON RM(10) ,SCM(10) ,AB(250)  
 1 XI(151,11) ,ETA(151,11) ,ZETA(151,11) ,  
 2 XM(10) ,YM(10) ,ZM(10) ,  
 3 DX(10) ,DY(10) ,SCDR(10) ,  
 4 SZ(10,250) ,SI(10,250) ,S2(10,250) ,  
 5 S3(10,250) ,TZ(10,25) ,T1(10,25) ,  
 6 T2(10,25) ,T3(10,25) ,FMT(12) ,  
 7 CPSI(25) ,SPSI(25)

COMMON MMEAN ,WKADV ,ICSTRT ,IAZ ,NRPI ,NTV ,DLRV ,  
 1 DELX ,VFESAT ,DI ,USIRT ,NA ,I ,IB ,  
 2 JG ,KT ,ZNIS ,ZN25 ,ZM3S ,FPI ,AL ,AM ,  
 3 AN ,BL ,BP ,BN ,CC1 ,CC4 ,CC7 ,CC10 ,  
 4 KA ,RB ,AA5 ,AA6 ,XV2 ,XV1 ,XV3 ,  
 5 IRTK ,IBN ,IWN ,IST2 ,DMPRAD ,TVZ ,TV1 ,TV2 ,  
 6 TV3 ,SVZ ,SV1 ,SV2 ,SV3 ,KAZ ,ISW4 ,  
 7 ISW5 ,KA ,DPRDS ,NB ,NR ,NSV ,NSA ,  
 8 VMAP1 ,FNA ,PI ,TPI ,ZNI ,ZM2 ,NRA ,  
 9 UMEGR ,KTRAD ,BLDRAD ,AZER ,ISW3 ,ZM3 ,VF ,

COMMON XQNTM  
 COMMON XUOFR(25,151),YUOFR(25,151),ZUOFR(25,151),VNRML(12,25)  
 COMMON EM(6),EN(6),QANZO(6),PHN(6),QMN(6),CMN(6),DMN(6)

```

COMMON DPMN(6),DUMN(6),PMNM1(6),QNMN1(6),RUNNO(4),TITLE(14)
COMMON FMT3(12),XDISK(12,25),YDISK(12,25),ZDISK(12,25),FMT4(12)
COMMON UDISK(12,25),VDISK(12,25),WDISK(12,25),IISW,JJSW
COMMON KKSU,LLSW,MMSW,NISW,XINJH,YINJN,ZINJN,JRAD,JAZER,JPTSL
COMMON AR,LIN,LJUT,LTAP2,LTAP4,LTAP8,IHROL,IMNOL,ISOL
COMMON XUP,XMAX,NINC,BLDLG,FINC,PSIND,TINC,JMAX,AMUO,PSIO
COMMON PSIOD,AMU,ATA,PSI,EPS,X,Y,Z,XP,ZP,RP,UVEL,VVEL,MVEL,P,T
COMMON TIME,JPT,JINC,KTAG,KFWD,KRVR,DPDY,DPDZ
COMMON MEPSOL,POLO,UOLD,VOLD,MOLD,TOLD,TIMOL,KOLU
COMMON XCLU,YOLD,ZOLD,XPULD,XPULD,ZPULD,AMUOL,ATAOL,PSIOL,EPSOL
COMMON XSAVE,YSAVE,ZSAVE,USAVE,VSAVE,WSAVE,AMUSV,ATASV,PSISV
COMMON EPSSV,PSAVE,MEPSV,NH,MEPS,RNDM,ALDEG,ALPHA,COSAL,SINAL

```

C

```
EQUIVALENCE (SZ,DUMMY)
```

C

```

EQUIVALENCE ( DUMMY(1),RE), (DUMMY(12),SCE), (DUMMY(23),SIDFE),
1 ( DUMMY(34),WZ), (DUMMY(45),MC), (DUMMY(89),WS),
2 ( DUMMY(133),A), (DUMMY(383),SCMD2), (DUMMY(393),SCE15),
3 ( DUMMY(404),SIDFM), (DUMMY(414),GNPSI),
4 ( DUMMY(514),SNPSI), (DUMMY(614),W)
EQUIVALENCE (DR,BLDRAD),(VF,VFS),(AT,ALDEG),(AIR,ALPHA)
EQUIVALENCE (AMUO,AMUO),(QMNZO(1),QMNZO(1)),(PSIO,PSIO)

```

C

C

C

```
XQNFM MUST BE A NEGATIVE NUMBER
```

C

```

AMUPT=AMU
ATAPT=ATA
PSIPT=PSI

```

C

```

VV=0.
WH=0.

```

C

```

XMDPT=XUP-0.5*XQNFM
XMQMD2=X-0.5*XQNFM

```

```

ZSINAL=Z*SINAL
ZCOSAL=Z*COSAL
C
C
C 101 XMDPT=XMDPT+XQNTM
C
C IF (XMDPT.LT.XMQMD2) GO TO 102
C
C THE CURRENT VALUES OF VV AND WW DO NOT REPRESENT THE TRUE VELOCITIES AT
C THE CURRENT POINT. HOWEVER, THEY WILL BE MADE TO DO SO ON GETTING OUT OF
C THIS LOOP, BY MULTIPLYING THEM BY XQNTM. TIME SAVING HA HA HA
C
C TRANSFORMATION FROM WIND COORDINATES TO DISK COORDINATES EQ 32
XPMCDPT=XMDPT*COSAL+ZSINAL MIUPOINT
ZPMCDPT=-XMDPT*SINAL+ZCOSAL
C
C TRANSFORMATION FROM DISK COORDINATES TO ELLIPSOIDAL COORDINATES EQ 35
FPSMPT=-SIGN(1.,ZPMCDPT) MIDPOINT
PSI=ATAN2(Y,-XPMCDPT)
ABCU=1.-XPMCDPT*XPMCDPT-Y*Y-ZPMCDPT*ZPMCDPT
RTABCD=SQRT(ABCD*ABCD+4.*ZPMCDPT*ZPMCDPT)
IF((ABCD+RTABCD).GT.0.) GO TO 7777
AMU=0.
ATA=SQRT(-ABCD)
IF((ABCD+RTABCD).LT.0.) WRITE(6,1)XPMCDPT,Y,ZPMCDPT,ABCD,RTABCD,AMU,
C 1 ATA
C 1 FORMAT(/' *((ABCD+RTABCD).LT.0. VALUES ARE: ',7E12.4,' IN VLCTS1*/'
C 1 /)
GO TO 6666
7777 AMU=0.7071067812*EPSMPT*SQRT(ABCD+RTABCD)
6666 CONTINUE
C
CALL CHAMP

```

```

C      VV=VV+DPDY
C      WW=WW+DPDZ
C      GO TO 101
C      102 VV=VV*XQNTM
C      WW=WW*XQNTM
C      COMPUTE DELTA, WHICH IS THE FINAL INCREMENT.
C      DELTA=XQNTM**2+XQNTM-XMDPT
C      XMDPT=X
C      TRANSFORMATION FROM WIND COORDINATES TO DISK COORDINATES
C      XPMDPT=XMDPT*UOSAL+ZSINAL
C      ZPMPT=-XMDPT*SINAL+ZCOSAL
C      TRANSFORMATION FROM DISK COORDINATES TO ELLIPSOIDAL COORDINATES
C      EPSMPT=-SIGN(1.,ZPMPT)
C      PSI=ATAN2(Y,-XPMDPT)
C      ABCD=1.-XPMPT*XPMPT-Y*Y-ZPMPT*ZPMPT
C      RTABCD=SQRT(ABCD*ABCD+4.*ZPMPT*ZPMPT)
C      IF((ABCD+RTABCD).GT.0.) GO TO 4444
C      AMJ=0.
C      ATA=SQRT(-ABCD)
C      WRITE(6,2)XPMPT,Y,ZPMPT,ABCD,RTABCD,AMJ,ATA
C      2  FORMAT(1 /*(ABCD+RTABCD)-LI.0. VALUES ARE:*,7E12.4,' IN VLCTS2*/)
C      1 /)
C      GO TO 3333
C      4444 AMJ=0.70710*7E12*EPSMPT*SQRT(ABCD+RTABCD)
C      ATA=-ZPMPT/AMJ
C      5333 MEPMPT=IFIX(1.05*EPSMPT)
C      CALL CHAMP

```

EQ 32  
MIDPOINT

EQ 35  
MIDPOINT

```

C      UVEL=UVFL+P-PHLD
C      VVEL=VV+DELTAX*UPDY
C      WVEL=WN+DELTAAX*TPDZ
C
C      AMU=AMUPT
C      ATA=ATAPT
C      PSI=PSIPT
C
C      IF (MEPMT.EQ.MEPS) GO TO 103
C
C      WRITE(6,104)KTAG,JRAD,JAZER,JPT,MEPMT,MEPS
104  FORMAT( /# MEPMT AND MEPS DO NOT AGREE JUST BEFORE RETURNING FRU
      1M VLCTS. KTAG=',11,',JRAD=',12,',JAZER=',14,',MEPMT=',
      212,',MEPS=',12,'*//')
C
C      103 RETURN
      END

```

\*\*\*VLCTS

\* \* \* \* \*  
 \* SUBROUTINE CHAMP \*  
 \* \* \* \* \*

\*\*\*CHAMP

SUBROUTINE CHAMP

DIMENSION DUMMY(2500)

DIMENSION RE(11),SCE(11),SIDFE(11),WZ(11),WC(4,11),WS(4,11),A(250)  
 1,SCMD2(10),SCE15(11),STDFM(10),CNPSI(4,25),SNPSI(4,25),M(275)  
 DIMENSION QMNZO(6)

COMMON RM(10) ,SCM(10) ,AB(250) ,  
 1 XI(151,11) ,ETA(151,11) ,ZETA(151,11) ,  
 2 XM(10) ,YM(10) ,ZM(10) ,  
 3 UX(10) ,UY(10) ,SCDR(10) ,  
 4 SZ(10,250) ,SI(10,250) ,S2(10,250) ,  
 5 S3(10,250) ,TZ(10,25) ,I1(10,25) ,  
 6 T2(10,25) ,T3(10,25) ,FMT(12) ,  
 7 CPSI(25) ,SPSI(25)

COMMON WMEAN ,WKADV ,IDSTR1,IAZ ,NRPI ,NTV ,DLTV ,DLRV ,  
 1 DELX ,VFSAT ,DT ,USTRT ,NA ,I ,J ,IR ,  
 2 JH ,KI ,ZNIS ,Z2S ,Z3S ,FPI ,AL ,AM ,  
 3 AN ,DL ,BN ,CC1 ,CC4 ,CC7 ,CC10 ,  
 4 RA ,KB ,AA5 ,AA6 ,XVZ ,XV1 ,XV2 ,XV3 ,  
 5 IRTR ,IBN ,IWN ,IST2 ,UMPRAD ,TVZ ,TV1 ,TV2 ,  
 6 TV3 ,SVZ ,SVL ,SV2 ,SV3 ,KAZ ,KAS ,ISW4 ,  
 7 ISW5 ,KA ,DPRGS ,NB ,NR ,NSV ,NRA ,  
 8 NWAPI ,FNA ,PI ,TPI ,ZNI ,ZNS ,ZNF ,  
 9 QMEGR ,RTRAI ,BLURAD ,AZER ,ISW3 ,ISHT ,VF ,  
 COMMON XQVFM  
 COMMON XUNFR(25,151),YUNFR(25,151),ZUNFR(25,151),VNRML(12,25)  
 COMMON EM(6),EV(6),QMNZO(6),PMN(6),QMN(6),CMN(6),DPA(6)

```

COMMON DPMN(6),DGMV(6),PMNM1(6),QMNM1(6),RUNND(4),TITLE(14)
COMMON FRT3(12),XDISK(12,25),YDISK(12,25),ZDISK(12,25),FMT4(12)
COMMON ULISK(12,25),VDISK(12,25),WDISK(12,25),LISH,JJSW
COMMON KKS,LLS,MMS,NNSW,XINJN,YINJN,ZINJN,JRAL,JZER,JPTSL
COMMON AK,LIN,LOUT,LTAP2,LTAP4,LTAP8,THROL,THNGL,ISCOL
COMMON XUP,XMAX,NINC,BLDLG,FNINC,PSIND,TINC,JMAX,AMUD,PSIO
COMMON PSIO,AMU,ATA,PSI,EPS,X,Y,Z,XP,ZP,RP,UVEL,WVEL,P,T
COMMON TIME,JPT,JINC,KTAG,KFWD,KRVR,DPDY,DPDZ
COMMON MEPSOL,POLD,UOLD,VOLD,WOLD,TOLD,TIMGL,KOLD
COMMON XOLD,YOLD,ZOLD,XPOLD,ZPOLD,AMUGL,ATAUL,PSIUL,EPSOL
COMMON XSAVE,YSAVE,ZSAVE,USAVE,VSAVE,MSAVE,AMUSV,ATASV,PSISV
COMMON EPSSV,PSAVE,MEPSV,MW,MEPS,RNDM,ALDEG,ALPHA,COSAL,SINAL

```

C

```

EQUIVALENCE (SZ,DUMMY)

```

C

```

EQUIVALENCE ( DUMMY(1),RE), ( DUMMY(12),SCE), ( DUMMY(23),STDFE),
1 ( DUMMY(34),WZ), ( DUMMY(45),WC), ( DUMMY(89),WS),
2 ( DUMMY(133),A), ( DUMMY(383),SCM2), ( DUMMY(393),SCE15),
3 ( DUMMY(404),STDFM), ( DUMMY(414),CNPS1),
4 ( DUMMY(514),SNPS1), ( DUMMY(614),W)

```

```

EQUIVALENCE (UR,BLDRAD),(VF,VFS),(AT,ALDEG),(ATR,ALPHA)
EQUIVALENCE (AMUD,AMUO),(QMNZO(1),QMNZO(11)),(PSIO,PSIO)

```

C

C

```

AMUAMU=AMU*AMU
AMSQ=1.-AMUAMU
RTAMSQ=SQRT(AMSQ)
ATAATA=ATA*ATA
ATSQ=1.+ATAATA
RTATSQ=SQRT(ATSQ)

```

C

C

```

IF(ATA.LT.0.0) GO TO 100Z

```

C

C

AIKEY=ATAN2(1.,ATA)

C  
C

P=0.  
DPDMU=0.  
LPUDET=C.  
UPDSI=0.

C  
C

PMN(1)=AMU  
PMN(2)=AMU\*(2.5\*AMUAMU-1.5)  
PMN(3)=-3.\*AMU\*RTAMSQ  
PMN(4)=AMU\*RTAMSQ\*(7.5-17.\*AMUAMU)  
PMN(5)=15.\*AMU\*AMU

C

QMN(1)=ATA\*ATREY-1.  
QMN(2)=-ATA\*ATREY\*(2.5\*ATAATA+1.5)+2.5\*ATAATA+2./3.  
QMN(3)=3.\*RTAMSQ\*(1.-ATA\*ATREY)-1./RTAMSQ  
QMN(4)=ATA\*RTAMSQ\*ATREY\*(17.5\*ATAATA+7.5)  
-RTAMSQ\*(17.5\*ATAATA+5./3.)-1./RTAMSQ  
QMN(5)=-15.\*ATA\*ATREY+15.\*ATAATA+10.-2./RTAMSQ

C

PMNMI(1)=1.  
PMNMI(2)=1.5\*AMUAMU-0.5  
PMNMI(3)=-RTAMSQ  
PMNMI(4)=RTAMSQ\*(1.5-7.5\*AMUAMU)  
PMNMI(5)=3.\*AMU

C

QMNMI(1)=ATKEY  
QMNMI(2)=-ATREY\*(1.5\*ATAATA+0.5)+1.\*ATA  
QMNMI(3)=ATKEY\*RTAMSQ-ATA/RTAMSQ  
QMNMI(4)=-ATREY\*RTAMSQ\*(7.5\*ATAATA+1.5)  
+7.5\*ATA\*RTAMSQ-ATA/RTAMSQ  
QMNMI(5)=-3.\*ATREY\*RTAMSQ+3.\*ATA+2.\*ATA/RTAMSQ

C



```
C 1002 WRITE(6,1003)ATA
1003 FORMAT(//1X,'HJM COME ATA BECAME NEGATIVE ? ( ATA= ',E15.7,' )',
1 // ' CALLED EXIT AROUND 1002 IN CHAMP.' )
CALL EXIT
RETURN
END
***CHAMP
```

C \* \* \* \* \*  
 C \* SUBROUTINE FRWRD \*  
 C \* \* \* \* \*

\*\*\*FRWRD

SUBROUTINE FRWRD  
 DIMENSION DUMMY(2500)

DIMENSION RE(11), SCE(11), STDFE(11), WZ(11), WC(4,11), WS(4,11), A(250)  
 1, SCMD2(10), SCE15(11), SILFM(10), CNPSI(4,25), SMPSI(4,25), M(275)  
 DIMENSION QMNZU(6)

COMMON RM(10) , SCM(10) , AB(250) ,  
 1 XI(151,11) , ETA(151,11) , ZETA(151,11) ,  
 2 XM(10) , YM(10) , ZM(10) ,  
 3 DX(10) , DY(10) , SCDR(10) ,  
 4 SZ(10,250) , SI(10,250) , S2(10,250) ,  
 5 S3(10,250) , IZ(10,25) , T1(10,25) ,  
 6 T2(10,25) , T3(10,25) , FMT(12) ,  
 7 CPSI(25) , SPSI(25)

COMMON WMEAN , WKADV , ILSTRT , IAZ , NRPI , JTV , DLTV ,  
 1 DELX , VFSAI , DT , USTRT , NA , J , DLTV ,  
 2 JB , KT , ZNIS , ZN2S , ZN3S , FPI , J , IB ,  
 3 AN , BL , BM , BN , CCI , CC4 , CC7 , CC10 ,  
 4 RA , RB , AA5 , AA6 , XVZ , XVI , XV3 ,  
 5 ITRK , IBN , IWN , I1ST2 , DMPKAD , TVZ , TV1 , TV2 ,  
 6 TV3 , SVZ , SV1 , SV2 , SV3 , KAZ , KAS , ISW4 ,  
 7 ISW5 , KA , DPRDS , NB , NR , NSV , NAUB , NRA ,  
 8 NWAPI , FNA , PI , TPI , ZNI , ZN2 , ZN3 , VF ,  
 9 OMEGR , RTRAD , BLDRAD , AZER , ISW3 , ISMT

COMMON XGNFM  
 COMMON XUDFR(25,151), YUJFR(25,151), ZUOFR(25,151), VNRML(12,25)  
 COMMON EM(6), EN(6), QMNZU(6), PMN(6), QMN(6), CMN(6), DMN(6)  
 COMMON DPMN(6), DCMN(6), PMNML(6), CMNML(6), CMNMI(6), RUNND(4), TITLE(14)



```

IF(EPS)1505,1506,1507
C
C
1506 WRITE(6,1511)
1511 FORMAT(IX,35HCALLED EXIT 1506 BECAUSE EPS VANISHES )
CALL EXIT
C
1505 IF(FPSOL)1516,1509,1510
C
1509 WRITE(6,1512)
1512 FORMAT(IX,40HCALLED EXIT 1509 BECAUSE EPSOL VANISHES )
CALL EXIT
C
1510 KFWI=KFWD+1
WRITE(6,1513)KFWI,KTAG,JPT,JINC
1513 FORMAT(IX,64HJUST CROSSED THE DISK FROM UPPER SIDE TO LOWER SIDE.
THIS IS THE ,12,43H TH FORWARD CROSSING. CURRENT VALUES KTAG=
2 ,11,7H JPT= ,13,8H JINC= ,12)
CALL CR5NG
GO TO 1516
C
1507 IF(LPSOL)1514,1509,1516
C
1514 KRVS=KRVS+1
WRITE(6,1515)KRVS,KTAG,JPT,JINC
1515 FORMAT(IX,64HJUST CROSSED THE DISK FROM LOWER SIDE TO UPPER SIDE.
THIS IS THE ,12,43H TH REVERSE CROSSING. CURRENT VALUES KTAG=
2 ,11,7H JPT= ,13,8H JINC= ,12)
CALL CR5NG
C
1516 GO TO (1517,1518,1518),MNSW
1517 CALL CHAMP
VVEL=VVEL+DPDY*(-1.+UVEL)*TINC
WVEL=WVEL+DPDZ*(-1.+UVEL)*TINC
UVEL=UVEL+P-POLD)

```

\*\*\*\*\*NSW

```
GO TO 1519
1518 CALL VLCTS
1519 WRITE(6,1508)JPT,JINC,KTAG,MEPS,T,TIME,X,Y,Z,P,UVEL,VVEL,WVEL
1508 FORMAT(1X,2I3,3X,11,2X,12,3X,9E12.4)
1503 CONTINUE
```

C

```
RETURN
END
```

\*\*\*FRWRO

C \* \* \* \* \*  
 C \* SUBROUTINE ADVNC \*  
 C \* \* \* \* \*

\*\*\*ADVNC

SUBROUTINE ADVNC

DIMENSION DUMMY(2500)

DIMENSION RE(11),SCE(11),STDFE(11),WZ(11),WC(4,11),MS(4,11),A(2,0)  
 1,SCMD2(10),SCF15(11),STDFM(10),CNPSI(4,25),SNPSI(4,25),W(275)  
 DIMENSION QMNZO(6)

COMMON RM(10) ,SCM(10) ,AB(250) ,  
 1 XI(151,11) ,ETA(151,11) ,ZETA(151,11) ,  
 2 XM(10) ,YM(10) ,ZM(10) ,  
 3 DX(10) ,DY(10) ,SCDR(10) ,  
 4 SZ(10,250) ,S1(10,250) ,S2(10,250) ,  
 5 S3(10,250) ,T2(10,25) ,T1(10,25) ,  
 6 T2(10,25) ,T3(10,25) ,FMT(12) ,  
 7 CPSI(25) ,SPSI(25)

COMMON WMEAN ,WKADV ,IDSTRT,IAZ ,NRPI ,NTV ,DLTV ,DLRV ,  
 1 DELX ,VFESAT ,DT ,DSTRT ,NA ,J ,IB ,  
 2 JB ,KT ,ZNLS ,ZN2S ,ZN3S ,FPI ,AL ,AM ,  
 3 AN ,BL ,BM ,CCI ,CC4 ,CC7 ,CC10 ,  
 4 RA ,RB ,AA5 ,AA6 ,XVZ ,XV1 ,XV2 ,XV3 ,  
 5 ITR ,IBN ,IMN ,IST2 ,DMPRAD ,IVZ ,TVI ,TV2 ,  
 6 TV3 ,SVZ ,SVL ,SV2 ,SV3 ,KAZ ,KAS ,ISM4 ,  
 7 ISW5 ,KA ,OPRUS ,NB ,NR ,NSV ,NRA ,  
 8 NWAPl ,FNA ,PI ,TPI ,ZNI ,ZN2 ,NAUB ,  
 9 OMEGR ,RTRAI ,BLDRAD ,AZER ,ISH3 ,ISWT ,ZN3 ,VF ,

COMMON XQNTM  
 COMMON XUOFR(25,151),YUOFR(25,151),ZUOFR(25,151),VNRML(12,25)  
 COMMON EM(6),EN(6),QMNZO(6),PMN(6),QMN(6),CMN(6),DPN(6)



```

C
C
ZP=-X*SINAL+Z*CCOSAL
TRANSFORMATION FROM DISK COORDINATES TO ELLIPSOIDAL COORDINATES EQS 35
EPS=-SIGN(1.,ZP)
PSI=ATAN2(Y,-XP)
ABCD=L.-XP*XP-Y*Y-ZP*ZP
RTABCD=SQRT(ABCD*ABCD+4.*ZP*ZP)
IF((ABCD+RTABCD).GT.0.) GO TO 7777
AMU=0.
ATA=SQRT(-ABCD)
WRITE(6,1)XP,Y,ZP,ABCD,RTABCD,AMU,ATA
1 FORMAT(/' /*(ABCD+RTABCD).LE.0. VALUES ARE:',F12.4,' IN ADVNC */'
/ /)
GO TO 6666
7777 AMU=0.707106/812*EPS*SQRT(ABCD+RTABCD)
ATA=-ZP/AMU
6666 MEPS=IFIX(1.05*EPS)
C
161
RETURN
END
***ADVNC

```

```

C      * * * * *
C      * SUBROUTINE CRSNG *
C      * * * * *

```

\*\*\*CRSNG

SUBROUTINE CRSNG

DIMENSION DUMMY(2500)

DIMENSION RE(11),SCE(11),SIDFE(11),WZ(11),MC(4,11),MS(4,11),A(250)  
 1,SCHD2(10),SCE15(11),STDFM(10),CNPSI(4,25),SNPSI(4,25),W(275)  
 DIMENSION QMNZO(6)

```

COMMON RM(10) ,SCM(10) ,AB(250)
1 XI(151,11) ,ETA(151,11) ,ZETA(151,11)
2 XM(10) ,YM(10) ,ZM(10)
3 DX(10) ,DY(10) ,SCDR(10)
4 SZ(10,250) ,S1(10,250) ,S2(10,250)
5 S3(10,250) ,T2(10,25) ,T1(10,25)
6 T2(10,25) ,T3(10,25) ,FMT(12)
7 CPSI(25) ,SPSI(25)

```

```

COMMON WMEAN ,WKADY ,IDSTRT,IAZ ,NRPI ,NTV ,DLTV
1 DFLX ,VFSAI ,DT ,DSTRT ,NA ,I ,J
2 JH ,KT ,ZNIS ,ZN2S ,ZNS3 ,FPI ,AL
3 AN ,BL ,BN ,CC1 ,CC4 ,CC7 ,CC10
4 RA ,KB ,AA5 ,AA6 ,XVZ ,XV1 ,XV2 ,XV3
5 IRTK ,IBN ,IWN ,IST2 ,DMPRAD,IVZ ,TV1 ,TV2
6 TV3 ,SVZ ,SV1 ,SV2 ,SV3 ,KAZ ,KAS ,ISW4
7 ISW5 ,KA ,DPROS ,NB ,NR ,NSV ,NRA
8 NMAP1 ,FNA ,PI ,TPI ,ZNI ,ZNS ,VF
9 UMEGR ,RTRAD ,BLDRAD,AZER ,ISW3 ,ISWT
COMMON XQNTM
COMMON XQJFR(25,151),YUJFR(25,151),ZUOFR(25,151),VNRML(12,25)
COMMON EM(6),EN(6),QMNZO(6),PMN(6),QMN(6),CMN(6),DMN(6)

```

```

COMMON      UPMN(6), QMNN(6), PMNM(6), QMMI(6), RUNND(4), TITLE(14)
COMMON      FMT3(12), XDISK(12,25), YUDISK(12,25), ZUDISK(12,25), FMT4(12)
COMMON      UUDISK(12,25), VUDISK(12,25), WUDISK(12,25), IISW, JJSW
COMMON      KKS, LLS, MMS, NNS, XIN, YIN, ZIN, J, RAD, JAZER, JPTSL
COMMON      A, LIN, LOU, LTAP, LTAP2, LTAP4, LTAP8, IHR, I, M, L, I, S, C, L
COMMON      X, P, XMAX, NINC, BLDG, FNINC, PSIND, PSINC, JMAX, AMU, PSIO
COMMON      PSIOD, AMU, ATA, PSI, EPS, X, Y, Z, XP, ZP, RP, UVEL, VVEL, P, T
COMMON      TIME, JPT, JINC, KTAG, KFW, KRVS, OPDY, DPZ
COMMON      MFPSOL, POLU, UOLD, VOLD, WOLD, TOLD, TIMOL, KOLD
COMMON      XULD, YULD, ZOLD, XPOLD, ZPOLD, AMUOL, ATAO, PSIGL, EPSOL
COMMON      XSAVE, YSAVE, ZSAVE, USAVE, VSAVE, WSAVE, AMUSV, ATASV, PSISV
COMMON      EPSSV, PSAVE, MEPSV, NW, MEPS, RNDM, ALDEG, ALPHA, COSAL, SINAL

```

```

EQUIVALENCE (SZ, DUMMY)

```

```

EQUIVALENCE ( DUMMY(1), RE), ( DUMMY(12), SCE), ( DUMMY(23), STDFE),
1 ( DUMMY(34), WZ), ( DUMMY(45), WC), ( DUMMY(89), WS),
2 ( DUMMY(133), A), ( DUMMY(383), SCMD2), ( DUMMY(393), SCE15),
3 ( DUMMY(404), STDFM), ( DUMMY(414), CNPSI),
4 ( DUMMY(514), SNPSI), ( DUMMY(614), M)

```

```

EQUIVALENCE (UR, BLDRAD), (VF, VFS), (AT, ALDEG), (ATR, ALPHA)
EQUIVALENCE (AMU, AMUO), (QMNZU(1), QMNZU(1)), (PSIO, PSIO)

```

```

PSAVE=P
AMUSV=AMU
ATASV=ATA
PSISV=PSI
USAVE=UVEL
XSAVE=X
YSAVE=Y
ZSAVE=Z

```

```

615 XP=XPULU+(XP-XPULU)*ZPOLD/(ZPOLD-ZP)
     Y=YULD+(Y-YULD)*ZPOLD/(ZPOLD-ZP)

```

```

C
C TRANSFORMATION FROM DISK COORDINATES TO WIND COORDINATES SPECIAL
X=XP*CU,AL
Z=XP*SI,VAL

C
C TRANSFORMATION FROM DISK COORDINATES TO ELLIPSOIDAL COORDINATES SPECIAL
PSI=ATAV2(Y,-XP)
ABCG=1.-KP*XP-Y*Y
IF(ABCG.GT(.001))GO TO 7777
AMU=0.
ATA=SQRT(-ABCG)
WRITE(6,1)XP,Y,ZP,ABCG,AMU,ATA
1  FORMAT(' /* (ABCG,LE,0).XP,Y,ZP,ABCG,AMU,ATA ARE: ',6E12.4,
1  ' ' <--IN CRSYS. #/!')
GO TO 6666
7777 AMU=0.7071007812*EPS*SQRT(ABCG)
ATA=0.

C
6666 CALL CHAMP

C
JJJ=C=JINC-1
WRITE(6,620)JPT,JJJ,C,KIAG,MEPS,X,Y,Z,P
620  FORMAT(1X,2I3,'.3 ',11,2X,12,27X,4E12.4,' <-- IMMEDIATELY ON CROSSING DISK.!)')
617  WRITE(6,611)
611  FORMAT(1X,57MEANWHILE, BACK AT THE NEW POSITION OF THE PARTICLE ,
1  ' )

C
616  UVEL=USAVE+2.*P*EPS
AMU=AMUSV
ATA=ATA,SV
PSI=PSI,SV
P=PSAVE
X=X,SAVE
Y=Y,SAVE

```

Z=ZSAVE

C

RETURN  
END

\*\*\*CRSNG

```

C      * * * * *
C      * SUBROUTINE VARFMT *
C      * * * * *
C
C      SUBROUTINE VARFMT(DMCH1,NCH1,NCLMN,DMCH2,NCH2,DMFMT)
C
C      DIMENSION  UMCH1(5),DMCH2(5),DMFMT(12),DMDM(20),DM(2)
C
C      DATA DM(1)/4H /
C      DATA DMDM /1H1,1H2,1H3,1H4,1H5,1H6,1H7,1H8,1H9,2H10,2H11,2H12,
C      1 2H13,2H14,2H15,2H16,2H17,2H18,2H19,2H20/
C
C      IF(NCLMN.GT.20)GO TO 101
C      DO 100 I=1,5
C      IP7=I+7
C      DMFMT(I)=DMCH1(I)
C      100 DMFMT(IP7)=DMCH2(I)
C
C      DMFMT(6)=DMDM(NCLMN)
C      DMFMT(7)=DM(1)
C
C      RETURN
C      101 WRITE(6,102)NCLMN
C      102 FORMAT(1H1,6HNCLMN=,14///6)SINCE THIS VALUE EXCEEDS 20, CALLED E
C      EXIT IN SUBROUTINE VARFMT  (////)
C      CALL EXIT
C      RETURN
C      END
C
C      **VARTMT

```



```

C
C
C      WRITE RUN-IDENTIFICATIONS.
C
C      WRITE(6,310)PICNO
310 FORMAT(1H1,10X,4A4)
C      WRITE(6,303)RUNNO,TITLE
303 FORMAT(////,INPUT TAPE LTAP8 DATASET WHICH WAS USED FOR THIS RWAK
C      LCPIL RUN WAS GENERATED IN THE CRNLIMOD RUN ENTITLED '//5X,4A4,
C      , , * , 5,2H' ,14A4,2H , //////////////)
C      WRITE(6 , 305)NA,NB,NR,NRPI,NW,NSV,NTV,NINC,AR,ALDEG,DR,VFS,
C      BLDLG,XUP,DLTV,DLRV,NRPI,(RE(I),I=1,NRPI)
305 FORMAT(IX,'PARAMETERS FOR THAT CRNLIMOD RUN WERE'//IX,'NA = ',
C      1 12,' , NB = ',12,' , NR = ',12,' , NRPI = ',12,' , NW = ',12,
C      2  , NSV+1 = ',12,' , NTV = ',11,' , NINC = ',12,' , AR = ',E15.8,
C      3  , ALDEG = ',F8.3,' , DR = ',F6.2,' , VFS = ',F6.2,' , BLDLG = ',
C      4  F10.3,' , XUP = ',F5.2,' , DLTV = ',F8.3,' , DLRV = ',F8.3//IX,
C      5  '(RE(I),I=1,'12,' ,//IX,(10E13.4))
C      WRITE(6 , 306) NRPI,(SCELI(I),I=1,NRPI)
306 FORMAT(//IX,'(SCELI(I),I=1,'12,' ,//IX,(10E13.4))
C
C      NRP2=1
C      NRP3=2
C      NMAP1=(NM*NA)+1
C      NMBRDS=NRPI+NTV
C      READ(7,341)NMPASS
341 FORMAT(12X,12)
C      WRITE(6,342)NMPASS,NMBRDS
342 FORMAT(////,TOTAL NUMBER OF PICTURE-PASSES IN THIS RWAKEPIC RUN
C      1 = NMPASS = ',13,///' NMBRDS = ',12)
C      READ MESH-WAKE CO-ORDINATES.
C      READ(8 ) ((AMFESH(KRAD,KAZER,KPTSL),YMESH(KRAD,KAZER,KPTSL),
C      /MESH(KRAD,KAZER,KPTSL),KAZER=1,NA),KPTSL=1,NSV)
C      308 CONTINUE
C      READ TIP TRAILING VORTEX CO-ORDINATES.
C      READ(9 ) ((ATRAL(NRP2,KAZER,KPTSL),YTRAL(NRP2,KAZER,KPTSL),

```

```

1          ZTRAL(NRP2,KAZER,KPTSL),KAZER=1,NA),KPTSL=1,NWAPI)
C
C      GO TO (302,301),NTV
C      READ ROOF TRAILING VORTEX CO-ORDINATES.
301 READ( 8 )((XTRAL(NRP3,KAZER,KPTSL),YTRAL(NRP3,KAZER,KPTSL),
1          ZTRAL(NRP3,KAZER,KPTSL),KAZER=1,NA),KPTSL=1,NWAPI)
302 CONTINUE
C
C      READ INJECTION CO-ORDINATES AND INDUCED VELOCITIES ON THE DISK.
READ( 8 ) ((XDISK(KRAD,KAZER),YDISK(KRAD,KAZER),
1          ZDISK(KRAD,KAZER),UDISK(KRAD,KAZER),
2          VDISK(KRAD,KAZER),WDISK(KRAD,KAZER),
3          VWRML(KRAD,KAZER),
4          KRAD=1,NMBRDS),KAZER=1,NA)
C
C      REMIND 8
C
C      WRITE CO-ORDINATES OF CHECKPOINTS IN WAKE AND VEL DISTRI ON DISK.
NADB=NA/NR
C
WRITE( 6 , 338) NRPI,NSV,NWAPI,NADB,XMESH(1,1,2),YMESH(1,1,2),
1  ZMESH(1,1,2),XMESH(NRPI,1,2),YMESH(NRPI,1,2),ZMESH(NRPI,1,2),
2  XMESH(1,1,NSV),YMESH(1,1,NSV),ZMESH(1,1,NSV),
3  XTRAL(NRP2,1,NWAPI),YTRAL(NRP2,1,NWAPI),ZTRAL(NRP2,1,NWAPI),
4  XMESH(1,NADB,2),YMESH(1,NADB,2),ZMESH(1,NADB,2),
5  XMESH(NRPI,NADB,2),YMESH(NRPI,NADB,2),ZMESH(NRPI,NADB,2),
6  XMESH(1,NADB,NSV),YMESH(1,NADB,NSV),ZMESH(1,NADB,NSV),
7  XTRAL(NRP2,NADB,NWAPI),YTRAL(NRP2,NADB,NWAPI),
8  ZTRAL(NRP2,NADB,NWAPI)
338 FORMAT(1I1,'CHECK POINTS IN WAKE. '//
1  1X,'(XUOFR,YUOFR,ZUOFR) AT (1,1,2) AND (NRPI,1,2),',/
2  1X,'(1,1,NSV) AND (NRP2,1,NWAPI)',',/'
3  1X,'(1,NADB,2) AND (NRPI,NADB,2)',',/'
4  1X,'(1,NADB,NSV) AND (NRP2,NADB,NWAPI)',',//

```





```

C      TEST FOR CONFLICT IN THE PARAMETERS FOR THE GRNLMOD AND THIS 'PIC' JOB.
      NOCHK=0
      IF((ISM.GT.3)XCHK=7)
      IF((NA.NE.(NJB*(JA/NJB)))/NOCHK=1)
      IF((JAZBL.GT.(NA/NJB)))/NOCHK=2)
      IF((NM.GT.NM)/NOCHK=3)
      IF((NNSV.GT.NSV).AND.(ISM.EQ.1))/NOCHK=4)
      IF((NNTV.GT.JTV)/NOCHK=5)
      DO 312 KRAD=1,N,RAD
      IF((JJRAD(KRAD)).GT.(NRPI+JTV))/NOCHK=6)
      IF((ISM.GT.1).AND.(JJRAD(KRAD).LE.NRPI).AND.(NNSY.GT.NSV))/NOCHK=7)
312 CONTINUE
      IF(NOCHK.EQ.0)GOTO 313
      WRITE(6,314)NOCHK
314 FORMAT(1X,'CALLED EXIT BECAUSE RWAKEPIC JOB PARAMETERS CONFLICT WITH
      GRNLMOD RUN PARAMETERS. NOCHK=',I2)
      RETURN 6
      CALL EXIT
313 CONTINUE
C
C      NMMAPI=(NM*NA)+1
      PSIBI=(JAZBI-1)*2.*PI/FYA
311 IF(PI-ABS(PSIBI))315,316,316
315 PSIBI=PSIBI*(1.-(2.*PI/ABS(PSIBI)))
      GO TO 311
316 PSIBI=180.*PSIBI/PI
C
C      CALL FACTOR(F)
C
C      DRAW IDENTIFICATION,PICTURE PARAMETERS.
      CALL SYMBOL(0.,9.8,0.14,PIEND,0.,16)

```

CALL SYMBOL(0.,9.,0.14,14HCORRESPONDUS TU ,0.,14)  
CALL SYMBOL(0.,8.7,0.14,RUAND,0.,16)

C

CALL PLOT(0.5,0.,-3)  
CALL SYMBOL(0.,8.3,0.14,7HYA =,0.,7)  
CALL SYMBOL(0.,8.,0.14,7HJAZBI =,0.,7)  
CALL SYMBOL(0.,7.7,0.14,7HPSIID =,0.,7)  
CALL SYMBOL(0.,7.4,0.14,7HNYB =,0.,7)  
CALL SYMBOL(0.,7.1,0.14,7HNYW =,0.,7)  
CALL SYMBOL(0.,6.8,0.14,7HNSV =,0.,7)  
CALL SYMBOL(0.,6.5,0.14,7HNTV =,0.,7)  
CALL SYMBOL(0.,6.2,0.14,7HNURAD =,0.,7)  
CALL SYMBOL(0.,3.2,0.14,7HIIPASS=,0.,7)  
CALL SYMBOL(0.,2.6,0.14,7HIISM =,0.,7)

C

CALL PLOT(1.,0.,-3)  
CALL NUMBER(0.,8.3,0.14,NA,0.,-1)  
CALL NUMBER(0.,3.,0.14,JAZBI,0.,-1)  
CALL NUMBER(0.,7.7,0.14,PSIID,0.,2)  
CALL NUMBER(0.,7.4,0.14,MNA,0.,-1)  
CALL NUMBER(0.,7.1,0.14,NNM,0.,-1)  
NNSV=NNSV-1  
CALL NUMBER(0.,6.8,0.14,NNSV,0.,-1)  
NNSV=NNSV+1  
CALL NUMBER(0.,6.5,0.14,NNTV,0.,-1)  
CALL NUMBER(0.,6.2,0.14,NNRAD,0.,-1)  
CALL NUMBER(0.,3.2,0.14,IIPASS,0.,-1)  
CALL NUMBER(0.,2.6,0.14,IISM,0.,-1)

C

CALL PLOT(2.,0.,-3)

C

DRAW AXES, ELLIPSE, ETC.

C

CO 334 J=1, >1

AJJ=FLOAT(J-1)

Y=2.\*AJJ/50.



```

PSIBK=PSIB1+FLOAT(KBN-1)*2.*PI/FLOAT(NNB)
320 IF(PI-ABS(PSIBK))318,319,319
318 PSIBK=PSIBK*(1.-(2.*PI/ABS(PSIBK)))
GO TO 320
319 X5=X1+2.*COS(ALPHA)*COS(PSIBK)
Y5=Y1+2.*SIN(PSIBK)
CALL PLOT(X1,Y1,+3)
CALL PLOT(X5,Y5,+2)

C
JAZBD=JAZB1+(KBN-1)*NA/NNB
GO 321 KRAD=1,NNRAD

C
JRAD=JKRAD(KRAD)
IF(JKAD.GT.NKPI)GO TO 333
DO 322 JPT=1,NNSV
JAZER=JAZBD-(JPT-1)
326 IF(JAZER.GT.0)GO TO 325
JAZER=JAZER+NA
GO TO 326
325 IF(JAZER.LE.MA)GO TO 327
JAZER=JAZER-NA
GO TO 325
327 XPOS(JPT)=X1-2.*XMesh(JRAD,JAZER,JPT)
YPOS(JPT)=Y1+2.*YMesh(JRAD,JAZER,JPT)
ZPOS(JPT)=Y2-2.*ZMesh(JRAD,JAZER,JPT)
322 CONTINUE
CALL LINE(XPOS,ZPOS,MNSV,1,0,1)
CALL LINE(XPOS,YPOS,MNSV,1,0,1)
GO TO 321

C
333 JTK=1
IF(JRAD.EQ.(NKPI+1))GO TO 339
JTOR=2
339 DO 328 JPT=1,NNWAP1

```

```

JAZER=JAZBD-(JPT-1)
330 IF(JAZER.GT.0)GO TO 329
JAZER=JAZER+NA
GO TO 330
327 IF(JAZER.LE.NA)GO TO 331
JAZER=JAZER-VA
GO TO 329
331 XPOS(JPT)=X1-2.*XTRAL(JTOR,JAZER,JPT)
YPOS(JPT)=Y1+2.*YTRAL(JTOR,JAZER,JPT)
ZPOS(JPT)=Z1-2.*ZTRAL(JTOR,JAZER,JPT)
328 CONTINUE
CALL LINE(XPOS,ZPOS,NNWAP1,1,0,1)
CALL LINE(XPOS,YPOS,NNWAP1,1,0,1)
321 CONTINUE
324 CONTINUE
CALL PLOT(22.,0.,-3)
GO TO 340
C
C
345 CONTINUE
C
C
C
C
C
STREAMLINES.      STREAMLINES.      STREAMLINES.
DO 347 KBN=1,NNB
JAZBD=JAZB1+(KBN-1)*NA/NNB
DU 348 KRAD=1,NNRAD
JRAU=JJRAU/(NNRAD)
IF(JRAD.GT.NRPI)GO TO 349
DU 350 JPT=1,NNSV
XPOS(JPT)=X1-2.*XMESH(JRAD,JAZBD,JPT)
YPOS(JPT)=Y1+2.*YMEH(JRAD,JAZBU,JPT)
ZPOS(JPT)=Z1-2.*ZMESH(JRAD,JAZBD,JPT)
CALL LINE(XPOS,ZPOS,NNSV,1,0,1)
CALL LINE(XPOS,YPOS,NNSV,1,0,1)
GO TO 348

```

```

C      349 JTOR=1
      IF(JRAD.EQ.(NRP1+1))GO TO 352
      JTOR=2
C      352 DO 353 JPT=1,NNAPI
          XPOS(JPT)=X1-2.*XTRAL(JTOR,JZBD,JPT)
          YPOS(JPT)=Y1+2.*YTRAL(JTOR,JZBD,JPT)
C      353 ZPOS(JPT)=Y2-2.*ZTRAL(JTOR,JZBD,JPT)
          CALL LINE(XPOS,ZPOS,NNWAP1,1,NA,KBN)
          CALL LINE(XPOS,YPOS,NNWAP1,1,NA,KBN)
C      348 CONTINUE
C      347 CONTINUE
C      CALL PLOT(22,0,0,-3)
C      GO TO 340
C      CONTOURS. CONTOURS. CONTOURS. CONTOURS. CONTOURS.
C      CONTOURS. CONTOURS. CONTOURS. CONTOURS. CONTOURS.
C      346 CONTINUE
          CALL SYMBOL(16,9.5,0.21,10HFRONT VIEW,0,10)
          CALL SYMBOL(X6M2,Y2,0.07,1H,0,1)
          CALL SYMBOL(X6,Y4,0.07,1H,0,1)
          CALL SYMBOL(X6,Y2,0.07,1H,0,1)
          CALL SYMBOL(X6,Y3,0.07,1H,0,1)
          CALL SYMBOL(X6P2,Y2,0.07,1H,0,1)
C      DO 354 KRAD=1,6NRAD
          JRAD=JJRAU(KRAD)
          IF(JRAD.GT.NRP1) GO TO 355
C      DO 356 JPT=1,NA
          XPOS(JPT)=X1-2.*XMESH(JRAD,JPT,NNSV)
          YPOS(JPT)=Y1+2.*YMESH(JRAD,JPT,NNSV)
          ZPOS(JPT)=Y2-2.*ZMESH(JRAD,JPT,NNSV)

```

```
356 X6PUS(JPT)=X6-2.*YMF$H(JRAD,JPT,NNSV)
XPOS(NAP1)=XPOS(1)
YPOS(NAP1)=YPOS(1)
ZPOS(NAP1)=ZPOS(1)
X6PUS(NAP1)=X6PUS(1)
GO TO 357
```

C  
C

```
355 JTOR=1
IF(JRAD.EQ.(NRPI+1))GO TO 359
JTOR=2
358 JPT=1,NA
XPOS(JPT)=X1-2.*XTRAL(JTOR,JPT,NNSV)
YPOS(JPT)=Y1+2.*YTRAL(JTOR,JPT,NNSV)
ZPOS(JPT)=Y2-2.*ZTRAL(JTOR,JPT,NNSV)
358 X6PUS(JPT)=X6-2.*YTRAL(JTOR,JPT,NNSV)
XPOS(NAP1)=XPOS(1)
YPOS(NAP1)=YPOS(1)
ZPOS(NAP1)=ZPOS(1)
X6PUS(NAP1)=X6PUS(1)
```

C

```
357 CALL LINE(XPOS,ZPOS,NAP1,1,0,1)
CALL LINE(XPOS,YPOS,NAP1,1,0,1)
CALL LINE(X6PUS,ZPOS,NAP1,1,0,1)
```

C

```
354 CONTINUE
```

C

```
CALL PLOT(22,0,0,-3)
WRITE(6,367)
```

```
367 FORMAT(/' FINISHED PLOTTING FOR THIS PICTURE-PASS.'/IHL)
340 CONTINUE
```

C

```
*RITE(6,335)
335 FORMAT(IHL,'SUCCESSFUL COMPLETION OF THIS RWAKEPIC RUN.')
CALL EXIT
```

\*\*WAKI'IC

END



```

C      DATA COMPNT/12H1 ST COS1 AT SIN2 ND COS2 ND SIN3 RD COS3 RD SIN4
      1TH COS4 TH SIN5 TH COS5 TH SIN6 TH COS6 TH SIN7 TH COS7 TH SIN8 TH
      2 COS9 TH SIN9 TH COS9 TH SIN10TH COS10TH SIN11TH COS11TH SIN12TH C
      30S12TH SIN /
C
      DATA HUNG/ 240AERY DYNAML LIFT,LBWT/FTFLAPWISE BEND,MOM,LB-IN AE
      1RO,PITCH,MOM, LB-FI/FTGUND GAMMA STH,SQFT/SECINDUCED VELOCITY, FT
      2/SECEFF,ANGLE OF ATTACK,RADSCONST,COMP,CH,NRML V.F/SIST COS,CH,NRM
      3L V.FT/SEC2ND COS,CH,NRML V.FT/SLOC3RD COS,CH,NRML V.FT/SECQUAZ,ST.
      4 , 50HSAMMA, SQFT/SEC,SPVWIZ FLOW LIFT,LBWT/FT /
C
      DATA SHIYCL/385.54996,3895+.479,10*1./
C
      DATA SSTUCL/171.98341,8599.6785,10*1./
C
      DATA SHMCL/84.996823,8466.6835,10*1./
C
      READ(2,1304)PLOTNO,PICNO,CRAD,XAZ
      1304 FORMAT(5X,4A4,2X,14A4/10X,-14.7,5X,E14.7)
C
      REWIND 3
C
      CALL PLOTS(BUILD(2000),2000)
      CALL PERT(4,0,0,-3)
C
      CALL(3) RUNJOB,RUNNO,TITLE,NR,NA,NB,BLDRAD,NRM,NRA,NRMA,NAM1D2,
      1 ISPNEC,FMT1,FMT2,(RM(J),J=1,NR),(RDM(J),J=1,NRM)
C
      CALL SYMBOL(0,1,0,14,37)THIS KSLTSPLT JOB USED TP3 DATASET CF,
      1 20,0,37)

```

```

C      CALL SYMBOL(0.5,1.,0.14,RUNL6L,90.,80)
C
C      CALL VARFMT(20H(/I
1      ,20,FM13)
C      ,20,NRM,20H(12.4))
C
C      NAPI=NA+1
C      FVA=FLOAT(MA)
C      JTAPE=1
C
C      JTAPC=J MEANS THAT THE TAPE IS NOW READY FOR READING THE J TH TYPE
C      QUANTITY OFF IT.
C
C      DO 1315 KAZ=1,NAPI
1315 XAZMTH(KAZ)=2.3358712316**KAZ*FLOAT(KAZ-1)/FVA
C      DO 1302 J=1,NK
C      PCTRM(J)=100.*NM(J)/BLDRAD
1302 XXRM(J)=0.011811*PCTRM(J)
C      DO 1303 J=1,NRM
C      PCTRM(J)=100.*RUM(J)/BLDRAD
1303 XARM(J)=0.011811*PCTRM(J)
C
C      SCLAX=1./(1.1811*XRAD)
C      SCLAZ=360./(2.3358712316**KAZ)
C
C      WRITE(6,1305) PLOTNO,PICNO,M,XRAD,SCLXX,XAZ,SCLAZ
1305 FORMAT(1H1//110X,4A4//1X,14A4//)' XRAD = ,E14.7,10X,'SCLAX = ',
1      ,E14.7,' RADII PER INCH'/' XAZ = ,E14.7,10X,'SCLAZ = ,E14.7,
2      , DEGREES PER INCH')
C      WRITE(6,1301)RUNL6L,RUNNO,ITILE
1301 FORMAT(///)' THIS RESULT-PLOTTING RUN USED THE LTAP3 DATASET GENER
ATED IN THE CRNL2MOD RUN ENTITLED'///5X,3H' ,2JA4,5H ' ,///
2      , WHICH USED THE LTAP2 DATASET GENERATED IN THE CRNL1MOD RUN CA
LLED'/// 8X,4A4, ' * ,2H' ,14A4,4H ' .)
C
C      READ(5,1306)NPOINTS,(JJQNT(J),J=1,NNUNTS)

```



NOT REPRODUCIBLE

```
AMT=J, 34567891  
CLAEU, 98765431  
  
JUNT=JJUNT(RQ, JY)  
1311 IF (JUNT.EQ. JTAPL) GO TO 1316  
      KEAT(3), KIP  
      REAT(3), KIP  
      JTAPE=JTAPL+1  
      IF (JTAPL.EQ. (11+ISP.FG)) GO TO 1311  
  
      WRITE(6, 1313) KUNTY, JUNT, JTAPE, ISPNFC  
1313 FORMAT(//) CALLED AT 1313. KUNTY=, 12, , JJUNT(KUNTY)=, 12,  
      , JTAPL=, 12, , ISPNFC=, 12)  
      CALL EXIT  
  
1314 GO 1328 J=1, 500  
1323 DUM4Y(J)=0.  
      NRADII=4R  
      IF (JUNT.EQ. 2) NRADII=NRM  
      NRAUAZ=NR  
      IF (JUNT.EQ. 2) NRAUAZ=NRMA  
  
      NOW BEGIN TO MAKE A "TIME-HISTORIES" PLOT.  
  
      READ(3) JJJJ, (QTY(I, J), J=1, NRADII), I=1, NA)  
      READ(3) ((A(NQ, JQ), NQC=1, NAMID2), JQ=1, NRADII),  
1      ((B(NQ, JQ), NQC=1, NAMID2), JQ=1, NRADII),  
2      (AZLRJ(J), J=1, NRADII)  
      NCMLOC=1+6*(JJUNT-1)  
      NDMPS=NUMLOC+5  
  
      IF (JUNT.EQ. 2) GO TO 1369  
  
      WRITE(6, 1370) (HUNG(I), I=NUMLOC, NDMPS), NR, NA  
1370 FORMAT(1H/1X, 6147//) QTY(I, J), J=1, NR), I=1, NA), 5X, 'NR=', 12, 5X,
```

```

1      'NA=', I2/)
WRITE(6, FMT1) (QTY(I, J), J=1, NR), I=1, NA)
WRITE(6, I371) NR, NAMID2
1371  FORMAT(////) (A(NV, JQ), J=1, NR), NNQ=1, NAMID2) ', 5X, 'NR=', I2,
1      'NAMID2=', I2/)
WRITE(6, FMT1) (A(NV, JQ), J=1, NR), NNQ=1, NAMID2)
WRITE(6, I372) NR, NAMID2
1372  FORMAT(////) (B(NV, JQ), J=1, NR), NNQ=1, NAMID2) ', 5X, 'NR=', I2,
1      'NAMID2=', I2/)
WRITE(6, FMT1) (B(NV, JQ), J=1, NR), NNQ=1, NAMID2)
WRITE(6, I373) NR
1373  FORMAT(////) (AZER(J), J=1, NR) ', 5X, 'NR=', I2/)
WRITE(6, FMT1) (AZER(J), J=1, NR)
1374  'NA=', I2/)
GO TO I378
1369  WRITE(6, I374) (FDNG(I), I=NUMLOC, NOMP5), NR, NA
1374  FORMAT(IHI/IX, 6A4/)// (QTY(I, J), J=1, NR), I=1, NA) ', 5X, 'NRM=', I2,
1      'NA=', I2/)
WRITE(6, FMT3) (QTY(I, J), J=1, NR), I=1, NA)
WRITE(6, I375) NR, NAMID2
1375  FORMAT(////) (A(NV, JQ), J=1, NR), NVQ=1, NAMID2) ', 5X, 'NRM=', I2,
1      'NAMID2=', I2/)
WRITE(6, FMT3) (A(NV, JQ), J=1, NR), NNQ=1, NAMID2)
WRITE(6, I376) NR, NAMID2
1376  FORMAT(////) (B(NV, JQ), J=1, NR), NNQ=1, NAMID2) ', 5X, 'NRM=', I2,
1      'NAMID2=', I2/)
WRITE(6, FMT3) (B(NV, JQ), J=1, NR), NNQ=1, NAMID2)
WRITE(6, I377) NR
1377  FORMAT(////) (AZER(J), J=1, NR) ', 5X, 'NRM=', I2/)
WRITE(6, FMT3) (AZER(J), J=1, NR)
1378  'NA=', I2/)
GO I367 J=1, NRADII
1367  I=1, NA

```

NOT REPRODUCIBLE

```

1367 QTY(I,J)=QTY(I,J)-AZERO(J)
C
      JTAPE=JTAPE+1
C
      IF (JJJJJ.EQ.JQNT) GO TO 1330
      WRITE(6,1331,JQNT,JJJJJ
1331 FORMAT(///' CALLED EXIT 1331.(JQNT.NE.JJJJJ) JQNT=',I4,'JJJJJ='',I4)
      CALL EXIT
1330 CONTINUE
      IF (IUNKNM.EQ.-1) GO TO 1349
      SCLHTY=SHTYGL(JQNT)/XQHTY
      GO TO 1350
C
1349 CALL SCALE(QTY,NRADAZ,4.,QMIN,SCLQ,1)
      CALL SCALE(DUMMY,240,4.,AMIN,SCLA,1)
      CALL SCALE(AZERO,NRADII,4.,AZRMIN,SCLAZR,1)
      WRITE(6,1368)AZRMIN,SCLAZR
1368 FORMAT(///' AZRMIN = ',E14.7,5X,'SCLAZR = ',E14.7///)
C
1350 WRITE(6,1329) (HUNG(I),I=NDMLDC,NOMPS),QMIN,SCLQ,AMIN,SCLA
1329 FORMAT(///'IX,6A4//' QMIN = ',E14.7,5X,'SCLQ = ',E14.7///
      I , AMIN = ',E14.7,5X,'SCLA = ',E14.7//)
C
      CALL PLOT(2.,5.,-3)
      INDY=1
C
      INDY=+1 MEANS THAT THE NEXT PLOT IS TO BE MADE ON THE UPPER LEVEL.
C
      IF (NNRAD.EQ.0) GO TO 1332
      CALL SYMBOL(0.,-1.5,0.21,PLGTNO,90.,16)
      CALL SYMBOL(2.,4.,8,0.21,HUNG(NOMLOC),0.,24)
      CALL SYMBOL(6.,5.,4.8,0.14,16H(TIME-HISTORIES) ,0.,16)
      CALL PLOT(2.,5.,-3)
      AXLGTH=2.3358712316*XAZ
      F=AXLGTH/4.
C

```

```

C      DO 1332 KRAU=1,NNRAD
      JRAD=JJKAU(KRAD)
      IF(JRAD.LE.NKRADII) GO TO 1341
      WRITE(6,1342)KRAD,JKAD,NRADII
1342  FORMAT(//' CALLED EXIT 1342. KRAD=',I3,' ,JKAU=',I3,' ,NRADII=',I3)
      CALL EXIT
C
1341  PCT=PCTRM(JRAD)
      IF (JQNT.EQ.2)PCT=PCFRDM(JRAD)
      CALL NUMBER(1.,3.5,0.14,PCT,0.,+1)
      CALL SYMBOL(1.65,3.5,0.14,4*KRAD,0.,+4)
C
      DO 1333 JPOS=1,NA
1333  YPOS(JPOS)=QTY(JPOS, JRAD)/SCLHTY
      YPOS(NAP1)=YPOS(1)
C
      IF((IUNKNV.EQ.1)GO TO 1351
C
      CALL PLOT(0.,2.,-3)
      CALL LINE(XAZM TH, YPOS, NAP1, 1, 0, 1)
      CALL PLOT(0.,-2.,-3)
C
      DRAW AZIMUTH AXIS.
      CALL PLOT(AXLGTH,2.,-3)
      CALL PLOT(0.,2.,+2)
      CALL PLOT(0.,0.,-3)
      CALL FACTOR(F)
      CALL AXIS(0.,0.,1H , -1, 4.,0.,0.,90.)
C
      CALL SYMBOL(3.2,-0.31,0.14,1H.,0.,1)
      CALL SYMBOL(3.05,-0.45,0.14,7HAZIMUTH,0.,7)
C
      CALL PLOT(0.,0.,-3)
      CALL FACTOR(1.)

```

NOT REPRODUCIBLE

```

C      DRAW THE JY AXIS.
      QMIN=-2.*SCLHY
      CALL AXIS(0.,0.,IH,1.,4.,0.,QMIN,SCLHY)
      GO TO 1332
1331  CALL LNLX(AZMTH,YP,S,VAP,1,0,1)
      CALL AXIS(0.,0.,1,DEGREES AZIMUTH,-15.,4.,0.,0.,SCLAZ)
      CALL AXIS(0.,0.,IH,1.,4.,90.,QMIN,SCLG)
C
1332  INDY=-INDY
      INDY=-1 MEANS THAT THE NEXT PLOT IS TO BE MADE ON THE LOWER CONCOURSE.
C
      IF (INDY)1334,1335,1336
1335  WRITE(6,1337)INDY
1337  FORMAT(//' CALLED EXIT 1335 BECAUSE INDY VANISHES. INDY=',I6)
      CALL EXIT
C
1334  CALL PLOT(0.,-4.5,-3)
      GO TO 1332
1336  CALL PLOT(5.,4.5,-3)
C
1332  CONTINUE
C
      IF (INDY)1346,1335,1347
1346  CALL PLOT(5.,-0.5,-1)
      GO TO 1348
1347  CALL PLOT(5.,-5.,-3)
C
1348  WRITE(6,1349)KQNTY
1349  FORMAT(//' FINISHED TIME-HISTORIES PLOTS FOR KQNTY=',I3)
C
C      NOW BEGIN TO MAKE THE HARMONIC COMPONENTS PLOTS.
C
      CALL SYMBOL(0.,3.,0.21,PLDNU,90.,16)
      CALL SYMBOL(2.,9.8,0.21,HU,(NUMLOC),0.,24)
      CALL SYMBOL(6.,9.8,0.14,1,1,(HARMONIC ANALYSIS),0.,19)

```



```

CALL AXIS(0.,0.,1H,1.,4.,90.,0.,SCLSTD)
CALL PLOT(5.,0.,-3)
C 1354 IF(NHARM.EQ.0)GO TO 1322
F=AXLGTH/2.
C
C 10 1322 KHARM=L,NNHARM
C
C JHARM=JJHARM(KHARM)
C IF(JHARM.LE.NAMID2) GO TO 1339
C
WRITE(6,1340) KHARM,JHARM,NAMID2
1340 FORMAT(//' CALLED EXIT 1340. KHARM=',I3,' JHARM=',I3,
1 ',NAMID2=',I3)
CALL EXIT
C
C COSINE COMPONENT PLOT.
C
C 1339 GO 1323 JPUS=L,HRADII
1323 YPOS(JPOS)=A(JHARM,JPOS)/SCLHRM
NOMLOC=1+4*(JHARM-1)
CALL SYMBOL(0.25,3.5,0.14,COMPNT(NOMLOC),0.,8)
C
C IF(IUNKNW.EQ.0)GO TO 1359
C
C IF(JUNT.EQ.2) GO TO 1324
CALL LINE(XXRM,YPOS,NR,1,0,1)
GO TO 1325
1324 CALL LINE(XXRDM,YPOS,NRM,1,0,1)
1325 CALL AXIS(0.,0.,1H,1.,4.,90.,AMIN,SCLA)
CALL AXIS(0.,0.,4HRNDM,-4,3,0.,0.,SCLXX)
GO TO 1362
C
C 1359 CALL PLOT(0.,2.,-3)

```

```

IF(JQNT.EQ.2)GO TO 1360
CALL LINE(XXRM,YPOS,NR,1,0,1)
GO TO 1361
1360 CALL LINE(XXRDM,YPOS,NRM,1,0,1)
C DRAW THE RADII AXIS.
1361 CALL PLOT(AXLGTH,0.,+3)
CALL PLOT(0.,0.,+2)
CALL PLOT(0.,-2.,-3)
CALL FACTOR(F)
CALL AXIS(0.,0.,1H,-1,2.,0.,0.,0.50)
CALL SYMBOL(1.2,-0.45,0.14,6HRADIUS,0.,6)
CALL PLOT(0.,0.,-3)
CALL FACTOR(1.)
C DRAW THE QTY AXIS.
QTMIN=-2.*SCLHRM
CALL AXIS(0.,0.,1H,1,4.,90.,QTMIN,SCLHRM)
C
C 1362 CALL PLOT(0.,-4.5,-3)
C
C SINE COMPONENT PLOT.
C
C DO 1326 JPOS=1,NRADII
1326 YPOS(JPOS)=8(JHARM,JPOS)/SCLHRM
C
C NOMLOC=4.*JHARM-1
CALL SYMBOL(0.25,3.5,0.14,COMPNT(NOMLOC),0.,8)
C
IF(IJUNKM.EQ.0)GO TO 1363
IF(IJQNT.EQ.2) GO TO 1316
CALL LINE(XXRM,YPOS,NR,1,0,1)
GO TO 1317
1316 CALL LINE(XXRDM,YPOS,NRM,1,0,1)
1317 CALL AXIS(0.,0.,1H,1,4.,90.,AMIN,SCLA)
CALL AXIS(0.,0.,4HRNDM,-4,1.,0.,0.,SCLXX)
GO TO 1366

```

```

C 1363 CALL PLOT(0.,2.,-3)
      IF(JUNT.EQ.2)GO TO 1364
      CALL LINE(XARM,YPC,NR,1,0,1)
      GO TO 1365
1364 CALL LINE(XARM,YPJS,NRM,1,0,1)
1365 CALL PLOT(AXLGTH,0.,+3)
      CALL PLOT(0.,0.,+2)
      CALL PLOT(0.,-2.,-3)
      DRAW THE RADII AXIS.
      CALL FACTOR(F)
      CALL AXIS(0.,0.,1H,-1,2.,0.,0.,0.50)
      CALL SYMBOL(1,2,-0.45,0.14,0RADIUS,0.,0)
      CALL PLOT(0.,0.,-3)
      CALL FACTOR(1.)
      DRAW THE QTY AXIS.
      CALL AXIS(0.,0.,1H,1,4.,90.,JTMIN,SCLHRM)
C 1366 CALL PLOT(5.,4.5,-3)
      1322 CONTINUE
C
      CALL PLOT(2.,-5.,-3)
      WRITE(6,1327)KQNTY
1327 FORMAT(///// FINISHED PLOTTING FOR KQNTY = ,I2)
C 1308 CONTINUE
C
      CALL SYMBOL(0.,1.,0.14,37THIS RSLTSPLT JOB USED TP5 DATASET OF,
1 90.,37)
      CALL SYMBOL(0.5,1.,0.14,RUABL,90.,80)
      CALL PLOT(1.,0.,-3)
C
      REMIND 3
      WRITE(6,1330)

```

NOT REPRODUCIBLE

1338 FORMAT(11H1// ' SUCCESSFUL COMPLETION OF THIS RSLTSPLT RUN. ')

RETURN

C  
C  
C  
C

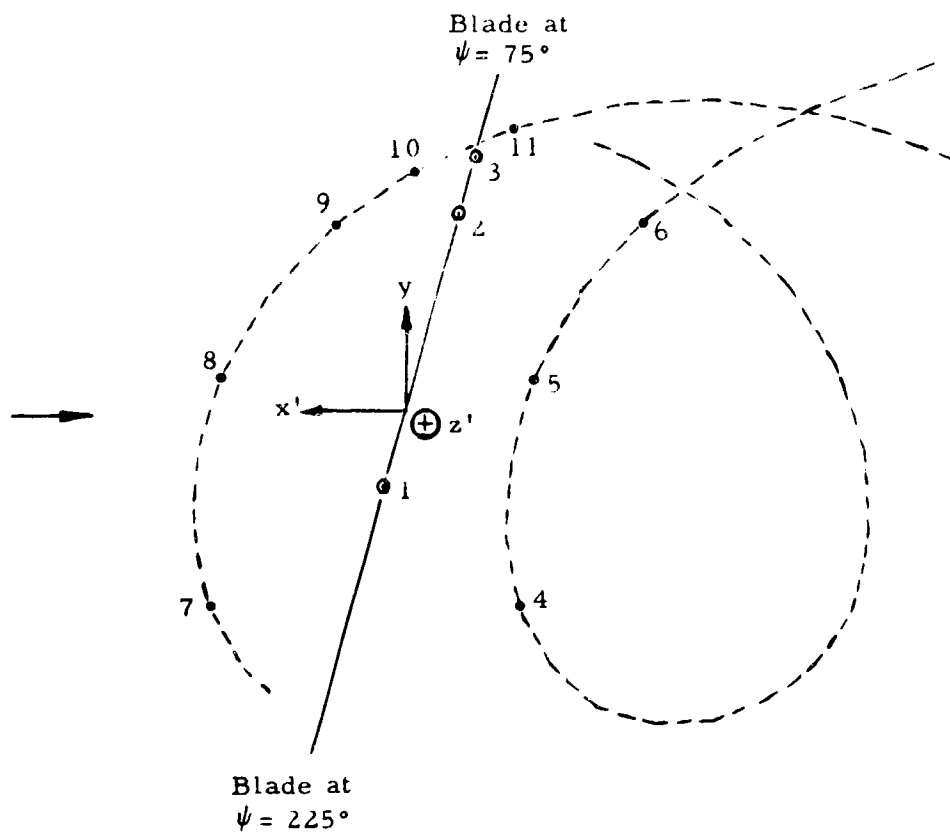
END

\*\*\*RSLTS

APPENDIX III

INDUCED VELOCITY AT SELECTED POSITIONS ON THE DISC DUE TO  
SELECTED SEGMENTS OF THE NEAREST TIP TRAIL

Table V shows the induced velocity due to nearby filaments of the trailed vorticity. Five instantaneous positions were chosen for points on the blades (see Figure 38), and the induced velocities resulting at these points due to selected short segments of the tip vortices (as positioned by the two geometries, CAL and UR) were computed for the  $\mu = 0.26$  flight condition of UH-1.



Coordinates ( $x'$ ,  $y$ ,  $z'$ ) of blade stations 1, 2, 3:

1. (+1.514, -4.434, -0.44)
2. (-3.649, +12.40, -0.679)
3. (-4.574, +15.86, -0.854)

See Table V for coordinates of wake segments as represented in the two wake geometries.

Figure 38. Positions of Selected Blade Stations and Selected Wake Trail Segments (UH-1,  $\mu = 0.26$ ).

TABLE V. INDUCED VELOCITY AT SELECTED BLADE STATIONS DUE TO  
SELECTED TIP TRAIL SEGMENTS (UH-1,  $\mu = 0.26$ )

i	j	k	Wake	Coordinates of Point A	Coordinates of Point B	$\Gamma_{AB}$	w' at M
1	4	5	CAL	-5.694, -12.14, +1.771	-6.180, +2.494, +2.370	325.0	-4.322
1	4	5	UR	-6.767, -12.07, +3.079	-7.773, +2.571, +3.454	327.6	-3.136
1	7	8	CAL	+12.23, -12.14, -0.625	+11.75, +2.494, -0.026	325.0	+2.828
1	7	8	UR	+12.11, -12.03, +0.353	+11.42, +2.470, +1.007	327.6	+2.909
2	9	11	CAL	+4.878, +11.99, +0.374	-6.221, +18.28, +0.773	231.1	+7.161
2	9	11	UR	+4.475, +11.76, +1.344	-6.574, +17.81, +1.835	229.4	+6.150
2	5	6	CAL	-6.180, +2.494, +2.370	-13.05, +11.99, +2.770	279.1	-2.725
2	5	6	UR	-7.773, +2.571, +3.454	-14.25, +11.92, +4.027	284.2	-2.016
3	10	11	CAL	-0.258, +15.67, +0.573	-6.221, +18.28, +0.773	220.0	+9.085
3	10	11	UR	-0.644, +15.31, +1.506	-6.574, +17.81, +1.835	215.6	+3.488

$\vec{e}_M$

See Figure 38.



UNCLASSIFIED

Security Classification

DOCUMENT CONTROL DATA - R & D

(Security classification of title, body of abstract and indexing annotation must be entered when the overall report is classified)

1. ORIGINATING ACTIVITY (Corporate author) University of Rochester Rochester, New York		2a. REPORT SECURITY CLASSIFICATION Unclassified	
		2b. GROUP	
3. REPORT TITLE AN ACTUATOR-DISC ANALYSIS OF HELICOPTER WAKE GEOMETRY AND THE CORRESPONDING BLADE RESPONSE			
4. DESCRIPTIVE NOTES (Type of report and inclusive dates) Final Report			
5. AUTHOR(S) (First name, middle initial, last name) M. Joglekar R. Loewy			
6. REPORT DATE December 1970		7a. TOTAL NO. OF PAGES 215	7b. NO. OF REFS 24
8a. CONTRACT OR GRANT NO. DAAJ02-68-C-0047 NEW		9a. ORIGINATOR'S REPORT NUMBER(S) USAAVLABS Technical Report 69-66	
8b. PROJECT NO. c. Task 1F162204A13904		9b. OTHER REPORT NO(S) (Any other numbers that may be assigned this report)	
d.			
10. DISTRIBUTION STATEMENT This document is subject to special export controls, and each transmittal to foreign governments or foreign nationals may be made only with prior approval of Eustis Directorate, U.S. Army Air Mobility R&D Laboratory, Fort Eustis, Virginia 23604.			
11. SUPPLEMENTARY NOTES		12. SPONSORING MILITARY ACTIVITY Eustis Directorate U.S. Army Air Mobility R&D Laboratory Fort Eustis, Virginia	
13. ABSTRACT In this analytical research, it is assumed that a helicopter rotor in forward flight can be represented by a flat plate. Expressions are developed relating the pressure field to the steady aerodynamic thrust and moment and the time-dependent flapping moment. This pressure field satisfies the zero pressure condition at the center and edge of the disc, the first and second harmonic variation in lift, and Laplace's equation.  A computer program was written to calculate the velocity field and streamlines. Two sample cases corresponding to high- and low-speed conditions for the UH-1 rotor were chosen for computation. Both cases showed the tip-vortex phenomenon.  In order to examine the sensitivity of blade load calculations to wake geometry, an existing airloads program was modified to accept the computed wake geometry. A comparison of results of this modified program with experimental data indicated that the effect of distorted wake is greater at low advance ratios than at high advance ratios. The reduced sensitivity at high advance ratios may be due to the wake being blown farther behind the rotor and/or the predominance of other aeroelastic parameters.			

DD FORM 1473

REPLACES DD FORM 1473, 1 JAN 64, WHICH IS OBSOLETE FOR ARMY USE.

UNCLASSIFIED

Security Classification

UNCLASSIFIED

Security Classification

14.	KEY WORDS	LINK A		LINK B		LINK C	
		ROLE	WT	ROLE	WT	ROLE	WT
	Helicopter Rotor Wake Wake Geometry Distorted Wake Helicopter Blade Loads Helicopter Aerodynamics						

UNCLASSIFIED

Security Classification